Cellular, molecular and behavioral analysis of neurodegeneration in a transgenic spinocerebellar ataxia type 1 (SCA1) model in zebrafish

Von der Fakultät für Lebenswissenschaften

der Technischen Universität Carolo-Wilhelmina zu Braunschweig

zur Erlangung des Grades eines

Doktors der Naturwissenschaften

(Dr. rer. nat.)

genehmigte

D i s s e r t a t i o n

von Mohamed Ahmed M. A. M. Elsaey

aus Port Said, Ägypten

1. Referent: Professor Dr. Reinhard W. Köster
2. Referent: Professor Dr. Martin Korte
eingereicht am: 07.07.2021
mündliche Prüfung (Disputation) am: 28.09.2021

Druckjahr 2021

"Printed with the support of the German Academic Exchange Service (DAAD)"

Vorveröffentlichungen der Dissertation

Teilergebnisse aus dieser Arbeit wurden mit Genehmigung der Fakultät für Lebenswissenschaften, vertreten durch den Mentor der Arbeit, in folgenden Beiträgen vorab veröffentlicht:

Publikationen

Elsaey, M. A.; Namikawa, K.; Köster, R. W. (2021): Genetic modeling of the neurodegenerative disease spinocerebellar ataxia type 1 in zebrafish. *International Journal of Molecular Sciences* 22 (14), 7351.

Tagungsbeiträge

Elsaey, M. A.; Namikawa, K.; Von Trotha, J. W.; Köster, R. W. (2021): Zebrafish stable transgenic model for SCA1 (poster). *Ataxia Investigators Meeting*, National Ataxia Foundation, Minneapolis, MN, USA.

Elsaey, M. A.; Namikawa, K.; Von Trotha, J. W.; Köster, R. W. (2020): Zebrafish transgenic neurodegeneration model for SCA1 (oral presentation). *Zoological Institute Seminar*, Braunschweig, Germany.

Elsaey, M. A.; Namikawa, K.; Köster, R. W. (2019): Zebrafish transgenic model for spinocerebellar ataxia type 1 (oral presentation). *Edinburgh Fish Technology*, Edinburgh, UK.

Elsaey, M. A.; Namikawa, K.; Köster, R. W. (2019): Zebrafish stable transgenic model for SCA1 (poster). *A State of Mind: Neural Communication in Health and Disease*, Braunschweig, Germany.

Elsaey, M. A.; Namikawa, K.; Köster, R. W. (2018): *In vivo* and *in vitro* expressing of the human pathological Ataxin-1 protein allows the disease modeling of spinocerebellar ataxia type 1 and consequently other polyglutamine disorders (poster). *What about Glia? New Concepts and Functional Roles*, Braunschweig, Germany.

I dedicate this work to
My parents Ahmed and Faten,
My wife Sara,
Ashraf, Abdallah, Ahmed, Shahinda,
Muhammad and Yunus

فَضْلُكُمْ يَا وَالِدَيَّ عَمَّنِي حَتَّى اللَّجَم
كُلُّ هَمٍّ قَدْ أَصَبْنَا زَادَكُمْ بِالطَّبْعِ هَم
إِنَّ كُلَّ مَا جَنَيْنَا مِنْ جُهُودِكُمْ نَجَم
وَالِدِي يَا خَيْرَ عَوْنٍ كَانَ لِي عِنْدَ الْمِحَن

أَنْتِ يَا مَنْ تَمْلِكِينَ جَنَّةً تَحْتَ الْقَدَم
كُلُّ أَلْفَاظِ لِسَانِي كُلُّ شُكْرٍ قَدْ رُهِن
اجْمَعُوا كُلَّ الْمَعَانِي مِن عرَابٍ أو عَجَم
لَا تُوافِي شُكْرَهُنَّ لَا تُجَاوِزُ الْعَدَم

Acknowledgements

This PhD thesis has been accomplished at the Department of Cellular and Molecular Neurobiology, Zoological Institute, Faculty of Life Sciences, Technical University of Braunschweig.

First of all, I would like to express my sincere gratitude to **Prof. Dr. Reinhard Köster** for supervising my PhD thesis and for his valuable support and advice regarding my work. I am also grateful to **Dr. Kazuhiko Namikawa** for teaching me patiently during the lab work and to **Dr. Jakob von Trotha** for his appreciated support.

My very special thanks go to **Prof. Dr. Martin Korte** for reviewing my thesis as a co-examiner and to **Prof. Dr. Robert Hänsch** for being the chairman of the doctoral examination board.

I would like to thank **Mr. Timo Fritsch** for his support in the fish facility and to my colleagues at the Department of Cellular and Molecular Neurobiology for fruitful discussions and technical assistance.

Thanks also to the Egyptian Ministry of Higher Education and Scientific Research and the German Academic Exchange Service (DAAD) for funding my PhD thesis via the German Egyptian Research Long-term Scholarship (GERLS).

Last but not least, I want to express my appreciation to all my friends for their continuous encouragement and their belief that I can do it.

Contents

Abstract ……..... 4

Zusammenfassung …….……..…….. 5

Arabic abstract ……...……..…….. 7

1 Introduction ……..…...……..…… 8

1.1 Spinocerebellar ataxia type 1 ……..….....……...…….…….. 8

1.2 Genetic modeling of the SCA1 disease ……..……...…….…… 13

1.3 The zebrafish cerebellum ……...…… 18

1.4 Is zebrafish a promising candidate for SCA1 disease modeling? ……...…...… 20

1.5 The aim of this study …….....…….……..…… 23

1.5.1 Generation of human pathogenic Ataxin-1-expressing stable transgenic zebrafish strain ……...…….…… 23

1.5.2 Characterization of neurodegeneration of SCA1-affected Purkinje cells ……..……...……...……..…...… 24

1.5.3 Assessment of physiological properties of SCA1-affected Purkinje cells ……...……... 24

1.5.4 Monitoring SCA1-induced behavioral changes in SCA1 transgenic zebrafish ……...……..…….…… 24

2 Materials and Methods ……...……. 26

2.1 Materials ……..…….....……...…….…… 26

2.1.1 Equipment ……..…...……...……..... 26

2.1.2 Software for data acquisition and analysis ……...……..…… 27

2.1.2.1 Software for imaging ……....… 27

2.1.2.2 Software for image processing, analysis and visualization ..… 27

2.1.2.3 Software for animal behavior tracking and analysis ……...… 28

2.1.2.4 Software for data analysis and visualization …….……...… 28

2.1.3 Bacterial strain for transformation ……..…….....……..…… 28

2.1.4 Chemicals ……..…….....……..……..…… 28

2.1.5 Enzymes ……..…….....……..……...…… 29

2.1.6 Antibodies ……...…….....…….……..……...…… 30

2.1.7 Solutions and media ……...…….....……..……...…… 31

2.1.7.1 Fish-related solutions …..…….. 31

2.1.7.2 Cloning solutions …..……..…….. 32

2.1.7.3 Histological-staining buffers …..……...……..……...…….. 32

2.1.8 Kits and reagents for high-affinity purification ……...…….....…… 33

2.1.9 Oligonucleotides ……...…..……..…….....… 33

2.1.10 Plasmid vectors for microinjection ……...…….....…..……...… 34

2.1.11 Zebrafish strains ……...…….....……..……...……...… 36

2.1.11.1 Wild-type zebrafish …..…….....…..…..….…….. 36

2.1.11.2 Transgenic lines …..……..……..……..….. 36

2.2 Methods ……...……..……...……...……..….. 39

2.2.1 Biotechnology methods and cloning procedures .....…….....…..…… 39

2.2.1.2 DNA digestion ……..……...… 39

2.2.1.2 DNA Purification ……..……...… 40

2.2.1.3 DNA Ligation ……..……..……...… 40

2.2.1.4 Plasmid transformation ……..……...… 41

2.2.1.5 Small-scale DNA preparation from bacteria (Mini Prep) ….… 42

2.2.1.6 Large-scale DNA preparation from bacteria (Midi Prep) ....… 43

2.2.1.7 Tol1 mRNA synthesis ……..……...… 44

2.2.2 Zebrafish husbandry and maintenance ……..……...……..…… 45

2.2.3 Microinjection of nucleic acids ……..……...……..… 46

2.2.4 Screening and generation of zebrafish stable transgenic strains …….... 46

2.2.5 Whole-mount immunohistochemistry ……..….. 47

2.2.6 Measuring the fish length and isolation of the brain ……..... 48

2.2.7 Histology and immunostaining of the zebrafish brain …..……...…….. 48

2.2.8 Ca^{2+}-activity analysis ….…….…….…... 50

2.2.9 Behavioral analysis ……..……..…... 50

2.2.10 Statistical analysis ……..……..……..…... 51

3 Results …… 52

3.1 Genetic modeling of SCA1 in zebrafish ……..…….…..…. 52

3.1.1 Genetic engineering and strategy for modeling SCA1 in zebrafish …... 52

3.1.2 Generation of stable transgenic zebrafish model for Purkinje cell-specific SCA1 ……...……..……..……..…... 55

3.1.3 Expression of human Ataxin-1 in the stable transgenic zebrafish strains ……..... 58

3.2 Neurodegenerative effects of the overexpression of human mutant Ataxin-1 on zebrafish Purkinje cells ……..……..…..…… 61

3.3 Age-related progredient loss of Purkinje cell population in zebrafish genetic model of SCA1 ……..……..…..…… 69

3.4 Physiological properties of zebrafish Purkinje cells expressing human Ataxin-1 ……... 73

3.5 SCA1 zebrafish display behavioral abnormalities …… 79

4 Discussion ……..…… 85

4.1 Genetic modeling of SCA1 in zebrafish ……...…....…… 85

4.2 Neurodegenerative effects of the polyglutamine toxicity ……...……...…… 86

4.3 Purkinje cell physiological deficits in the SCA1 zebrafish model …….…… 90

4.4 Behavioral abnormalities in the SCA1 zebrafish model …….…...… 92

4.5 Conclusion and outlook ……..…… 94

5 Appendix ……..…….…… 96

5.1 List of figures ……..…….....……...…...…… 96

5.2 List of tables ……..……..……...…...…… 99

5.3 List of abbreviations ……...…..…….....……...…...……...… 100

6 References ……..……..…. 103

Abstract

Spinocerebellar ataxia type 1 (SCA1) is a late-onset neurodegenerative disease caused by expansion of the polyglutamine (polyQ) tract in Ataxin-1 protein (Atx1). The cellular mechanisms of how the altered function of Atx1 causes progressive neurodegeneration of the cerebellum are still not fully understood. Zebrafish (*Danio rerio*) is a powerful organism for *in vivo* bioimaging of disease mechanisms and compound studies. Therefore, this study aimed to establish a genetic model of SCA1 in zebrafish accessible for observing affected Purkinje cells (PCs) using fluorescent protein reporters and biosensors and for monitoring the behavioral performance of affected fish in relation to their disease progression. Three stable transgenic zebrafish strains were generated expressing the membrane-targeted red fluorescent reporter GAPmScarlet only or together with the human protein Atx1 (30Q or 82Q) in bidirectional DNA constructs under control of a PC-specific enhancer. These strains were subjected to long term *in vivo* monitoring of PC degeneration. They were also subjected to calcium imaging at larval stages. Furthermore, long term behavioral analysis was performed.

The SCA1 zebrafish strain expressing Atx1[82Q] developed a larval cerebellum indistinguishable from the control strains. However, calcium-transient activity revealed onset of PC abnormal physiology already evident at 6 and 12 days post fertilization (dpf). Yet an age-dependent progressive degeneration of PCs was observed starting at 40 dpf. Although this neuropathology did not result in gross locomotor deficits, late juveniles at 2 months post fertilization (mpf) as well as adults at 3 mpf with advanced PC loss demonstrated a strongly-reduced exploratory behavior. However, early juvenile SCA1 fish at 40 dpf did not display behavioral deficits probably due to less-pronounced PC degeneration. This novel SCA1 neurodegeneration model in zebrafish, mimicking human SCA1 pathology, is a powerful tool to reveal the causative mechanisms of cytotoxicity *in vivo*. Moreover, this model can be used for validating candidate compounds against such a devastative neurological disease for their efficacy, side effects and blood brain barrier passage.

Zusammenfassung

Die spinozerebelläre Ataxie Typ 1 (SCA1) ist eine spät auftretende neurodegenerative Erkrankung, die durch eine Expansion des Polyglutamin-Trakts (polyQ) im Ataxin-1-Protein (Atx1) verursacht wird. Die zellulären Mechanismen, wie die veränderte Funktion von Atx1 eine fortschreitende Neurodegeneration des Kleinhirns verursacht, sind noch nicht vollständig verstanden. Der Zebrafisch (*Danio rerio*) ist ein leistungsfähiger Organismus für das *in vivo* Bioimaging von Krankheitsmechanismen und Wirkstoffstudien. Daher zielte diese Studie darauf ab, ein genetisches Modell von SCA1 im Zebrafisch zu etablieren, das für die Beobachtung betroffener Purkinje-Zellen (PC) mit Hilfe von Fluoreszenzprotein-Reportern und Biosensoren zugänglich ist, sowie für die Beobachtung des Verhaltens betroffener Fische in Abhängigkeit von ihrem Krankheitsverlauf. Es wurden drei stabile transgene Zebrafischstämme generiert, die den membrangezielten rot fluoreszierenden Reporter GAPmScarlet allein oder zusammen mit dem humanen Protein Atx1 (30Q oder 82Q) in bidirektionalen DNA-Konstrukten unter Kontrolle eines PC-spezifischen Enhancers exprimieren. Es folgten langfristige *in vivo* Studien der drei Linien mit besonderem Augenmerk auf das degenerative Verhalten der Purkinje Zellen, sowohl in Larven als auch in adulten Tieren. Hierfür wurden unter anderem Kalzium-Bildgebungsanalysen im Larvenstadium und Langzeit-Verhaltensanalysen im Alter von 40 Tagen nach der Befruchtung (dpf), 2 und 3 Monaten nach der Befruchtung (mpf) durchgeführt.

Der SCA1-Zebrafischstamm, welcher Atx1[82Q] exprimierte, entwickelte ein larvales Kleinhirn, das sich nicht von dem der Kontrollstämme unterschied. Die Kalzium-Transientenaktivität zeigte jedoch den Beginn der abnormalen Physiologie des PC bereits am 6. und 12. dpf. Dennoch wurde eine altersabhängige progressive Degeneration der PCs erst ab 40 dpf beobachtet. Obwohl diese Neuropathologie nicht zu groben lokomotorischen Defiziten führte, zeigten die späten Juvenile im Alter von 2 mpf sowie adulte Fische im Alter von 3 mpf mit fortgeschrittenem PC-Verlust ein stark reduziertes Erkundungsverhalten. Die früh-juvenilen SCA1-Fische im Alter von 40 dpf zeigten jedoch keine Verhaltensdefizite, wahrscheinlich aufgrund einer weniger ausgeprägten PC-Degeneration. Dieses neuartige SCA1-Neurodegenerationsmodell im Zebrafisch, das die menschliche SCA1-Pathologie nachahmt, ist ein leistungsfähiges Werkzeug, um die ursächlichen Mechanismen der Zytotoxizität *in vivo* aufzudecken und besser zu verstehen. Darüber hinaus kann dieses Modell zur Validierung von Wirkstoffkandidaten gegen eine solch verheerende neurologische

Erkrankung hinsichtlich ihrer Wirksamkeit, Nebenwirkungen und Blut-Hirn-Schranken-Passage verwendet werden.

نبذة مختصرة

مرض الرَّنَح النُّخاعي المُخَيْخي من النوع الأول هو مرض عصبي متأخر الظهور لم يكتشف له علاج حتى الآن. يسبب هذا المرض ضمورًا وفقدانًا تدريجيًا للخلايا العصبية بالمخيخ؛ مما يؤدي إلى خلل تدريجي في الاتزان الحركي، بالاضافة إلى خلل نفسي وإدراكي في بعض الحالات المتأخرة، وينتهي بالوفاة. هذا المرض ناجم عن خلل جيني يؤدي إلى استطالة السلسلة متعددة الجلوتامين في بروتين أتاكسين ١. لا تزال الآليات الخلوية لكيفية تسبب الخلل الوظيفي لهذا البروتين في حدوث الضمور العصبي التدريجي للمخيخ غير مفهوم تمامًا. تعد سمكة الزرد، بوصفها كائنًا حيًا يتميز ببرقاته الشفافة فى مراحل النمو المبكرة، مناسبة للتصوير الحيوي لآليات الأمراض، ولدراسة تأثير المركبات المختلفة بوصفها علاجات محتملة لهذه الأمراض دون الحاجة إلى تشريحها. لذلك، تهدف هذه الدراسة إلى إنشاء نموذج يحاكي مرض الرَّنَح النُّخاعي المُخَيْخي من النوع الأول في سمكة الزرد يمكن عن طريقه مراقبة خلايا بوركينجي التي تعد أكثر الخلايا العصبية المتأثرة بهذا المرض، كما يمكن مراقبة التغير السلوكي للأسماك المصابة مع تقدم المرض.

باستخدام تقنيات الهندسة الوراثية، أُنتجت سلالات من أسماك الزرد المعدلة وراثيًا تحمل البروتين البشري الطبيعي أو مسبب المرض داخل خلايا بوركينجي. خضعت هذه السلالات لمراقبة طويلة المدى في أعمار مختلفة حتى البلوغ. تمت مراقبة وظيفة خلايا بوركينجي وشكلها، بالإضافة إلى مراقبة الأداء السلوكي للأسماك. لقد لوحظ في نتائج هذه الدراسة أن سلالة الأسماك التي تحمل البروتين البشري مسبب المرض تحتوي على مخيخ لا يمكن تمييزه شكلًا عن سلالة الأسماك التي تحمل البروتين الطبيعي. ولكن كشفت دراسة وظيفة خلايا بوركينجي بوضوح عن ضعف في نشاط هذه الخلايا العصبية في عمر ٦ و١٢ يومًا. كما لوحظ ضمور تدريجي يزداد مع تقدم العمرلخلايا بوركينجي بدءًا من عمرالأربعين يومًا. وعلى الرغم من أن السلالة الحاملة لهذا المرض العصبي لم تظهر عجزًا حركيًا كبيرًا، فقد أدت شدة الضمور وفقدان كم كبير من خلايا بوركينجي في الأسماك ذات عمر الشهرين وكذلك الأسماك البالغة عند عمر ثلاثة شهور إلى انخفاض شديد فى السلوك الاستكشافي مقارنة بأسماك السلالة غير الحاملة للمرض. يعد هذا النموذج أول نموذج يحاكي مرض الرَّنَح النُّخاعي المُخَيْخي من النوع الأول في أسماك الزرد، وهو وسيلة فعالة للكشف عن الآليات المسببة لضمور خلايا بوركينجي. علاوة على ذلك، يمكن استخدام هذا النموذج لاختبار العديد من المركبات المرشحة كعلاجات لهذا المرض العصبي من حيث فعاليتها وآثارها الجانبية وقدرتها على المرور للمخ.

1 Introduction

1.1 Spinocerebellar ataxia type 1

Spinocerebellar ataxia type 1 is an adult onset, autosomal dominant neurodegenerative disease caused by a cytosine-adenine-guanine (CAG)-repeat expansion mutation in the human *ataxin-1* gene (*Atx1*), resulting in abnormal expansion in the polyQ tract of the Ataxin-1 protein (Atx1). This protein contains a polyQ tract of variable length in its N-terminus, with non-interrupted polyQ-stretches of above 40 glutamine residues leading to SCA1 symptoms and neurodegeneration (Nethisinghe et al. 2018). The length of this tract inversely correlates with the age of onset and directly correlates with the severity of pathogenesis and progression of SCA1 (Zoghbi and Orr 2000). In SCA1 patients, motor coordination, visuospatial performance, psychiatric health and cognitive abilities successively decline leading to death (Pérez Ortiz and Orr 2018). The symptoms of the disease begin usually in the twenties or thirties of age and they get worse in an age-dependent progressive manner (Orr et al. 1993). The mutated Atx1 protein causes progressive neurodegeneration of cerebellar PCs which ends with atrophy of the cerebellum (Fig. 1.1) and death within 10-30 years after first appearance of the disease onset (Pérez Ortiz and Orr 2018; Wang et al. 2016).

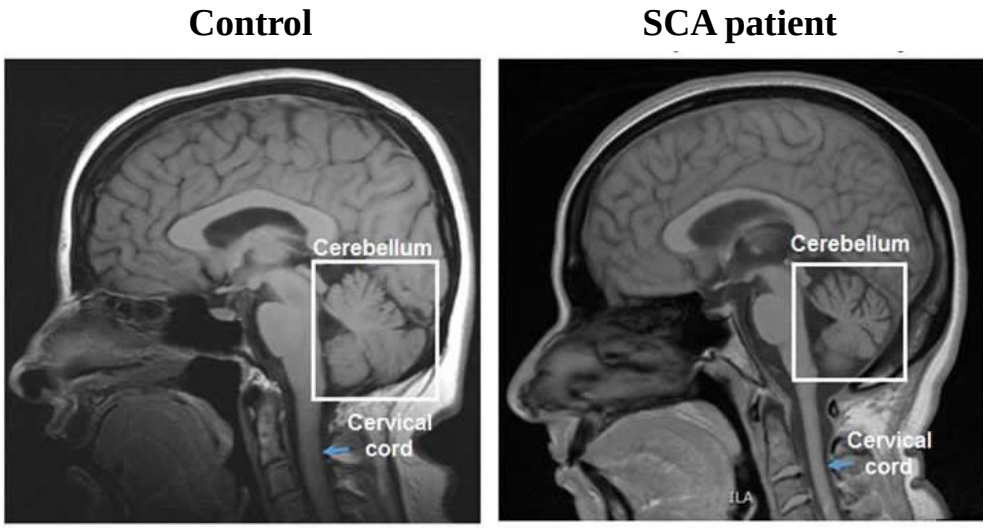

Figure 1.1 Sagittal MRI from unaffected control (left) and SCA patient (right)

MRI from a SCA-affected patient reveals cerebellar degeneration and cervical spinal cord thinning. Modified from (Wang et al. 2016).

The length of the wild-type Atx1 protein is 816 amino acids. However, this varies according to the length of polyQ tract which is normally 4 to 36 glutamine residues and 38 to 83 uninterrupted glutamine residues in SCA1-affected patients (Nethisinghe et al. 2018; Rocha et al. 2019). The polyQ tract is positioned at the N-terminal region of the protein (starting at amino acid 197). In addition, the **A**ta**x**in-1 and **H**MG-box protein 1 (AXH) domain (amino acids 570-689) is functional in the interactions of the Atx1 protein either with itself or with the most of the Atx1 interactors (Chen et al. 2004; Goold et al. 2007; Zoghbi and Orr 2009). Furthermore, the **n**uclear **l**ocalization **s**ignal (NLS) (amino acids 771-776) is the responsible signal for Atx1 translocation into the nucleus. The C-terminal residue of the NLS contains serine residue (Ser^{776}) which can be phosphorylated by the kinases (Klement et al. 1998; Zoghbi and Orr 2009) (Fig. 1.2). The function of the human Atx1 protein is not fully understood so far (Nethisinghe et al. 2018). However, it has been shown that Atx1 is involved in motor coordination, cognitive function and β-**a**myloid **p**recursor **p**rotein (APP) processing (Matilla et al. 1998; Crespo-Barreto et al. 2010; Zhang et al. 2010). It plays a role in transcriptional regulation and RNA metabolism (Matilla-Dueñas et al. 2008). Atx1 is also required for remodeling of extracellular matrix through forming a transcriptional repression complex with the transcriptional repressor Capicua (Lee et al. 2011).

Figure 1.2 Human Ataxin-1 protein

Structural and functional domains of Atx1 protein. AXH, NLS and aa stand for Ataxin-1 and HMG-box protein 1, nuclear localization signal and amino acids, respectively. Modified from (Chen et al. 2004; Chiara et al. 2009; Rocha et al. 2019; Zoghbi and Orr 2009).

Formerly, some highly-informative studies have been accomplished to reveal causal mechanisms of the SCA1 pathology. However, the knowledge of the cellular and molecular mechanisms underlying SCA1-mediated neurodegeneration is still incomplete. Thus, no treatment is existent for SCA1 disease, and cure is limited to symptom amelioration. SCA1 disease is characterized by the presence of large inclusion bodies of the mutant polyQ Atx1 in the nuclei of affected neurons (Zoghbi and Orr 2009). These protein aggregates play a

significant role in the polyQ-caused pathogenesis (Taroni and DiDonato 2004). Moreover, the abnormal polyQ expansion in the Atx1 protein induces its pathogenesis by altering the interactions of Atx1 with its interactor proteins (Nethisinghe et al. 2018). Thus, both protein aggregation as well as abnormal protein interactions are the polyQ-mediated pathogenic pathways in SCA1 that finally lead to the cytotoxicity and cell death (Kang and Hong 2009) (Fig. 1.3).

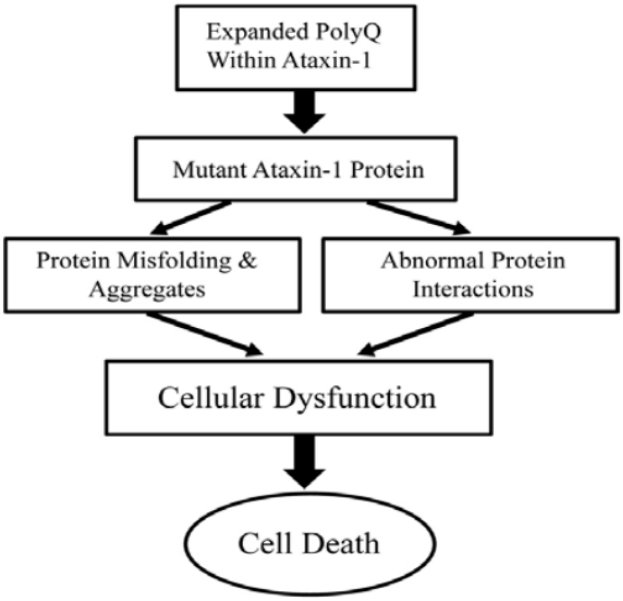

Figure 1.3 Schematic model of SCA1 pathology

The pathogenic pathways leading to cytotoxicity in SCA1 are protein aggregation and abnormal protein interactions (Kang and Hong 2009).

Wild-type Atx1 is present in the cell in two large protein complexes at least. In the first complex, Atx1 is bound to the transcriptional repressor **C**ap**ic**ua (CIC) and it is not phosphorylated at Ser^{776} phosphorylation site. In the other complex, Atx1 is bound to the RNA splicing regulator m**R**NA-**b**inding **m**otif protein **17** (RBM17) and phosphorylated at Ser^{776} site (Fig. 1.4A). However, in case of the mutant Atx1 with abnormally-expanded polyQ tract, an imbalance of the two complexes occurs in which less Atx1 is bound to CIC and more Atx1 is associated with RBM17 (Fig. 1.4B). Both the expansion of the polyQ tract and the phosphorylation of Ser^{776} increase the interaction of Atx1 with RBM17 (Zoghbi and Orr 2009). Consequently, it is suggested that SCA1 pathogenesis is caused by both a gain-of-function mechanism and a loss-of-function mechanism. Additionally, it was also reported that

the entire loss of Atx1 did not induce SCA1 pathogenesis (Matilla et al. 1998). Taken together, it may be that the core reason of SCA1 pathogenesis is a gain-of-function mechanism and that the partial loss-of function mechanism is a minor cause (Zoghbi and Orr 2009).

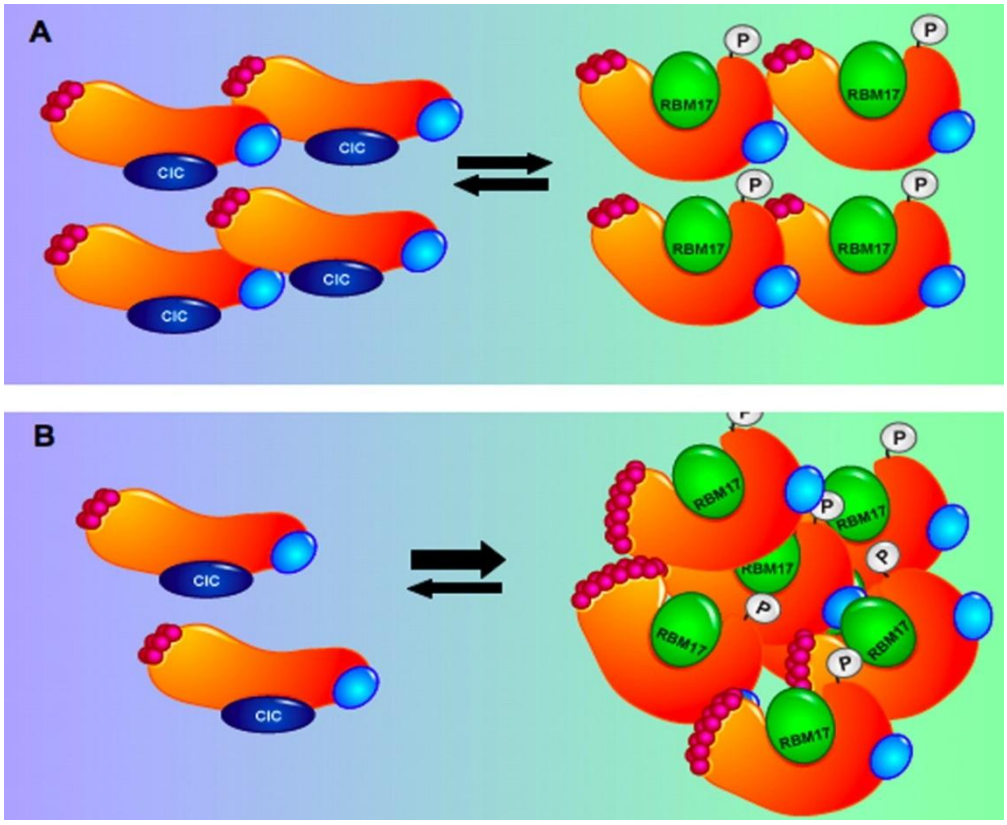

Figure 1.4 Illustration of the abnormal protein interactions in SCA1

The abnormal expansion of the polyQ tract alters the balance of Atx1 protein complexes:

(A) Wild-type Atx1 is either bound to the transcriptional repressor Capicua (CIC) and not phosphorylated at Ser^{776} site, or bound to the RNA splicing regulator mRNA-binding motif protein 17 (RBM17) and phosphorylated at Ser^{776} site.

(B) Mutant Atx1 with abnormally-expanded polyQ tract shows imbalance in protein interactions with less Atx1 bound to CIC and more Atx1 associated with RBM17.

The orange shape represents Atx1 protein and the violet circles represent glutamine residues (Zoghbi and Orr 2009).

Interestingly, pathology of the mutant Atx1 protein does not depend only on the abnormally-expanded polyQ tract in the N-terminal region of the protein, but also on some domains in the C-terminal region. These domains are needed for the toxicity of the protein. First of all, the

Atx1 AXH domain is crucial for its interactions with transcriptional factors (Kim et al. 2013). These interactions are affected in case of the mutant Atx1 resulting in cytotoxicity. Furthermore, NLS which triggers Atx1 translocation into the nucleus plays an important role in the pathogenesis of the mutant Atx1 as it was proven in previous studies that the mutant Atx1 induces its toxicity in the nuclei of the affected cell, where it interacts with the transcription and RNA processing regulators (Nóbrega and Pereira de Almeida 2018). This was confirmed when the human mutant Atx1[82Q] protein with a non-functional NLS was expressed in mice as these animals did not show SCA1 pathology (Klement et al. 1998).

1.2 Genetic modeling of the SCA1 disease

The current knowledge about cellular and molecular mechanisms underlying SCA1 pathology is basically derived from modeling this disease in mouse, fruit fly and cell culture, taking advantage of the specific benefits of these models. For instance, transgenic mouse models have been an influential tool to understand molecular mechanisms of PC cytotoxicity and neurodegeneration as well as the subsequent behavioral deficits in the SCA1-affected mice, with the observed phenotypes mimicking those of SCA1 human patients (Burright et al. 1995; Emamian et al. 2003; Tsuda et al. 2005). After identification of the SCA1 causative gene, which is *ataxin-1* (Zoghbi et al. 1991; Ranum et al. 1991), and the gene's mutation involved in the protein's dysfunction, which is abnormal expansion of CAG repeats coding for the polyQ tract in the Ataxin-1 protein (Orr et al. 1993), the first SCA1 animal model was established by generating a stable transgenic mouse model of neurodegeneration.

Referring to the first SCA1 animal model, the human mutant *Atx1[82Q]* gene with an expanded polyQ tract was expressed in mice PCs under the control of the PC-specific *pcp2* promoter. In addition, Burright and coworkers (1995) established control transgenic mice expressing the human non-pathogenic *Atx1[30Q]* gene with a polyQ sequence of normal length (Burright et al. 1995). It was reported that the human pathogenic gene with abnormally-expanded sequence of CAG repeats could induce PC neurodegeneration (Fig. 1.5) and ataxia in mice when expressed in their PCs. However, expression of the human non-pathogenic gene *Atx1[30Q]* in mice PCs did not produce neither PC degeneration nor ataxic phenotype in the transgenic mice. In conclusion, it was demonstrated that this established SCA1 mouse model expressing human SCA1 gene offers an *in vivo* model for studying the cellular and molecular disease mechanisms as well as testing potential therapeutic approaches for ameliorating such an untreatable neurological disorder (Burright et al. 1995).

Control mouse Purkinje cells **SCA1 mouse Purkinje cells**

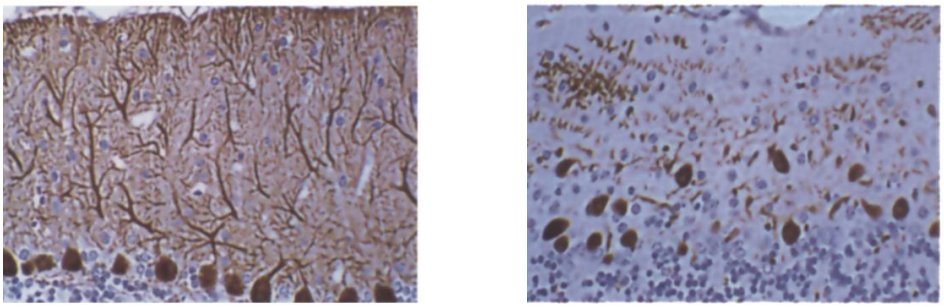

Figure 1.5 Purkinje cell morphology in unaffected control mouse (left) and transgenic mouse model of SCA1 (right)

Immunohistochemical antibody staining against calbindin (PC marker) in brain sections from 17-week-old mice reveals neurodegeneration of PCs and disorganized PC layer in the SCA1-affected mice (right) compared with the typical appearance of cerebellar cortex in the healthy control mice (left) (Burright et al. 1995).

Afterwards, further trials to model SCA1 disease in experimental animals were performed aiming at obtaining a more precise simulation of the human disease. For example, Watase and coworkers (2002) argued that the previously-established SCA1 mouse model (Burright et al. 1995) displayed only a phenotype related to the deficiency of Purkinje neurons and lives a normal lifespan. In their point of view, this model expressing the human mutant *Atx1[82Q]* gene in PCs is different from SCA1-affected human patients who not only show progressive impairment of motor coordination due to neurodegeneration of PCs, but also progressively develop cognitive deficits, ending up with a complex stage of the disease which leads to earlier death. Instead, it was hypothesized that introducing the human mutation into the corresponding mouse gene through a knock-in strategy would offer a more accurate model; since the gene expression from the endogenous locus should provide precise temporal and spatial expression patterns (Watase et al. 2002).

Therefore, knock-in transgenic mice carrying either 78 or 154 CAG repeats through targeting the 78Q or 154Q repeat expansion into the mouse *Sca1* locus (Lorenzetti et al. 2000) were established. The artificially-expanded 154Q repeats were used to enable inducing a robust neurodegeneration in the short lifespan of mice. On the one hand, the transgenic mice strain *Sca1[78Q]* did not display a robust phenotype, however, these mice displayed mild and late-onset behavioral alterations. On the other hand, the transgenic strain *Sca1[154Q]* successfully

mimicked several features of the human SCA1 disease, from neurodegeneration (Fig. 1.6A-D) to progressive ataxia (Fig. 1.6E) and cognitive impairment, meaning that the Q154 expanded tract was long enough to induce the desired disease phenotypes in mice just with the endogenous levels of mutated mouse *Atx1* and without the need for overexpressing human pathogenic *Atx1* allele. It was concluded that such a SCA1 mouse model offers a more reliable tool to understand the disease pathological mechanisms and to investigate promising cures (Watase et al. 2002).

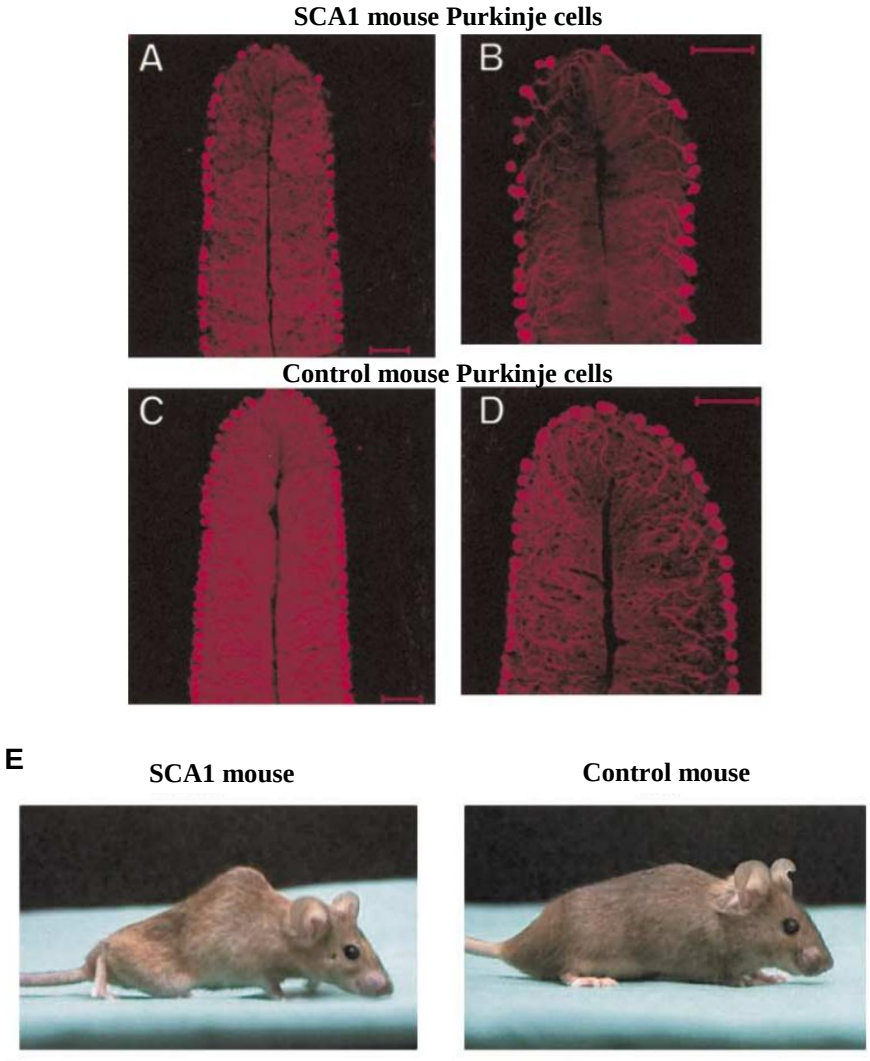

Figure 1.6 Phenotypes of a SCA1 knock-in mouse model

(A-D) Immunostaining against calbindin (PC marker) in brain sections from 34-week-old mice reveals neurodegeneration of PCs and changed cerebellar morphology in the SCA1-affected mice (A, B) compared with the control mice (C, D) to the typical appearance of cerebellar cortex in the healthy control mice. Scale bar: 100 µm.
(E) Ataxic phenotype in a SCA1-affected mouse (left) compared with a healthy control mouse (right).
Modified from (Watase et al. 2002).

Furthermore, some SCA1 mouse models were generated with certain genetic characteristics in order to investigate specific pathway/s involved in the SCA1 pathology. A clear example for this kind of modeling is the transgenic mouse expressing the mutant allele *Atx1[82Q]-A*^{776} instead of the original human mutant *Atx1[82Q]-Ser*^{776} allele (Emamian et al. 2003). In this SCA1 mouse model, the human mutant *Atx1[82Q]* allele was overexpressed in Purkinje neurons after the serine residue at the position 776 (Ser^{776}), the phosphorylation site of the Atx1 protein (see Fig. 1.2), was replaced by an alanine residue at the same position (A^{776}) to enable understanding the role of phosphorylation of Atx1 in SCA1 pathogenesis. Since the transgenic mice expressing *Atx1[82Q]-A*^{776} displayed a significantly-weaker disease phenotype with a robust decrease in the ability of the pathogenic Atx1 protein to aggregate and form inclusion bodies in the nuclei of PCs (Fig. 1.7), it was suggested that the phosphorylation site Ser^{776} of Atx1 plays a vital role in SCA1 pathology together with the abnormally-expanded polyQ tract and the targeted localization of Atx1 into the nuclei of PCs (Emamian et al. 2003).

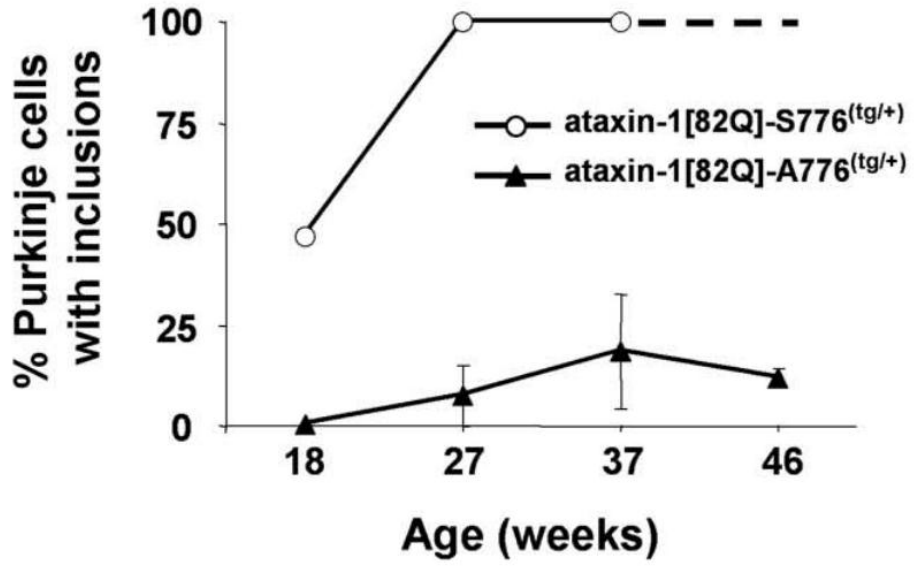

Figure 1.7 *Atx1[82Q]-A*^{776} shows a decreased rate of formation of nuclear inclusions in Purkinje cells of a transgenic mouse model of SCA1

The SCA1-affected transgenic mice expressing the human pathogenic *Atx1[82Q]-A*^{776} allele with a mutated phosphorylation site display a reduced ability of the pathogenic Atx1 protein to form nuclear inclusions in PCs compared to the SCA1-affected transgenic mice expressing the human pathogenic *Atx1[82Q]-Ser*^{776} allele with a normal phosphorylation site, demonstrating the importance of the phosphorylation of Atx1 in SCA1 toxicity (Emamian et al. 2003).

In addition to the mouse models, a *Drosophila* model for SCA1 disease was generated (Fernandez-Funez et al. 2000). In order to generate this SCA1 disease model in *Drosophila*, either the non-pathogenic *Atx1[30Q]* or the pathogenic *Atx1[82Q]* human alleles were expressed in the eye retina of transgenic flies. It was shown that not only the expression of *Atx1[82Q]*, but also the quite high expression of *Atx1[30Q]* could produce disease phenotypes. This retina degeneration model in fruit fly has provided rapid screening for genes involved in mediating Atx1Q-induced cell death (Fernandez-Funez et al. 2000; Tsuda et al. 2005). While in *Drosophila* SCA1 needs to be modeled in heterotypic cell populations due to the lack of a cerebellum in invertebrates, mice find their limitations in longitudinal *in vivo* studies for monitoring disease progression, such as *in vivo* time-lapse microscopy of dynamic cell biological processes. Therefore, a genetic model of SCA1 in cerebellar PCs of a vertebrate accessible for high resolution *in vivo* microscopy as well as behavioral and pharmacological investigations would be valuable and likely further informative.

1.3 The zebrafish cerebellum

The cerebellum, the foremost affected part by the SCA1 disease, is part of the vertebrate brain derived from the dorsal region of the anterior-most hindbrain (Hibi et al. 2017). It functions in motor control and learning, in addition to higher emotional and cognitive functions. It is important for the integration of sensory perception and motor coordination (Bae et al. 2009). The structure of its neuronal circuitry is highly conserved among vertebrates. In teleosts, nearly all cell types of the human cerebellum can be found displaying a highly-conserved morphology, connectivity and function (Hibi and Shimizu 2012; Matsui et al. 2014). However, there are a few differences between teleost and mammalian cerebellum. Mainly, the mammalian cerebellum lacks eurydendroid cells (ECs) and, in its place, the deep cerebellar nuclei (DCN) play a functionally-homologous role, as they receive the axons of PCs with inhibitory signals and send efferent axons outside the cerebellum. The DCN are located ventrally, far from PCs, whereas ECs are located in the vicinity of the PC region (Namikawa et al. 2019a). PCs of the cerebellum are among the most vulnerable neuronal populations that are affected by SCA1 cytotoxicity (Zoghbi and Orr 2009). They are GABAergic inhibitory neurons discovered by the anatomist Jan Evangelista Purkyně in 1837 (Gruol et al. 2016; Chang et al. 2020). PCs are among the brain's largest neurons and they play the key role in cerebellar computations (Purves et al. 2001; Chang et al. 2020).

The zebrafish cerebellum consists of three domains: the valvula cerebelli (Va), the corpus cerebelli (CCe) and the lobus caudalis cerebelli (LCa), from rostral to caudal. As in mammals, the Va and CCe consist of three layers: the molecular layer (ML), the Purkinje cell layer (PCL) and the granular layer (GL) (Fig. 1.8A). The zebrafish cerebellum contains different types of neurons, including PCs, ECs, granule cells (GCs), Golgi cells and stellate cells (Fig. 1.8B). The climbing fibers (CFs) are afferent fibers which project from the neurons in the inferior olivary nucleus and form synapses with PCs. The mossy fibers (MFs) are the other type of afferent fibers to the cerebellum which project from the neurons in the precerebellar nuclei and form synapses with GCs. The signals from the MFs are transported by the axons of GCs which are called parallel fibers (PFs) to the PC dendrites. In addition, stellate cells send inhibitory signals to the PC dendrites. All of these information are integrated in PCs and sent through their axons to ECs which send the output signals outside the cerebellum (Bae et al. 2009; Dohaku et al. 2019; Namikawa et al. 2019a) (Fig. 1.8B).

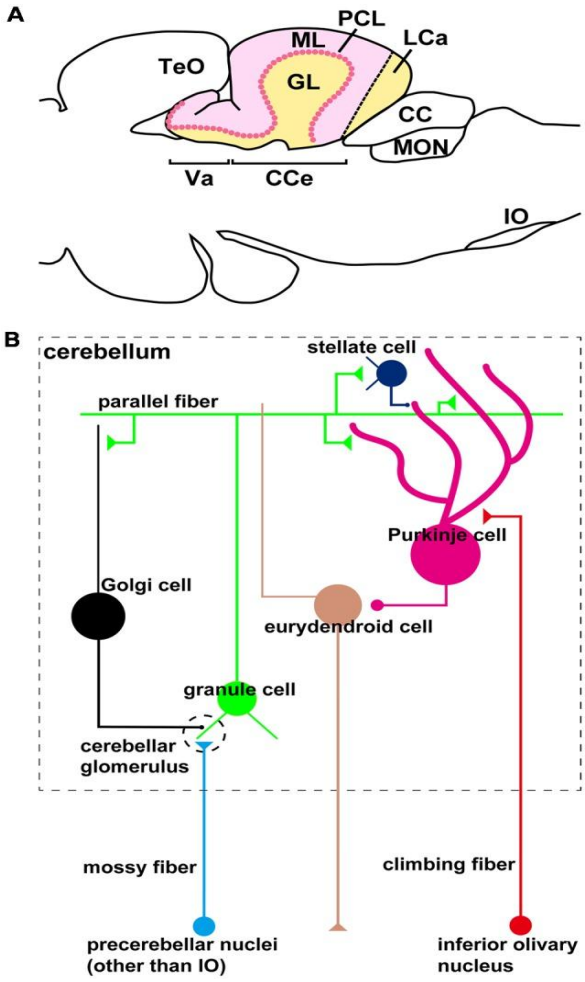

Figure 1.8 The zebrafish cerebellum

(A) Schematic Illustration of the cerebellar sagittal section. Va, CCe, LCa, ML, PCL, GL, TeO, CC, MON and IO stand for valvula cerebelli, corpus cerebelli, lobus caudalis cerebelli, molecular layer, Purkinje cell layer, and granular layer, tectum opticum, crista cerebellaris, medial octavolateralis nucleus and inferior olivary nucleus, respectively. Anterior is to the left.
(B) Schematic Illustration of the cerebellar neural circuitry.
(Dohaku et al. 2019)

1.4 Is zebrafish a promising candidate for SCA1 disease modeling?

There is a high degree of similarity between zebrafish and mammals in terms of genetics, physiology and anatomy (Zon and Peterson 2005). Recently, zebrafish represents an emerging tool for modeling complex brain diseases (Meshalkina et al. 2017) and it is speedily becoming a widespread model organism in neuropharmacology (Kalueff et al. 2014). Genetic methods in zebrafish have been rapidly expanding in the past years making zebrafish genetically tractable and allowing for the easy generation of transient and stable transgenic animals. Due to the transparency of the embryos, using zebrafish as model organism offers the unique possibility to observe cellular and subcellular mechanisms underlying differentiation and degeneration of the cells in a living vertebrate model organism (Lieschke and Currie 2007). The high fecundity of zebrafish as well as the small size and fast development of their embryos could be useful for *in vivo* drug screening and evaluation (Zon and Peterson 2005).

Since the cerebellum is highly conserved between zebrafish and human in genetics, structure and function, zebrafish offers a powerful model to study the cerebellar neuronal networks *in vivo*. The zebrafish cerebellum is unfolded and directly located underneath the skin of dorsal hindbrain which makes it optimal for *in vivo* cellular and subcellular studies (Matsui et al. 2014). Advances in imaging technologies also allow for investigating detailed cellular and molecular processes in the zebrafish brain (Schramm et al. 2021). In addition, Namikawa and colleagues (2019) could recently identify a compact enhancer element that induces expression specifically in zebrafish cerebellar PCs, the most vulnerable cells affected by SCA1. This compact regulatory element of 258 base pairs (bp), *cpce* (***c****a8* promoter-derived **PC**-specific **e**nhancer element), was isolated from upstream of the zebrafish gene *carbonic anhydrase VIII* (*ca8*) and successfully used to induce green fluorescent protein (GFP) expression in PCs of a stable transgenic zebrafish strain. Such expression is observed at 4 dpf with the early differentiation of PCs (Fig. 1.9A) and lasts until adulthood (Fig. 1.9B) (Namikawa et al. 2019b). This tool made zebrafish PCs accessible for exclusive expression of desired genes including the human SCA1-causing *Atx1[82Q]* allele and fluorescent protein reporters and biosensors.

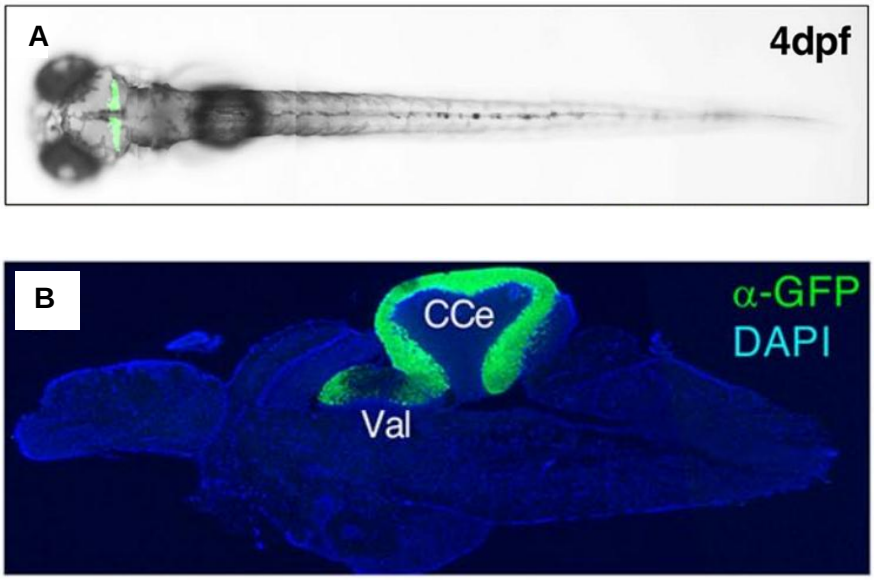

Figure 1.9 Expression pattern of PC-specific GFP under control of the regulatory element *cpce* (*ca8* promoter-derived PC-specific enhancer element) in Tg(*en.cpce-E1B:GFP*)^{bz13} stable transgenic strain

(A) The green fluorescence reveals the PC-specific expression of GFP in 4 dpf larval zebrafish.
(B) Immunohistochemical staining against GFP (green) counterstained by DAPI (blue) in a sagittal brain section reveals the PC-specific expression of GFP in adult zebrafish.
Modified from (Namikawa et al. 2019a).

Furthermore, the SCA1 protein Atx1 as well as the other cellular proteins known to be involved in the SCA1 toxicity, such as CIC and RBM17, are conserved in zebrafish (Woods et al. 2005; Carlson et al. 2009b; Chen et al. 2014; Mehjabin et al. 2019). This suggests that the pathological pathways of SCA1 can be recapitulated in zebrafish. The *Atx1* gene was investigated in zebrafish and two homologs, *Atx1a* and *Atx1b*, were identified. These zebrafish homologs encode for proteins expressed in the zebrafish cerebellum with conserved domains essential for SCA1 pathology (Carlson et al. 2009b; Vauti et al. 2020) (Fig. 1.10). Carlson and colleagues (2009) recommended that modeling of SCA1 in zebrafish can result in a useful model for studying the pathology of SCA1 as well as screening of the toxicity and bioactivity of many potential drugs before testing on large animal models. Therefore, establishment of a SCA1 zebrafish model promises to be rewarding for characterizing disease etiology and further validating compounds to inhibit disease progression.

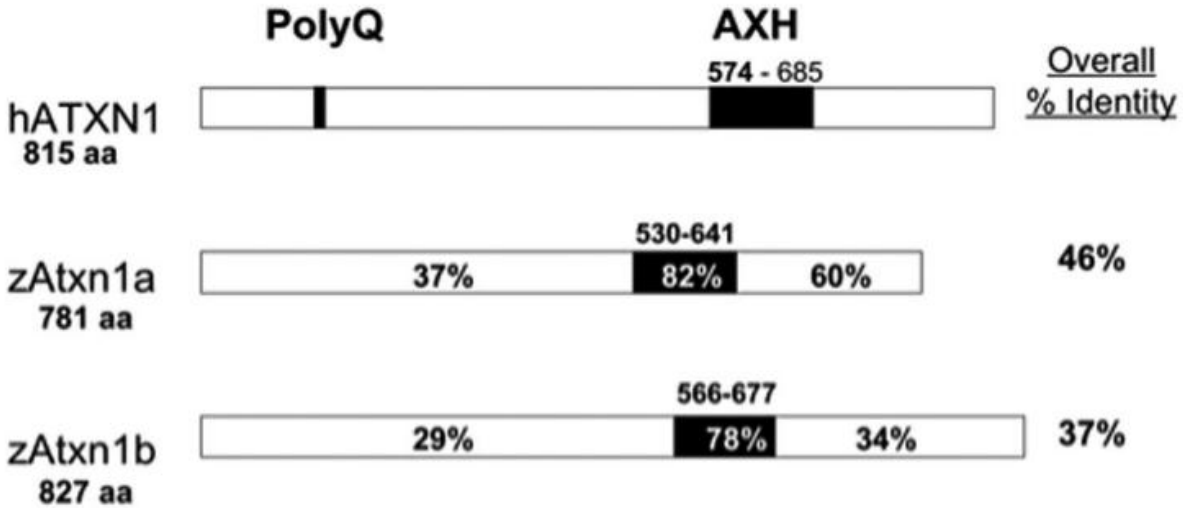

Figure 1.10 Comparison of the Ataxin-1 protein between human and zebrafish

Zebrafish expresses two Ataxin-1 homologs which show conservation with human Ataxin-1. The percentage shown on zebrafish homologs is the percentage of amino-acid identity with human Ataxin-1. There is high identity in the AXH domain (in black), the functional domain in the interactions of the Ataxin-1 protein with the most of its interactors. The total number of amino acids in each protein is shown under the protein's name (Carlson et al. 2009b).

1.5 The aim of this study

The aim of this study is to establish a stable transgenic zebrafish model for the neurodegenerative polyQ disease SCA1. Thus far, SCA1 has been *in vivo*-modelled in mouse and fruit fly, and these models have provided a deep understanding about the molecular mechanisms and cellular processes underlying mutant Atx1-induced cytotoxicity. However, such pathological mechanisms are not fully understood (Rousseaux et al. 2018; Lee et al. 2021), and there is no treatment against the SCA1 disease yet (Bondar et al. 2018; Nitschke et al. 2021). Therefore, it would definitely be of advantage if an additional model could be available allowing for monitoring and bioimaging the SCA1-induced pathological progression in PCs *in vivo*.

The accessibility of SCA1-affected PCs at zebrafish larval stages by *in vivo* bioimaging, the small size of these larvae and their aquatic environment well-suited for pharmacological treatments and behavioral analysis, as well as the previously-identified PC-specific enhancer element in zebrafish (Namikawa et al. 2019b) are important advantages. Therefore, the current study aims at inducing PC neurodegeneration in zebrafish by overexpressing the human pathogenic Atx1 protein using the characterized enhancer to generate the first transgenic zebrafish model for SCA1. This model will allow for further complementing the previously-described animal models for a deeper understanding of the cellular and molecular mechanisms of SCA1 pathology in addition to an *in vivo* evaluation of promising neuroprotective substances against neurodegeneration. The aim of the study can be accomplished through the following objectives:

1.5.1 Generation of human pathogenic Ataxin-1-expressing stable transgenic zebrafish strain

It might be feasible to generate transient transgenic Atx1[82Q]-expressing zebrafish larvae to study the SCA1 pathological mechanisms as well as to validate the effectiveness of the compounds to moderate disease progression. However, the mosaic nature of transgene expression with varying expression levels could cause difficulty to validate the speed of SCA1 disease progression and further complicating the comparison of the effectiveness of neurodegeneration inhibiting compounds. This study therefore aims to generate a stable transgenic zebrafish strain in which human Atx1[82Q] is expressed throughout the entire PC

population and inherited into the next generations. In these fish, Atx1[82Q] is expressed at comparable levels in all PCs.

1.5.2 Characterization of neurodegeneration of SCA1-affected Purkinje cells

PC degeneration in zebrafish genetic model of SCA1 is investigated in an age-dependent manner in order to answer the following questions:

- Could the human pathogenic Atx1 induce neurodegeneration of zebrafish PCs?
- How robust is this PC neurodegeneration in zebrafish?
- When does this neurodegeneration of PCs start in zebrafish?
- Does this disease model show age-related progredient disturbances of the PCL in zebrafish reminiscent of the progredient neurodegenerative SCA1 disease in human patients?

1.5.3 Assessment of physiological properties of SCA1-affected Purkinje cells

Physiological properties of PCs are assessed *in vivo* using calcium imaging. Here, some important questions need to be answered:

- Does the neuronal activity of zebrafish PCs get affected by overexpression of the human pathogenic Atx1[82Q]?
- When could PCs display these functionality abnormalities?

1.5.4 Monitoring SCA1-induced behavioral changes in SCA1 transgenic zebrafish

Although the anatomical organization and the function of the zebrafish cerebellum has been shown to be conserved (Bae et al. 2009; Matsui et al. 2014), the contribution of degenerating PCs to altered zebrafish behavior still remains to be investigated. This study aims to answer the following questions:

- Does SCA1-induced PC degeneneration result in behavioral deficits?

- Which phase of PC neurodegeneration could induce behavioral changes in SCA1 transgenic zebrafish?
- Does this zebrafish disease model display age-related progressive behavioral deficits in a direct relationship with the disturbances in PCL mimicking the progressive SCA1 disease?

2 Materials and Methods

2.1 Materials

In the subsequent subsections, the materials used to perform the experiments of this study are listed.

2.1.1 Equipment

Various devices were used in the different experiments. The technical equipment used in this study is listed in **table 2.1**.

Table 2.1 Equipment

Device	Description	Supplier
Confocal laser scanning microscope	LSM 880	Zeiss, Oberkochen, Germany
Confocal laser scanning microscope	TCS SP8	Leica Microsystems, Wetzlar, Germany
Fluorescence stereomicroscope	M205 FA	Leica Microsystems, Wetzlar, Germany
Stereomicroscope	S8 APO	Leica Microsystems, Wetzlar, Germany
Centrifuge	5415C	Eppendorf, Hamburg, Germany
Thermoshaker	Thermoshaker 5436	Eppendorf, Hamburg, Germany
Vortex	REAX2000	Heidolph, Schwabach, Germany
Rotator	LD-79	Labinco BV, Breda, the Netherlands
Incubator	B 6120	Heraeus, Hanau, Germany
Electrophoresis power Supply	EC105	Thermo Fisher Scientific, Schwerte, Germany

Gel electrophoresis chambers	40-0708	peQlab Biotechnologie GmbH, Erlangen, Germany
Spectrophotometer	DeNovix DS-11+	Biozym, Hessisch Oldendorf, Germany
Vertical pipette puller	Dki 700C	David Kopf Instruments, Tujunga, CA, USA
Microinjector	FemtoJet 4x	Eppendorf, Hamburg, Germany
Micromanipulator	MN-151	Narishige scientific instrument lab., Tokyo, Japan
Pipetboy	ACU 2	Integra Biosciences, Biebertal, Germany
Cryostat	CM3050 S	Leica Microsystems, Wetzlar, Germany
Vibratome	VT1000 S	Leica Microsystems, Wetzlar, Germany

2.1.2 Software for data acquisition and analysis

In this study, there are different types of data. In the subsequent sections, the software programs that were used for acquisition, processing and analysis of such data are listed.

2.1.2.1 Software for imaging

- ZEISS ZEN (black edition), associated with the ZEISS LSM 880 confocal microscope, Zeiss, Oberkochen, Germany.
- LAS X, Leica Microsystems, Wetzlar, Germany.
- NIS-Elements D 5.11.01, Nikon, Düsseldorf, Germany.

2.1.2.2 Software for image processing, analysis and visualization

- ZEISS ZEN (black edition), associated with ZEISS LSM 880 confocal microscope, Zeiss, Oberkochen, Germany.
- ZEISS ZEN 3.0 (blue edition), Zeiss, Oberkochen, Germany.
- LAS X, Leica Microsystems, Wetzlar, Germany.

- ImageJ 1.52c, National Institutes of Health (NIH), Bethesda, MD, USA.
- Volocity 6.3, PerkinElmer, Waltham, MA, USA.
- Imaris 9.6.0, Oxford instruments, Zurich, Switzerland.
- Adobe Illustrator CC 2018, Adobe, San José, CA, USA.

2.1.2.3 Software for animal behavior tracking and analysis

- EthoVision XT 12, Noldus, Wageningen, the Netherlands.
- VLC media player 3.0.11 Vetinari, VideoLAN, Paris, France.

2.1.2.4 Software for data analysis and visualization

- GraphPad Prism 9, Insightful Science, San Diego, CA, USA.
- SnapGene 5, Insightful Science, San Diego, CA, USA.
- Microsoft Office 2016, Microsoft, Redmond, WA, USA.

2.1.3 Bacterial strain for transformation

Escherichia coli bacterial strain XL1-Blue (Bullock et al. 1987) with ampicillin selection was used as competent cells for high efficiency transformation and amplification of target plasmids DNA.

2.1.4 Chemicals

The chemicals used in this study are listed in **table 2.2**.

Table 2.2 Chemicals

Chemical	Supplier
Tricaine	Sigma-Aldrich, Taufkirchen, Germany
Mivacurium chloride[12]	Santa Cruz Biotechnology, Dallas, TX, USA
Paraformaldehyde (PFA)	Carl Roth, Karlsruhe, Germany
HPLC water	Carl Roth, Karlsruhe, Germany

6x Gel loading dye Purple	New England Biolabs, Frankfurt am Main, Germany
1kb DNA ladder	New England Biolabs, Frankfurt am Main, Germany
Phenol red solution 0.5%	Sigma-Aldrich, Taufkirchen, Germany
N-Phenylthiourea (PTU)	Sigma-Aldrich, Taufkirchen, Germany
Normal goat serum (NGS)	Vector laboratories, Burlingame, CA, USA
Triton X-100	Sigma-Aldrich, Taufkirchen, Germany
Sodium chloride (NaCl)	Sigma-Aldrich, Taufkirchen, Germany
Magnesium sulfate ($MgSO_4$)	Carl Roth, Karlsruhe, Germany
Dithiothreitol (DTT) 100 mM	Promega, Walldorf, Germany
RiboLock RNase Inhibitor	Thermo Fisher Scientific, Schwerte, Germany
Ethanol (EtOH)	Sigma-Aldrich, Taufkirchen, Germany
Methanol (MeOH)	VWR International, Darmstadt, Germany
Mayer's Hematoxylin solution	Sigma-Aldrich, Taufkirchen, Germany
Eosin solution	Sigma-Aldrich, Taufkirchen, Germany
Entellan mounting medium	Sigma-Aldrich, Taufkirchen, Germany
Fluoro-Gel	Electron Microscopy Sciences, Hatfield, PA, USA

2.1.5 Enzymes

The enzymes used in the biotechnology methods and cloning procedures in this study are listed in **table 2.3**.

Table 2.3 Enzymes

Enzyme	Supplier
Restriction endonucleases	New England Biolabs, Frankfurt am Main, Germany
T4 Ligase	Thermo Fisher Scientific, Schwerte, Germany
Klenow	New England Biolabs, Frankfurt am Main, Germany
Phusion DNA Polymerase	Thermo Fisher Scientific, Schwerte, Germany
DNase I (RNase-free)	Thermo Fisher Scientific, Schwerte, Germany
T3 RNA Polymerase	Promega, Walldorf, Germany
T7 RNA Polymerase	Promega, Walldorf, Germany
Sp6 RNA Polymerase	Promega, Walldorf, Germany

2.1.6 Antibodies

The antibodies used for immunohistochemistry in this study are listed in **table 2.4**.

Table 2.4 Antibodies

Antibody	Host	Antigen	Dilution	Supplier	ID
Anti-HA	Rat	HA-tag	1:1000	Chromotek, Planegg, Germany	#7C9
Anti-ZebrinII	Mouse	Aldolase C	1:500	Prof. R. Hawkes (Brochu et al. 1990)	
Alexa Fluor 488	Goat	Mouse IgG	1:1000	Thermo Fisher Scientific, Schwerte, Germany	#A-11001

2.1.7 Solutions and media

The standard solutions for zebrafish use and care were modified from the previous studies (Kimmel et al. 1995; Matthews et al. 2002). Moreover, the standard laboratory buffers were prepared as described in the previous studies (Sambrook and Russell 2001).

2.1.7.1 Fish-related solutions

The fish-related solutions used in this study are listed in **table 2.5**.

Table 2.5 Fish-related solutions

Solution	Ingredients
30% Danieau medium	0.12 mM $MgSO_4$ 0.18 mM $Ca(NO_3)_2$ 0.21 mM KCl 1.5 mM HEPES (pH 7.2) 17.4 mM NaCl The medium was filled up to 1 liter with ddH_2O
0.3% *N*-Phenylthiourea (PTU) stock solution	1.2 g PTU 400 ml 30% Danieau medium
Anti-pigmentation medium: 0.003% PTU/Danieau medium	10 ml 0.3% PTU 990 ml 30% Danieau medium
Egg water	0.04 g/l Sea salt in ddH_2O
Tris buffer (1 M, pH 9.5)	121.14 g Tris(hydroxymethyl)aminomethane was filled up to 1 liter with ddH_2O The pH was adjusted to 9.5
0.2% Tricaine stock solution	200 mg Tricaine powder 97.9 ml ddH_2O The pH was adjusted to ~7 with Tris (1 M, pH 9.5)
0.04% Tricaine for anaesthesia	0.04% Tricaine in 30% Danieau medium (v/v)

PBS	10 mM Na_2HPO_4 2 mM KH_2PO_4 137 mM NaCl 2.7 mM KCl The pH was adjusted to 7.4

2.1.7.2 Cloning solutions

The cloning solutions used in this study are listed in **table 2.6**.

Table 2.6 Cloning solutions

Solution	Ingredients
LB-Medium	10 g Bacto-tryptone 5 g Yeast extract 10 g NaCl 1 Liter ddH_2O The pH was adjusted to 7.4
LB-Agar	10 g Bacto-tryptone 5 g Yeast Extract 10 g NaCl 15 g Agar 1 Liter ddH_2O

2.1.7.3 Histological-staining buffers

The solutions used for Hematoxylin-Eosin staining and immunohistochemical staining in this study are listed in **table 2.7**.

Table 2.7 Fixation and staining buffers

Solution	Ingredients
20% Triton stock solution	10 ml Triton X-100 The detergent solution was filled up to 50 ml with ddH_2O
PBST (Phosphate-buffered saline with Triton)	0.3% Triton in 1x Phosphate-buffered saline (PBS) (v/v)
4% PFA	40 g Paraformaldehyde (PFA) 1 Liter ddH_2O The pH was adjusted to 7.2
Fixation buffer	4% PFA in PBST (v/v)
PBST DMSO	1% Dimethyl Sulfoxide (DMSO) in PBST (v/v)
NGS Blocking buffer	10% NGS (Normal Goat Serum) in PBST DMSO (v/v)

2.1.8 Kits and reagents for high-affinity purification

The kits used in this study for high-affinity extraction and purification of nucleic acids are listed in **table 2.8**.

Table 2.8 Purification kits

Kit	Supplier
FastGene Gel/PCR Extraction Kit	NIPPON Genetics EUROPE, Düren, Germany
RNeasy Mini Kit 250	QIAGEN, Hilden, Germany
RNeasy Midi Kit 50	QIAGEN, Hilden, Germany

2.1.9 Oligonucleotides

It was important after each cloning step to confirm by sequencing that the number of CAG repeats in both non-pathogenic *Atx1[30Q]* and mutant *Atx1[82Q]* human alleles were kept the

same during the cloning procedures in the successive cloning steps. In addition, it was important before injection to confirm by sequencing that *Atx1[30Q]* and *Atx1[82Q]* were N-terminally fused to an HA-tag for immunohistochemical detection. The Oligonucleotides used for these purposes are listed in **table 2.9**.

Table 2.9 Oligonucleotides

Oligonucleotide	Sequence	Stock no.
Human Atx1, upstream PolyQ, for for sequencing of the polyQ sequence in human *Atx1*	5' TCCCAGCTGGAGGCCTATTC 3'	#3472
Human Atx1, downstream PolyQ, rev for sequencing of the polyQ sequence in human *Atx1*	5' GTATTGCATGACGACCTGGGA 3'	#3473
Human Atx1, N-terminus, rev for sequencing of the HA-tag sequence	5' TCGGAGGACCGGCTGGTGGC 3'	#1674

2.1.10 Plasmid vectors for microinjection

pA-4xmir181aT-GAPmScarlet-E1b-8×ca8-E1b-4xmir181aT-pA **(Stock no. #5158)**

This vector drives overexpression of the membrane-targeted red fluorescent reporter *GAPmScarlet* in the cell membranes of zebrafish Purkinje neurons. GAP is a membrane-targeting signal isolated from the amino terminus of the zebrafish neuronal protein **G**rowth **A**ssociated **P**rotein 43 (GAP-43) ((Zuber et al. 1989). mScarlet is a bright red fluorescent protein that demonstrates high performance in cellular microscopy (Bindels et al. 2017). The PC-specific expression occurs under control of the 258-bp enhancer element *cpce* isolated from upstream of the zebrafish gene *ca8*. Adding 2x4 copies of the enhancer element *cpce* in opposite orientation and flanking it on both sides with *E1b* basal promoter, multiple cloning site, 4 copies of *miRNA181a*T (*mir181aT*) target fragment and *SV40 polyadenine* (*pA*) sequence mediates robust PC-specific expression of two different transgene cassettes (Namikawa et al. 2019b). However, there is only one transgene cassette, *GAPmScarlet,*

expressed in this vector. In addition, the both sides are flanked by Tol1 transposon recognition sites (Koga et al. 2008).

pA-4xmir181aT-GAPmScarlet-E1b-8×ca8-E1b-HA:Atx1[30Q]-4xmir181aT-pA **(Stock no. #3417)**

This vector drives overexpression of the human non-pathogenic allele *Atx1[30Q]* in the nuclei of zebrafish Purkinje neurons in addition to the membrane-targeted red fluorescent reporter *GAPmScarlet* in the cell membranes of Purkinje neurons. The human non-pathogenic allele *Atx1[30Q]* is N-terminally tagged with an HA-tag for the staining purposes. The PC-specific expression occurs under control of the 258-bp enhancer element *cpce* isolated from upstream of the zebrafish gene *ca8*. Adding 2x4 copies of the enhancer element *cpce* in opposite orientation and flanking it on both sides with *E1b* basal promoter, multiple cloning site, 4 copies of *mir181aT* target fragment and *SV40 pA* sequence mediates robust PC-specific expression of two different transgene cassettes, *GAPmScarlet* and *Atx1[30Q]* (Namikawa et al. 2019b). In addition, the both sides are flanked by Tol1 transposon recognition sites (Koga et al. 2008).

pA-4xmir181aT-GAPmScarlet-E1b-8×ca8-E1b-HA:Atx1[82Q]-4xmir181aT-pA **(Stock no. #5187)**

This vector drives the overexpression of human pathogenic allele *Atx1[82Q]* in the nuclei of zebrafish Purkinje neurons in addition to the membrane-targeted red fluorescent reporter *GAPmScarlet* in the cell membranes of Purkinje neurons. The human pathogenic allele *Atx1[82Q]* is N-terminally tagged with an HA-tag for the staining purposes. The PC-specific expression occurs under control of the 258-bp enhancer element *cpce* isolated from upstream of the zebrafish gene *ca8*. Adding 2x4 copies of the enhancer element *cpce* in opposite orientation and flanking it on both sides with *E1b* basal promoter, multiple cloning site, 4 copies of *mir181aT* target fragment and *SV40 pA* sequence mediates robust PC-specific expression of two different transgene cassettes, *GAPmScarlet* and *Atx1[82Q]* (Namikawa et al. 2019b). In addition, the both sides are flanked by Tol1 transposon recognition sites (Koga et al. 2008).

2.1.11 Zebrafish strains

2.1.11.1 Wild-type zebrafish

Zebrafish of the *brass* strain, a reduced melanin mutant strain (Gross and Perkins 2008), was used as wild-type fish in this study. This strain has less pigmentation on the body surface caused by melanocyte deficiency, which affects the melanin synthesis. Therefore, embryos and early larvae of this line are easily-accessible for observing the fluorescent proteins by fluorescence microscopy.

2.1.11.2 Transgenic lines

The following stable transgenic lines were generated by microinjection of the desired DNA construct into the cytoplasm of one cell stage embryos of the *brass* strain:

Tg: *GAPmScarlet-8×ca8*

This transgenic line was generated by microinjection of a DNA construct expressing the membrane-targeted red fluorescent reporter *GAPmScarlet* under control of the PC-specific enhancer element *cpce* isolated from upstream of the zebrafish gene *ca8* (Namikawa et al. 2019b). GAP is a membrane-targeting signal isolated from the amino terminus of the neuronal protein **G**rowth **A**ssociated **P**rotein 43 (GAP-43) ((Zuber et al. 1989).

This line was generated to overexpress the membrane red fluorescent protein GAPmScarlet in specific neuronal cell type (PCs) to monitor the morphology of Purkinje neurons and to quantify the area of their population at different ages. The stock number of plasmid vector injected to generate this transgenic line is #5158.

Tg: *GAPmScarlet-8×ca8-HA:Atx1[30Q]*

This transgenic line was generated by microinjection of a bidirectional DNA construct expressing the human non-pathogenic allele *Atx1[30Q]* together with the membrane-targeted red fluorescent reporter *GAPmScarlet* under control of the PC-specific enhancer element *cpce* isolated from upstream of the zebrafish gene *ca8* (Namikawa et al. 2019b). The HA-tag was fused to the N-terminus of the Atx1[30Q] protein.

This line was generated to overexpress the human non-pathogenic full-length gene *Atx1[30Q]* in a specific neuronal cell type (PCs) that is the most vulnerable one affected by the SCA1 disease. In addition, the red fluorescent protein GAPmScarlet was coexpressed to monitor the morphology of Purkinje neurons and to quantify the area of their population at different ages. The HA-tag was used for the immunostaining of the protein. The stock number of plasmid vector injected to generate this transgenic line is #3417.

Tg: *GAPmScarlet-8×ca8-HA:Atx1[82Q]*

This transgenic line was generated by microinjection of a bidirectional DNA construct expressing the human SCA1-causing pathogenic allele *Atx1[82Q]* together with the membrane-targeted red fluorescent reporter *GAPmScarlet* under control of the PC-specific enhancer element *cpce* isolated from upstream of the zebrafish gene *ca8* (Namikawa et al. 2019b). The HA-tag was fused to the N-terminus of the Atx1[82Q] protein.

This line was generated to overexpress the human mutant full-length gene *Atx1[82Q]* in a specific neuronal cell type (PCs) that is the most vulnerable population affected by the SCA1 disease. In addition, a membrane red fluorescent protein GAPmScarlet was coexpressed to monitor the morphology of Purkinje neurons and to quantify the area of their population at different ages. The HA-tag was used for the immunostaining of the protein. The stock number of plasmid vector injected to generate this transgenic line is #5187.

Tg: (*-7.5ca8:GFP*)^{bz12}

The zebrafish of this transgenic strain express a green fluorescent protein exclusively in PCs under control of the *ca8* promoter-derived PC-specific enhancer element *cpce* (Namikawa et al. 2019b; Chang et al. 2020). This transgenic line was crossed with the control, *Atx1[30Q]* and *Atx1[82Q]* transgenic lines to establish double transgenic zebrafish expressing the reporter protein GFP together with GAPmScarlet only, Atx1[30Q] or Atx1[82Q] specifically in PCs. This experiment was used to reveal whether the transgene expression in the control, *Atx1[30Q]* and *Atx1[82Q]* established strains was confined to the PC population.

Tg: (*2xcpce-E1b:KALNFB, he1.1:mTagBFP2*)^{bz14} X (*14xUAS:GCaMP6s*)^{mpn101}

The carriers of Tg(*2xcpce-E1b:KALNFB, he1.1:mTagBFP2*)^{bz14} and Tg(*14xUAS:GCaMP6s*)^{mpn101} are expressing the genetically-encoded Ca^{2+} indicator GCaMP6s, with the calcium-binding protein calmodulin (CaM) and the reporter protein GFP

(Chen et al. 2013), specifically in PCs under control of Gal4/UAS system mediated by the Gal4 variant, KALNFB (Namikawa et al. 2019b). This transgenic line was crossed with the control, *Atx1[30Q]* and *Atx1[82Q]* transgenic lines to establish triple transgenic zebrafish expressing Ca^{2+} indicator GCaMP6s together with GAPmScarlet only, Atx1[30Q] or Atx1[82Q] specifically in PCs. This experiment was used to compare the physiological properties of zebrafish PCs between the control, *Atx1[30Q]* and *Atx1[82Q]* transgenic strains.

2.2 Methods

2.2.1 Biotechnology methods and cloning procedures

Three plasmids DNA were constructed expressing the membrane-targeted red fluorescent reporter *GAPmScarlet* only (control), or together with the human non-pathogenic allele *Atx1[30Q]* or the human SCA1-causing mutant *Atx1[82Q]* in bidirectional vectors. GAP is a membrane-targeting signal isolated from the N-terminus of the zebrafish neuronal protein Growth Associated Protein 43 ((Zuber et al. 1989). mScarlet is a bright red fluorescent protein which shows great performance in cellular imaging (Bindels et al. 2017). Both human alleles *Atx1[30Q]* and *Atx1[82Q]* were N-terminally fused to an HA-tag for immunohistochemical detection. The bidirectional expression occurs under control of the 258-bp regulatory element *cpce* (*ca8* promoter-derived PC-specific enhancer element). This small genomic element is isolated from upstream of the zebrafish gene *carbonic anhydrase VIII* (*ca8*) and is able to specifically drive expression in zebrafish PCs starting at their time point of differentiation at 2.5 dpf (Namikawa et al. 2019b). Adding 2x4 copies of the enhancer element *cpce* in opposite orientation and flanking it on both sides with *E1b* basal promoter (Huang et al. 2006), multiple cloning site, 4 copies of *miRNA181aT* target fragment and *SV40 polyadenine* sequence mediates robust PC-specific expression of two different transgene cassettes (Namikawa et al. 2019b). In addition, the both sides are flanked by Tol1 transposon recognition sites (Koga et al. 2008). The biotechnology methods and cloning procedures for constructing these plasmids DNA were as follows:

2.2.1.1 DNA digestion

Digestion solutions were prepared according to the following protocol:

Vector solution: 1 µl of the plasmid DNA (1 µg/µl) + 1 µl per restriction enzyme + 3 µl 10x buffer + HPLC water to a total volume of 30 µl.

Insert solution: 2 µl of the plasmid DNA (1 µg/µl) + 1 µl per restriction enzyme + 3 µl 10x buffer + HPLC water to a total volume of 30 µl.

Both solutions were incubated at 37 °C for at least 1 hour.

The solutions were electrophoresed on 1% agarose/TAE gel and stained with ethidium bromide for at least 10 minutes. The required bands were cut out from the gel and transferred into a 1.5-ml reaction tube.

2.2.1.2 DNA Purification

Vector and insert DNA were purified out of the gel using gel extraction kit according to the following protocol:

500 µl PN buffer was added to each gel slice in both reaction tubes.

Gel was dissolved on a thermoshaker at 55 °C and maximum speed for at least 5 minutes.

The mixture was then added (max. 800 µl) onto a purification column (FastGene Gel/PCR Extraction Kit, NIPPON Genetics EUROPE).

It was centrifuged at 8,000 rpm for 10 - 15 seconds.

Flow-through was thrown away.

600 µl PE buffer was added onto the column.

The column was afterwards centrifuged at 8,000 rpm for 10 - 15 seconds.

Subsequently, it was placed in a new collection tube.

The column was dried by centrifugation at maximum speed for 2.5 minutes.

It was placed in a new 1.5-ml reaction tube.

25 µl sterile water was pipetted directly to the column membrane (without touching it).

It was then centrifuged at maximum speed for 1 minute.

2.2.1.3 DNA Ligation

Digested and purified DNA of both vector and insert was used for ligation according to the following protocol:

2 µl vector solution + 6 µl insert vector solution were mixed.

1.5 µl T4-ligase buffer was added to the mixture.

0.5 µl T4-ligase was added.

5 µl HPLC water was also added.

The ligation mix was then incubated at room temperature for 20 minutes.

It was cooled down on ice before starting the transformation.

2.2.1.4 Plasmid transformation

Transformation is the process by which the competent bacterial cells uptake and express the exogenous plasmid DNA using the following protocol:

Competent bacteria which usually kept at -80 °C were thawed on ice.

50 µl of bacterial solution was added to the ligation mix and they were mixed by pipetting.

The mixture was incubated on ice for 15 - 30 minutes.

It was heat shocked at 42 °C (water bath) for 45 seconds to induce bacterial uptake of the plasmid DNA.

It was then cooled down on ice for 2 - 3 minutes.

300 µl Luria Bertani (LB) medium (without any antibiotic) was added.

The mixture was incubated on a thermoshaker at 37 °C and 900 - 1000 rpm for 15 minutes to 1 hour.

It was afterwards centrifuged for 1 minute at maximum speed.

300 µl of the supernatant were thrown away for condensing the bacteria.

The bacterial pellet was resuspended in the remaining supernatant and spread well onto a selection agar plate containing the right antibiotic.

The plate was incubated overnight at 37 °C until the suitable size of bacterial colonies appeared.

2.2.1.5 Small-scale DNA preparation from bacteria (Mini Prep)

For analysing the bacterial colonies prepared with cloning procedures, isolation of small-scale plasmid DNA from bacteria was performed according to the following protocol:

Some selected bacterial colonies were inoculated separately in 2 ml LB-medium containing the selective antibiotic.

They were incubated in a shaker overnight (~ 16 hours) at 37 °C and 180 rpm.

Each bacterial solution was transferred into a 1.5-ml reaction tube.

It was centrifuged at maximum speed for 2.5 minutes to form a bacterial pellet.

The supernatant was thrown away by using vacuum pump then a DNA isolation and purification kit (RNeasy Mini Kit 250, QIAGEN) was used in the next steps.

150 µl RNase containing resuspension buffer was used to resuspend the pellet by vortexing.

150 µl alkaline lysis buffer was added and mixed by inverting the tube.

150 µl neutralization buffer was applied and mixed by inverting the tube to coagulate denatured proteins and precipitate the bacterial debris.

The mixture was afterwards centrifuged at maximum speed for 5 minutes.

Subsequently, the supernatant was transferred into a new 1.5-ml reaction tube.

100% ethanol was added to 1.5 ml.

The mixture was vortexed well and centrifuged at maximum speed for 5 minutes.

The supernatant was discarded and the DNA pellet was dried in room temperature.

The DNA pellet was resuspended in 50 µl ddH_2O.

For selecting the positive bacterial colonies, 2 µl of each DNA solution were mixed with 0.25 µl per restriction enzyme, 1.5 µl 10x buffer and ddH_2O to 15 µl, incubated at 37 °C for at least 30 minutes and checked for the target vector and insert bands on 1% agarose/TAE gel (electrophoresis).

2.2.1.6 Large-scale DNA preparation from bacteria (Midi Prep)

In order to get a large amount of the required plasmid DNA, the target DNA from a positive bacterial colony was amplified, isolated and purified according to the following protocol:

The selected bacterial colony was cultured in 100 ml LB-medium containing the selective antibiotic.

It was incubated in a shaker overnight (~ 16 hours) at 37 °C and 180 rpm.

The bacterial solution was transferred into two 50-ml Falcon tubes.

The solution was centrifuged at 4 °C and 4500 rpm for 10 minutes to form a bacterial pellet.

The supernatant was discarded and a DNA isolation and purification kit (RNeasy Midi Kit 50, QIAGEN) was used in the next steps.

8 ml RNase containing resuspension buffer was used to resuspend the pellet by vortexing.

8 ml alkaline lysis buffer was added and mixed by inverting the tube.

The solution was incubated at room temperature for 3 minutes.

During lysis buffer treatment, the purification column was equilibrated by washing with 12 ml equilibration buffer.

8 ml neutralization buffer was applied and mixed well by inverting the tube to coagulate denatured proteins and precipitate the bacterial debris.

The mixture was loaded onto the column.

After the whole cell lysate ran through, the column was washed with 5 ml equilibration buffer.

Subsequently, the column's filter was removed and the column's membrane was washed with 8 ml washing buffer.

DNA was eluted from the membrane by 5 ml elution buffer and collected in a 50-ml Falcon tube.

3.5 ml isopropanol was added and mixed by vortexing.

The mixture was centrifuged at 4 °C and 5000 rpm for 30 minutes and the supernatant was then discarded.

The DNA pellet was transferred using 500 µl 70% ethanol into a 1.5-ml reaction tube and centrifuged at maximum speed for 5 minutes.

The supernatant was completely thrown away with a pipette and the pellet was dried in room temperature for 5 minutes.

The DNA pellet containing the target plasmid DNA was resuspended well in 200 µl HPLC water.

The concentration of DNA was measured by a spectrophotometer (DeNovix DS-11+, Biozym).

The DNA solution was diluted with HPLC water to the concentration of 1 µg/µl and stored in -20 °C.

2.2.1.7 Tol1 mRNA synthesis

mRNA encoding for the transposon Tol1 was prepared according to the following protocol:

12 µg plasmid DNA template for Tol1 mRNA synthesis was digested with 2.5 µl appropriate restriction enzyme for 2 hours at 37 °C in HPLC water added to a total volume of 30 µl.

1 µl linearized plasmid DNA solution was checked by gel electrophoresis to confirm that DNA was completely restricted.

DNA was purified with a purification column (FastGene Gel/PCR Extraction Kit, NIPPON Genetics EUROPE) and eluted by 30 µl RNase-free water in a special RNase-free tube.

The concentration of DNA was measured by a spectrophotometer (DeNovix DS-11+, Biozym).

The mixture of mRNA synthesis reaction was then prepared in a special RNase-free tube at -20 °C:
Linearized plasmid DNA (1 µg)

10x transcription buffer (Roche) (5 µl)
NTP/Cap mixture (5 µl)
RiboLock RNase Inhibitor (Thermo Fisher Scientific) (2 µl)
Appropriate RNA polymerase (1.5 µl)
RNase-free water (up to 50 µl)

This mixture was incubated for 2 hours at 37 °C and 1.5 µl RNase-free DNase I (Roche) was then added to the mixture and the mixture was further incubated for 15 minutes at 37 °C. The synthesized mRNA was purified and eluted by 50 µl RNase-free water in a special RNase-free tube.

The concentration of mRNA was measured by a spectrophotometer (DeNovix DS-11+, Biozym) and diluted to 250 ng/µl. The solution was stored at -20 °C in a special RNase-free tube.

2.2.2 Zebrafish husbandry and maintenance

Zebrafish of the *brass* strain, a reduced melanin mutant strain (Gross and Perkins 2008), were used for performing the experiments of this study. The establishment of stable transgenic strains, the experimental procedures and the animal numbers were approved by "Niedersächsisches Landesamt für Verbraucherschutz und Lebensmittelsicherheit". The animal protocol's approval number is 33.19-42502-04-18/3013. Zebrafish maintenance and experiments were carefully performed in compliance with European accepted standards and German legislation (Directive 2010/63/EU, license AZ 325.1.53/56.1-TUBS) and according to the legal animal welfare requirements (Aleström et al. 2019). The fish were kept in an aquarium which is connected to a filtering system to ensure a high water quality. The light/dark cycle in the fish facility was set to 14 hours light and 10 hours darkness and the temperature was maintained at 28 °C. Mature fish were crossed in one-liter cages containing a fish pair overnight and the obtained embryos were collected in the following morning in petri dishes containing egg water and kept in a 28-°C incubator. After a few hours, the dead embryos were removed and the egg water was changed with 30% Danieau medium which was being changed daily. At 6 dpf, the larvae were transferred into the fish facility. For live imaging experiments and whole-mount immunohistochemistry at larval stages, the Danieau medium was supplemented with 0.003% PTU starting from 0.5 dpf to suppress pigmentation.

2.2.3 Microinjection of nucleic acids

Three injection solutions were prepared in order to generate three transgenic strains. Each solution consisted of the desired circular plasmid DNA at a concentration of 25 ng/µl, mRNA encoding the transposon Tol1 at a concentration of 25 ng/µl and phenol red at a concentration of 0.05% (1:10 of a 0.5% stock solution). The phenol red was used as a color marker to distinguish injected embryos from uninjected ones. The injection solution was freshly prepared for each injection experiment. In order to establish each transgenic strain, microinjection of the relevant prepared solution was performed into the cytoplasm of the one cell stage embryos. A glass microcapillary was pulled with a vertical pipette puller (Dki 700C) to be used as a sharp-tipped injection needle. Few microliters of the solution were filled into the needle which was then fixed on a micromanipulator (MN-151). The embryos were sorted in a Petri dish inside grooves of 1.5% solidified agarose gel. They were fixed in an orientation where the cell is at the top and the yolk is at the bottom. After that, the injection was performed under a stereomicroscope (Leica S8 APO) using the micromanipulator (MN-151). The injected embryos were transferred into a 28-°C incubator.

2.2.4 Screening and generation of zebrafish stable transgenic strains

In order to obtain stable transgenic zebrafish of the F2 generation, which propagate PC-specific mScarlet, Atx1[30Q] or Atx1[82Q] expression in a Mendelian manner, the injected larvae were checked under a fluorescence stereomicroscope (Leica M205 FA) at 4 dpf after the early PC differentiation. The positive carriers which showed red fluorescence in PCs were collected and moved to the fish facility at 6 dpf in order to be raised as a P0 generation. After 3 months, the young adults were screened by crossing with wild-type fish and the offspring was checked for red fluorescence in PCs at 4 dpf. The carrier larvae were raised to obtain adult F1 generation fish. Afterwards, these adult fish were crossed with wild-type fish to get, raise and analyze F2 generation carriers.

2.2.5 Whole-mount immunohistochemistry

In order to detect the human Atx1 protein in zebrafish PCs, whole-mount immunohistochemistry on 4 dpf larval zebrafish was performed according to the following protocol modified from a previous report (Kani et al. 2010):

10-20 carrier larvae from each transgenic line were sedated in 0.05% Tricaine for 10 minutes in a 2-ml tube. The medium was then completely removed and the larvae were fixed with 1 ml cold 4% PFA/PBST in the same tube. The tube was shaken on a shaker for 3 hours at 4 °C.

The larvae were washed with 1 ml PBST for 10 minutes. They were incubated in 1 ml cold acetone for 15 minutes at -20 °C and then washed once with 1 ml PBST and twice with 1 ml PBS-DT for 10 minutes each. They were incubated in 500 µl 5% normal goat serum/PBS-DT for 1 hour at room temperature on a shaker (blocking).

The larvae were incubated in 500 µl of the primary antibody solution (1^{ry} antibody 1:1000 dilution, 1% BSA, 1% DMSO and 0.1% Triton in PBS) overnight at 4 °C on a shaker. The anti-HA antibody (Chromotek) was used as the primary antibody for detecting the HA-tagged human Atx1 protein. The larvae were then washed with 1 ml PBST six times for 10 minutes each.

They were incubated in 500 µl of the secondary antibody solution (2^{ry} antibody 1:1000 dilution, 1% BSA, 1% DMSO and 0.1% Triton in PBS) for 2 hours at room temperature on a shaker. The Alexa Fluor 488 anti-mouse IgG antibody (Thermo Fisher Scientific) was used as the secondary antibody. The larvae were then washed with 1 ml PBST six times for 10 minutes each.

The stained larvae were embedded in 1% low-melting agarose/PBS inside imaging chambers with glass bottom. The fluorescent images of PCs were obtained with a confocal laser scanning microscope (ZEISS LSM 880). The images for the figures were constructed from Z-stack planes by ZEISS ZEN software (associated with ZEISS LSM 880) and processed using ImageJ 1.52c software.

2.2.6 Measuring the fish length and isolation of the brain

Firstly, 0.04% tricaine was used as an anesthetic compound to anesthetize the fish at 40 dpf, 2 mpf and 3 mpf. Then, each fish was cooled down on ice and afterwards the length of the body form the anterior tip of the jaw until the caudal indentation of the tail fin (fork length) was measured using a ruler. After that, the fish was decapitated and the head was transferred to a Petri dish with cold 1x PBS for further dissection under a stereomicroscope (Leica S8 APO). All the organs and tissues such as the gills and eyes were removed using two forceps until reaching the skull. The skull was then broken and removed carefully to not damage the brain. The brain was smoothly moved into cold 4% PFA/PBS and incubated overnight at 4 °C for fixation. In the next morning, the brain was washed with cold 1x PBS three times for 5 minutes each. The fixed brain was then ready for imaging using laser scanning confocal microscopy (ZEISS LSM 880) or for sectioning, depending on the experiment. The images were constructed from Z-stack planes by ZEISS ZEN (black edition) software (associated with ZEISS LSM 880) and processed using ImageJ 1.52c software. The figures were prepared using Adobe Illustrator CC 2018 software. For quantification, the area of the PC region was measured using Volocity 6.3 software.

2.2.7 Histology and immunostaining of the zebrafish brain

The fixed brain of adult zebrafish was cut to 70 µm-thick sagittal sections using a vibratome (Leica VT1000 S) for Hematoxylin-Eosin staining or 40 µm-thick sagittal sections using a cryostat (Leica CM3050 S) for immunohistochemistry. In terms of Hematoxylin-Eosin staining, the brain was pre-embedded in 1% low-melting agarose/PBS at 37 °C for 30 minutes. The brain was then transferred into a special embedding mold. The agarose gel was removed and the brain was embedded in 3% agarose/PBS for making the block for cutting. The orientation of the brain was quickly adjusted after adding the 3% agarose as it solidifies very fast. After this adjustment, the agarose block was left to cool down to room temperature and the cutting was then performed at a frequency of 80 Hz in the vibratome's cutting box filled with 1x PBS. The 70 µm-thick cerebellar sagittal sections were mounted on a SuperFrost glass slide (Thermo Fisher Scientific), dried at 40 °C and stained with Hematoxylin-Eosin according to the following protocol:

The glass slide with the brain sections was rinsed in tap water for 5 minutes and then in Mayer's Hematoxylin solution for 8 minutes. It was shortly rinsed 3 times in tap water and once in freshly-prepared ethanol/HCl (200 ml absolute ethanol + 6 ml 37% HCl).

The slide was washed under running tap water for 10 minutes and then rinsed in Eosin solution for 1 minute. It was rinsed shortly in 70% ethanol once, for 2 minutes in 80% ethanol twice and for 2 minutes in 96% ethanol twice.

It was then rinsed twice in xylene for 2 minutes, a drop of entellan was added on the slide using a glass rod, and a coverslip was gently put onto the slide allowing the entellan to spread and cover all the brain sections. The slide was finally dried at 37 °C and the stained sections were visualized by stereomicroscopy (Leica S8 APO).

In terms of immunohistochemistry, the fixed brain was incubated in 30% sucrose/PBS overnight at 4 °C. It was then embedded in optimal cutting temperature compound (OCT) and frozen at -80 °C. For cutting, the temperature of the cryostat (Leica CM3050 S) was adjusted at -20 °C. Cerebellar sagittal sections of 40 µm thickness were cut, mounted on a SuperFrost glass slide (Thermo Fisher Scientific), and immunostained according to the following protocol modified from a previous report (Kani et al. 2010):

The cerebellar sections were washed with PBST for 1 hour then incubated in 5% normal goat serum/PBS-DT for 1 hour at room temperature (blocking). Afterwards, the sections were incubated in the primary antibody solution (1^{ry} antibody, 1% BSA, 1% DMSO and 0.3% Triton in PBS) overnight at 4 °C. The primary antibody was either the anti-HA antibody (1:2000 dilution) for detecting the HA-tagged human Atx1 protein, or the anti-ZebrinII antibody (1:500 dilution). ZebrinII is a polypeptide antigen expressed exclusively in PCs. The anti-ZebrinII antibody stains somata, dendrites and axons of PCs (Brochu et al. 1990).

The sections were washed with PBST six times for 10 minutes each. They were the incubated in the secondary antibody solution (2^{ry} antibody 1:1000 dilution, 1% BSA, 1% DMSO and 0.3% Triton in PBS) for 2 hours at room temperature. Alexa Fluor 488 anti-mouse IgG antibody was used as the secondary antibody. The sections were then washed with PBST six times for 10 minutes each.

A coverslip was gently mounted on the glass slide using a mounting medium (Fluoro-Gel, Electron Microscopy Sciences). After drying at 37 °C, the fluorescent images of PCs were

obtained by laser scanning confocal microscopy (ZEISS LSM 880) and fluorescence stereomicroscopy (Leica M205 FA). The images for the figures were constructed from Z-stack planes and processed using ImageJ 1.52c software.

2.2.8 Ca^{2+}-activity analysis

Control, *Atx1[30Q]* and *Atx1[82Q]* transgenic strains were crossed with Tg(*2xcpce-E1b:KALNFB, he1.1:mTagBFP2*)^{bz14} x Tg(*14xUAS:GCaMP6s*)^{mpn101} carriers to establish triple transgenic zebrafish expressing the genetically-encoded Ca^{2+} indicator GCaMP6s, with the calcium-binding protein calmodulin (CaM) and the reporter protein GFP (Chen et al. 2013), specifically in PCs mediated by the Gal4 variant, KALNFB (Namikawa et al. 2019b). The obtained carriers, showing red fluorescence of mScarlet in the PC membrane and green fluorescence of GFP in the PC cytoplasm, were collected at 4 dpf under a fluorescence stereomicroscope (Leica M205 FA). At 6 dpf and 12 dpf, larvae with different genotpye were anaesthetized for one minute in 100 µl 30% Danieau medium containing Mivacurium chloride[12] at a concentration of 0.5 mg/ml (Mattern et al. 2020).

The larvae were then embedded in 2% low-melting agarose/PBS and image stack recording (5 planes each 10µm apart) of their PCL at 1.1 Hz intervals was performed by digital light-sheet microscopy (Leica TCS SP8 DLS) for a duration of 333 seconds (370 frames). After the imaging, GCaMP6s fluorescent emission was analyzed in the third PC plane of all fish using ImageJ 1.52c software. The first 66 frames (60 seconds) were considered as habituation period and were neglected in the data analysis. The subsequent 10 frames were used as a baseline signal. The average of mean grey values of the baseline frames (F0) was subtracted from the mean grey value of each subsequent frame (F) to calculate (F-F0)/F0 for each frame. Moreover, the average ΔF/F0 for each fish was calculated to statistically compare the three fish groups.

2.2.9 Behavioral analysis

The novel tank diving test is a behavioral test used to characterize the exploratory behavior in zebrafish. The novel tank was positioned in front of a video camera for optimal recording. There was enough light in the tank's background to have an appropriate contrast for accurate tracking and analysis. The video recording by EthoVision XT 12 software was started and the individual zebrafish was gently transferred with a net into the novel tank. The net was moved

carefully in the water allowing the fish to swim out. The tracking of the fish by the software started automatically after detection of the fish in the adjusted arena. The fish's behavior in the tank was recorded for 6 minutes and then the fish was gently returned to its home tank (Cachat et al. 2010). Afterwards, the video analysis was performed automatically by the software according to the adjusted analysis profile with the desired parameters to be assessed. The assessed parameters were the percentage of time spent in the upper half of the novel tank, the latency until the first visit to the upper half, the whole distance traveled in the tank, the number of transitions to the upper half and the average, the minimum and the maximum swimming velocity. The results were then exported to Microsoft Excel sheets for further statistical analysis.

2.2.10 Statistical analysis

Goodness-of-fit tests, Shapiro-Wilk and Kolmogorov-Smirnov, were used to evaluate the deviation of data distribution from normal Gaussian distribution at a significance level of 0.05 (Dallal and Wilkinson 1986; Royston 1995). Two-way ANOVA with post hoc Tukey's test was used to evaluate the statistical significance of differences between experimental groups. Data are presented as mean ± SEM. p-Values which are indicated as *$p < 0.05$, **$p < 0.01$, ***$p < 0.001$ and ****$p < 0.0001$ refer to significant differences. Experimental numbers of the animals per group are reported in the respective figure legends. GraphPad Prism 9 software was used for statistical analysis and graph plotting.

3 Results

The establishment of a SCA1 genetic model in zebrafish easily-accessible for monitoring of neurodegeneration and disease progression, unraveling pathological mechanisms underlying the disease phenotypes, as well as testing potential treatment compounds and strategies, could be a step towards developing therapeutic approaches. There are already some other established animal models, however, providing a zebrafish SCA1 model to the ataxia researchers will add some more advantages such as *in vivo* live imaging of the transparent larval carriers, cheap maintenance and large numbers of offspring providing sufficient specimens for various studies.

3.1 Genetic modeling of SCA1 in zebrafish

3.1.1 Genetic engineering and strategy for modeling SCA1 in zebrafish

The strategy of this study for generating a zebrafish SCA1 model is to overexpress the human SCA1-causing gene *Atx1[82Q]* specifically in zebrafish PCs, the most vulnerable cells to SCA1 pathology in human patients. Not only the SCA1-causing gene, but also a fluorescent reporter, GAPmScarlet (Bindels et al. 2017), was expressed to allow for monitoring of affected PCs. Therefore, a bidirectional DNA vector was employed to enable the expression of both genes under control of the same PC-specific enhancer and consequently at the same spatiotemporal manner (Namikawa et al. 2019b). Furthermore, two other DNA vectors were constructed to establish two control fish strains. One of these control vectors expressed the human non-pathogenic gene *Atx1[30Q]* instead of *Atx1[82Q]* together with the fluorescent reporter and the other vector expressed only the fluorescent reporter (Fig. 3.1A-C).

In order to prove that the number of CAG repeats in both non-pathogenic (30Q) and pathogenic mutant (82Q) alleles of human *Atx1* were kept the same without alteration during the cloning procedures in the successive cloning steps, the constructed plasmids DNA were sequenced using the oligonucleotides *Human Atx1, upstream PolyQ, for* and *Human Atx1, downstream PolyQ, rev* for optimal sequencing of the polyQ sequence in human *Atx1*. The stock number of these oligonucleotides is 3472 and 3473, respectively. The sequencing data confirmed the successful cloning. The sequencing of the DNA construct expressing the

human non-pathogenic allele *Atx1[30Q]* revealed that the number of CAG repeats was stably kept at 30 without alteration during the cloning procedures. The plasmid stock number is 5648, in which detailed cloning procedure is provided. Additionally, the sequencing of the DNA construct expressing the human SCA1-causing allele *Atx1[82Q]* revealed that the number of CAG repeats was stably kept at 82 without alteration during the cloning procedures. The plasmid stock number is 5187, in which detailed cloning procedure is provided.

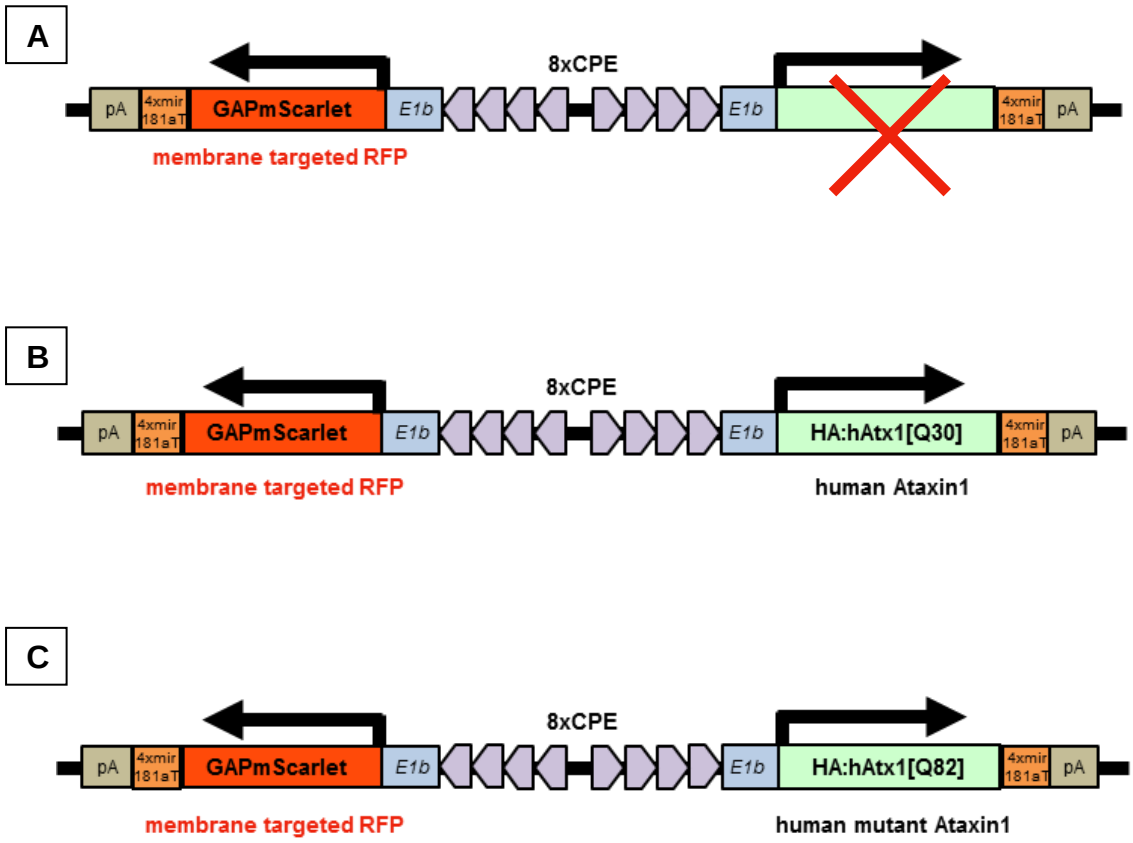

Figure 3.1 Genetic modeling of the human SCA1 disease in zebrafish

Schematic drawing of expression constructs for PC-specific coexpression of the red fluorescent reporter protein mScarlet targeted to the cytoplasmic membrane, and non-pathogenic *Atx1[30Q]* or mutant pathogenic *Atx1[82Q]* human allele.

(A) Bidirectional DNA construct with expression of only the membrane-targeted red fluorescent reporter GAPmScarlet under control of *ca8* promoter-derived PC-specific enhancer element.

(B) Bidirectional DNA construct with coexpression of the human non-pathogenic protein Atx1[30Q] together with the membrane-targeted red fluorescent reporter GAPmScarlet under control of *ca8* promoter-derived PC-specific enhancer element.

(C) Bidirectional DNA construct with expression of the human SCA1-causing mutant protein Atx1[82Q] together with the membrane-targeted red fluorescent reporter GAPmScarlet under control of *ca8* promoter-derived PC-specific enhancer element.

The 2x4 copies of the enhancer element were added in opposite orientation and flanked on both sides with *E1b* basal promoter, multiple cloning site, 4 copies of *mir181aT* target fragment to eliminate ectopic expression in tectal neurons and retinal cells, and *SV40 pA* sequence. This mediated robust PC-specific expression of two different transgene cassettes. All bidirectional transgene cassettes were flanked by Tol1 transposon recognition sites.

3.1.2 Generation of stable transgenic zebrafish model for Purkinje cell-specific SCA1

The three DNA constructs were separately microinjected into one-cell stage zebrafish embryos together with mRNA encoding the transposon Tol1 to promote genomic integration and germline transmission of the respective transgene cassettes early during development (Kikuta and Kawakami, 2009). At 4 dpf the injected larvae were screened and founders with broad GAPmScarlet expression throughout the PC population were raised to adulthood (P0 generation). Germline transmission was examined by crossing individual P0 fish with wild-type fish and screening of the filial F1 generation for PC-specific mScarlet fluorescence. Such carriers were raised to adulthood and crossed with wild-type fish to confirm stable transmission of the fluorescent reporter to the F2 offspring in a mendelian ratio (Fig. 3.2). Transgenic embryos of the F2 generation when analyzed at 4 dpf by laser scanning confocal microscopy were found to display continuous non-mosaic expression of the fluorescent reporter GAPmScarlet throughout the PCL (Fig. 3.3a-c).

To confirm that the expression is specific for PCs, adult carriers from the three strains were crossed with carriers from the Tg(*-7.5ca8:GFP*)^{bz12} transgenic line which expresses GFP specifically in PCs (Namikawa et al., 2019). The transgenic embryos obtained from this mating showed double positive expression of red and green fluorescent proteins in PCs when they were analyzed at 4 dpf by laser scanning confocal microscopy (Fig. 3.3a-f). Colocalization of the red flourescence (GAPmScarlet) and the green fluorescence (GFP) in the cytoplasmic membrane and the cytoplasm of PCs, respectively, and the nonexistence of any unspecific red signal proved that transgene expression in the three established lines was confined to the PC population, the most vulnerable cell population to SCA1 disease (Fig. 3.3g-i).

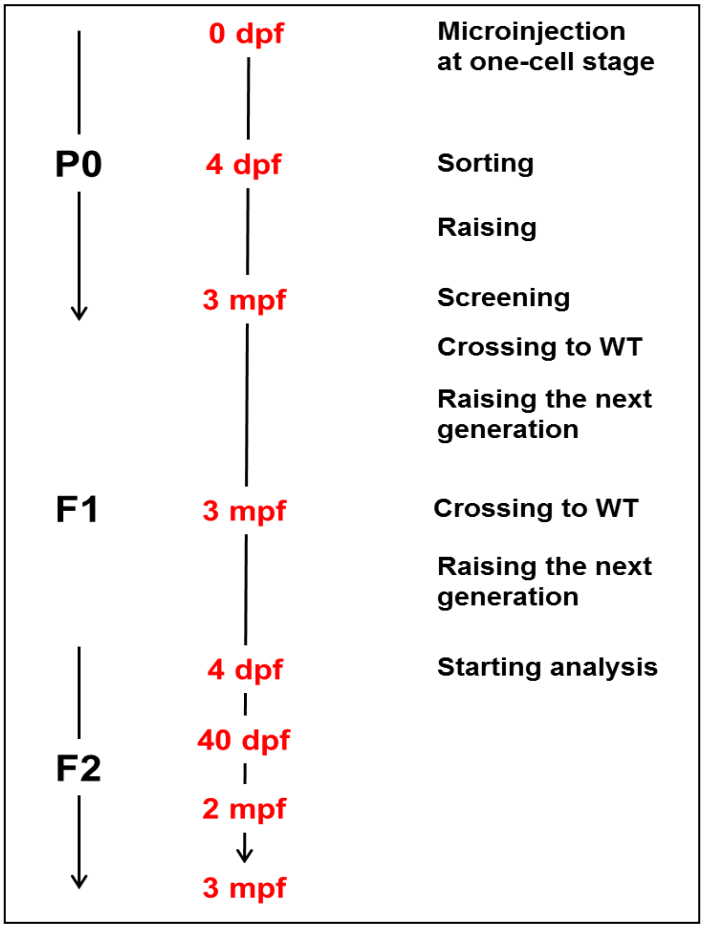

Figure 3.2 Generation of stable transgenic zebrafish model for PC-specific SCA1

Schematic outline of screening and breeding procedure performed to obtain stable transgenic zebrafish of the F2 generation, which propagate PC-specific *mScarlet* and *Atx1* expression in a Mendelian manner. The generation of each of the three transgenic lines established in this study started with injecting the associated cloned DNA construct together with mRNA encoding the transposon Tol1 into wild-type zebrafish zygotes at 0 dpf. The injected larvae which showed red fluorescence in PCs at 4 dpf were raised in the fish facility to get adult P0 generation carriers at 3 months post fertilization (mpf). Such adults were screened by crossing with wild-type fish and the offspring were checked for red fluorescence in PCs. The positive carriers were raised to get adult F1 generation fish. Afterwards, these adult fish were crossed with wild-type fish to raise and analyze F2 generation carriers starting after the beginning of PC differentiation in 4 dpf larval stage, then at early and late juvenile stages (40 dpf and 2 mpf, respectively) until adulthood (3 mpf).

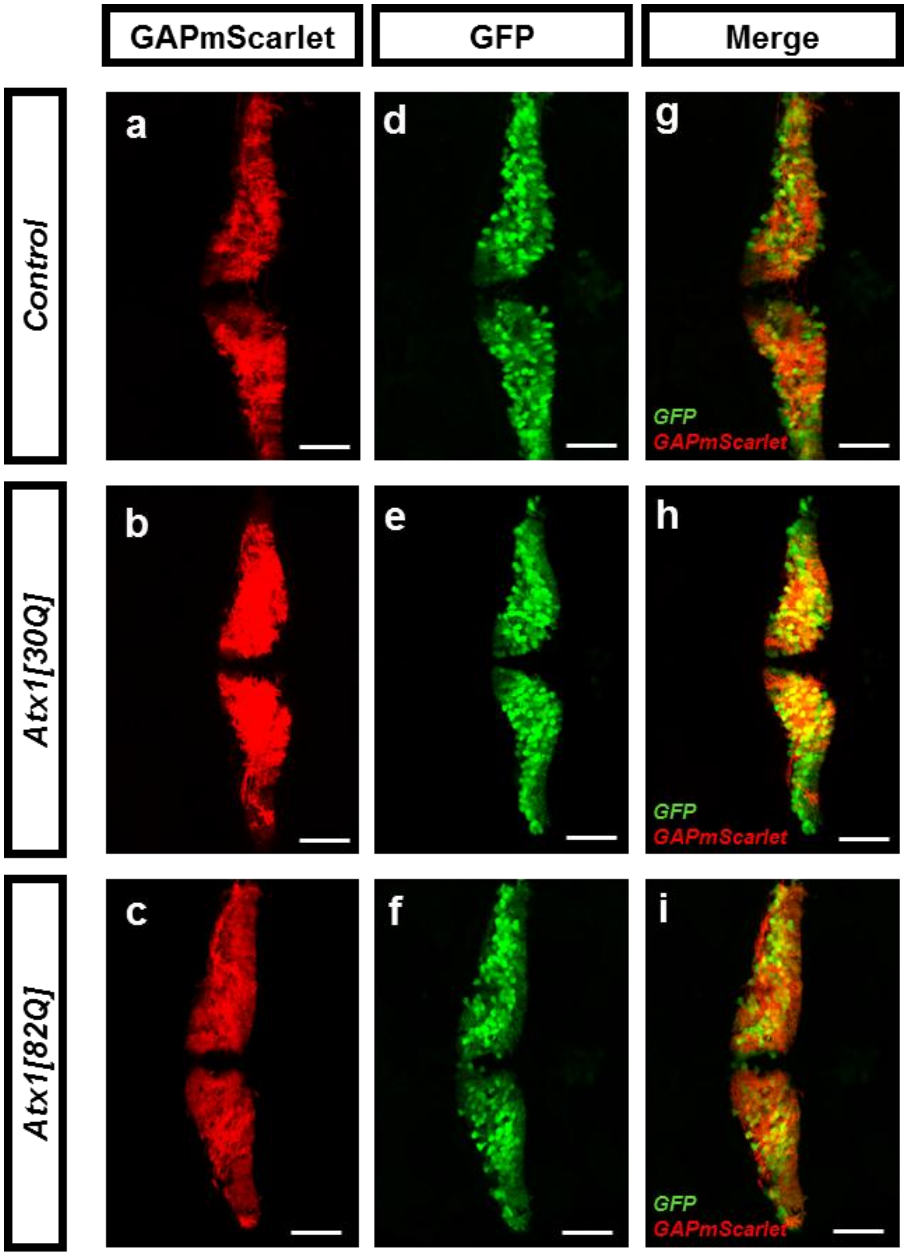

Figure 3.3 Expression pattern of GAPmScarlet in the established transgenic strains compared with PC-specific GFP in the transgenic strain Tg(*-7.5ca8:GFP*)^{bz12}

Analysis of membrane-targeted GAPmScarlet expression (a-c) compared with PC-specific GFP cytoplasmic expression (d-f) and their colocalization in PCs (g-i) in 4 dpf embryos of the F2 generation of the established control (upper row), *Atx1[30Q]* (middle row) and *Atx1[82Q]* (lower row) transgenic strains. These results show that transgene expression in the three generated strains is confined to PCs. The images display a dorsal view of the larval zebrafish cerebellum, anterior is to the left. Scale bar: 50 µm.

3.1.3 Expression of human Ataxin-1 in the stable transgenic zebrafish strains

To investigate whether GAPmScarlet fluorescence in PCs was accompanied by protein expression of the human *Atx1* allele, HA-immunohistochemistry was performed. In the *Atx1[30Q]* transgenic 4 dpf larval zebrafish, the expression of non-pathogenic HA-tagged hAtx1[30Q] with normal number of polyQ repeats was observed in PCs throughout the entire PC population after immunostaining against HA-tag. GAPmScarlet red fluorescent reporter protein was observed as well in the cytoplasmic membranes of zebrafish PCs (Fig. 3.4A). In the *Atx1[82Q]* transgenic 4 dpf larval zebrafish, the expression of pathogenic mutant HA-tagged hAtx1[82Q] with abnormal number of polyQ repeats was observed in PCs throughout the entire PC population after immunostaining against HA-tag. GAPmScarlet red fluorescent reporter protein was observed as well in the cytoplasmic membranes of zebrafish PCs (Fig. 3.4B). Both HA-tagged human proteins, Atx1[30Q] and Atx1[82Q], showed aggregates in PCs (Fig. 3.4A, B, respectively, white arrows).

This analysis revealed that human Atx1[30Q] and Atx1[82Q] were coexpressed with GAPmScarlet in PCs throughout the entire population indicating that GAPmScarlet serves as a reliable intravital marker for human *Atx1*-allele expression. Such expression of human SCA1-causing Atx1[82Q] protein in zebrafish Purkinje neurons in a stably inherited manner through fish generations is the first step towards modeling of the SCA1 inherited disorder in zebrafish. Expression of human non mutant Atx1[30Q] protein in zebrafish Purkinje neurons in a similar stably inherited manner through fish generations offers a baseline control for proper comparisons with SCA1 fish in the different experiments. It is also important to mention that no signs of neurodegeneration were detected in PCs of the *Atx1[82Q]* transgenic strain at larval stages. Therefore, PCs of juvenile and adult stages were investigated.

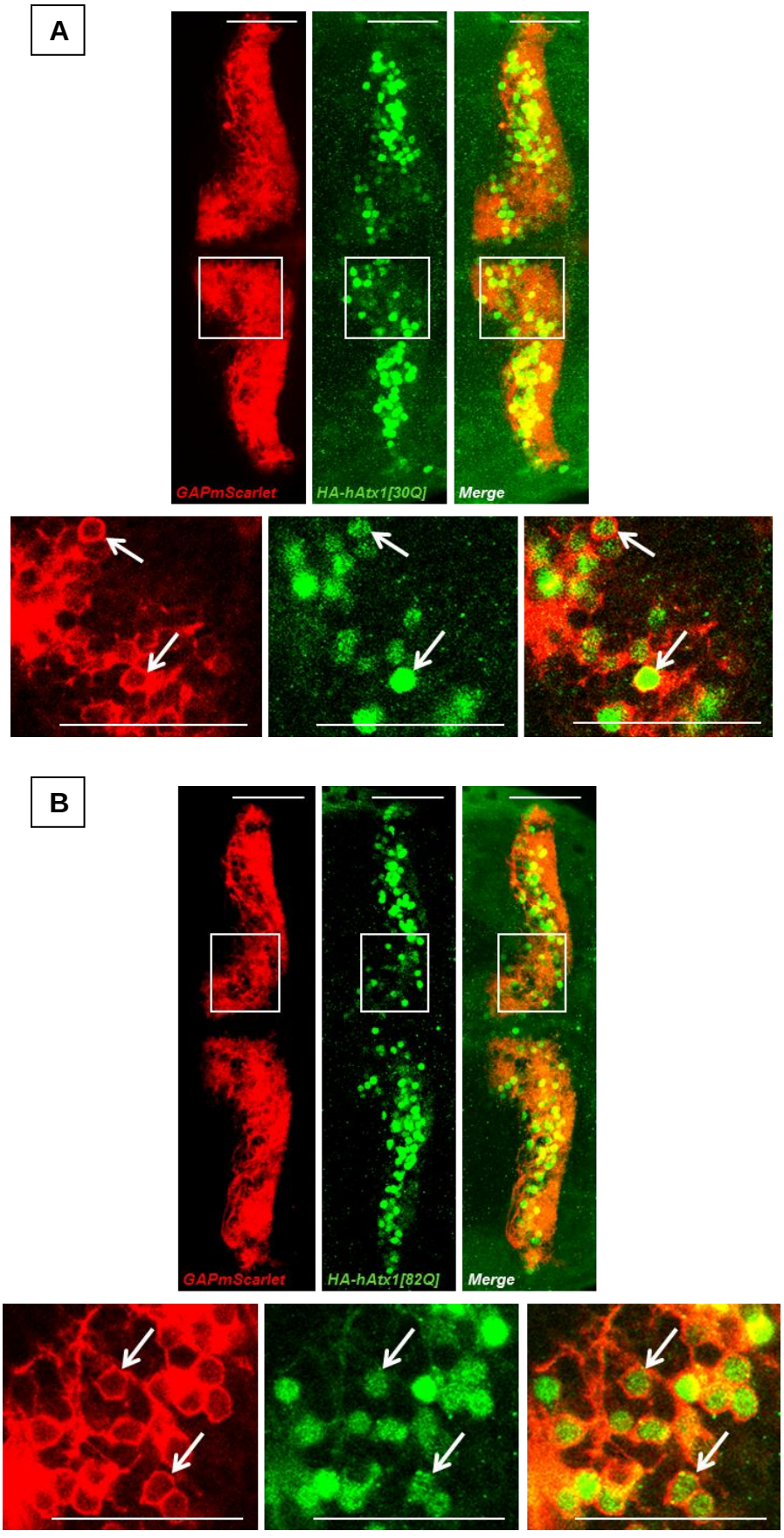

Figure 3.4 Analysis of human *Atx1*-allele expression in the stable zebrafish transgenic strains

Anti-HA immunostaining of the HA-tagged proteins, hAtx1[30Q] (A) and hAtx1[82Q] (B), shows their expression in PCs (green fluorescence) in 4 dpf larvae of the F2 generation of the established transgenic *Atx1[30Q]* and *Atx1[82Q]* strains, respectively. Such green signals are surrounded by the PC-specific membrane-localized red fluorescent protein GAPmScarlet (white arrows). The images display a dorsal view of the larval zebrafish cerebellum, anterior is to the left. Scale bar: 50 µm.

3.2 Neurodegenerative effects of the overexpression of human mutant Ataxin-1 on zebrafish Purkinje cells

In order to reveal the effect of transgene expression on developing and mature PCs, heterozygous F2 offspring of the control, *Atx1[30Q]* and *Atx1[82Q]* stable transgenic strains were raised. Expression of the red fluorescent membrane-targeted GAPmScarlet in PCs was investigated by confocal microscopy. Embryonic development appeared to occur indistinguishably between control fish, *Atx1[30Q]* fish expressing the human non-pathogenic allele with a polyQ stretch of 30 non-interrupted glutamine residues and *Atx1[82Q]* fish expressing the human pathogenic allele with a polyQ stretch of 82 non-interrupted glutamine residues. Larvae from all three alleles displayed a continuous bright red fluorescence throughout the PC population. Therefore, transgenic carriers were raised to early juvenile (40 dpf) (Fig. 3.5), late juvenile (2 mpf) (Fig. 3.6) and young adult (3 mpf) (Fig. 3.7) stages. At these time points, the brains were dissected for microscopy analysis of PCs at further detail. PCs still expressed the red fluorescent reporter protein confirming the continued expression of the transgene throughout adulthood as demonstrated previously (Namikawa et al., 2019).

At 40 dpf PCs in the control (Fig. 3.5a), *Atx1[30Q]* (Fig. 3.5b) and *Atx1[82Q]* (Fig. 3.5c) heterozygous transgene carriers formed a continuous layer covering the corpus cerebelli with both cerebellar hemispheres being separated by the dorsal midline (Fig. 3.5a white dashed line). No major signs of cerebellar atrophy like shrinkage in tissue or discontinuous patches of fluorescent PCs could be identified at this developmental age. Nevertheless, in contrast to controls and *Atx1[30Q]* zebrafish, confocal microscopy of the PC population in *Atx1[82Q]*-expressing juveniles depicted speckles of brighter fluorescence suggestive of aggregation, cellular shrinkage and onset of neurodegeneration. This could be confirmed with a higher magnification imaging of selected PC areas (Fig. 3.5a-c, white squares) showing individual cells (Fig. 3.5d-f). PCs expressing Atx1[82Q] showed abnormal morphology (Fig. 3.5f, white arrows). However, PCs expressing Atx1[30Q] (Fig. 3.5e, white arrows) or GAPmScarlet only (Fig. 3.5d, white arrows) showed regular morphology with no signs of neurodegeneration.

In late juvenile fish of 2 months of age the controls (Fig. 3.6a) and *Atx1[30Q]* (Fig. 3.6b) fish displayed a continuous PC population marked by red fluorescence in both hemispheres. This regularity and continuity of PC population in both hemispheres of the corpus cerebelli continued to young adulthood in 3 months old fish with a PC population displaying a dense

continuous layer of red fluorescent cells (Fig. 3.7a, b). In contrast to this, 2 months old juvenile *Atx1[82Q]* fish showed irregularities in their fluorescent PC population with signs of neurodegeneration based on the observance of areas of decreased or even absent red fluorescence (Fig. 3.6c). In order to show such irregularities on the cellular level, higher magnification imaging of selected cerebellar regions was performed (Fig. 3.6a-c, white squares). This revealed substantial difference among PCs in the SCA1 juveniles (Fig. 3.6f, white arrows), which displayed robust onset of neurodegeneration, and PCs in the control (Fig. 3.6d, white arrows) and *Atx1[30Q]* (Fig. 3.6e, white arrows) juveniles, which displayed normal appearance.

Furthermore, young adults showed an escalation of such abnormalities where the PC population in *Atx1[82Q]* carriers was significantly disrupted with a severely disturbed outline, large discontinuities of cells, a small size and a granular appearance (Fig. 3.7c). Confocal microscopy of selected PC areas at higher magnification (Fig. 3.7c, white square) revealed condensed PC somata of unusually bright fluorescence likely caused by cell shrinkage and condensation of the fluorophore (Fig. 3.7f, white arrows) and fluorescent cellular debris indicative for an ongoing degeneration of PCs, while in control (Fig. 3.7a) and *Atx1[30Q]* carriers (Fig. 3.7b) a regular PC population was observed. Having a closer look at selected areas of PC region in these control transgenic strains (Fig. 3.7a, b, white squares), the individual PCs displayed a regular morphology with neither condensed cell somata of unusually bright fluorescence nor cellular debris (Fig. 3.7d, e). In addition, a fine web of neuropil formed by PC dendrites was visible.

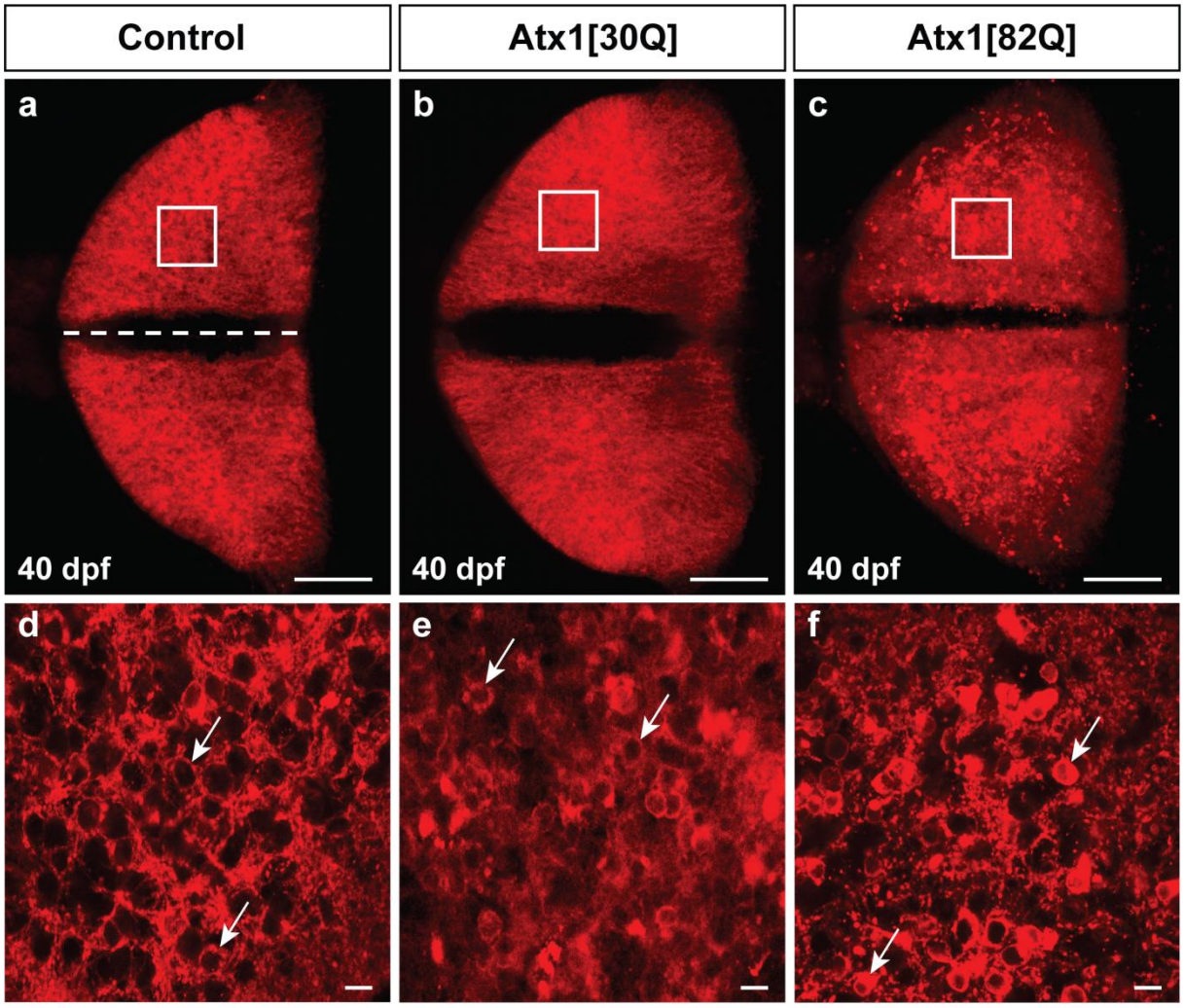

Figure 3.5 Neurodegenerative effects of overexpression of the human mutant Atx1[82Q] on Purkinje cells of the early juvenile zebrafish

Morphology of zebrafish cerebellum at 40 dpf juveniles of the F2 generation of the established transgenic strains (a-c), shown by the PC-specific membrane-targeted red fluorescent protein GAPmScarlet, reveals signs of neurodegeneration of PC population in the SCA1 transgenic zebrafish (right column) when compared to the control (left column) and *Atx1[30Q]* (middle column) transgenic strains. On the cellular level (d-f), there are signs of neurodegeneration of PCs in the *Atx1[82Q]* transgenic strain (f, white arrows) which are not observed in control (d, white arrows) and *Atx1[30Q]* (e, white arrows) strains. These data suggest that signs of PC neurodegeneration started to appear at the early juvenile stages expressing human pathogenic Atx1[82Q]. The images are representative for each experimental group (n = 7, 7 and 6 in the control, *Atx1[30Q]* and *Atx1[82Q]* groups, respectively) and display a dorsal view of early juvenile zebrafish cerebellum, anterior is to the left. Scale bar (a-c): 100 µm, (d-f): 10 µm.

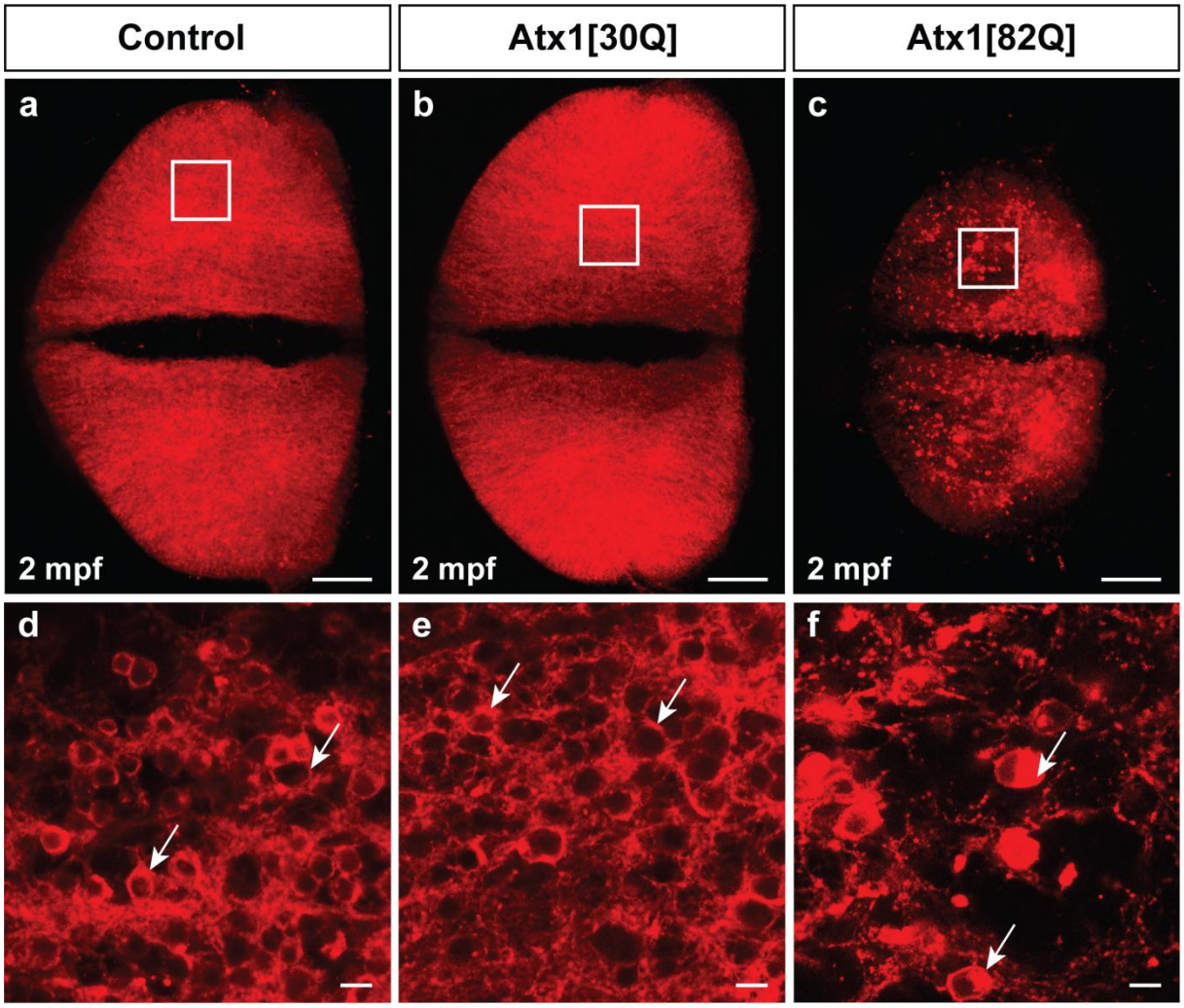

Figure 3.6 Neurodegenerative effects of overexpression of the human mutant Atx1[82Q] on Purkinje cells of the late juvenile zebrafish

Morphology of zebrafish cerebellum at 2 mpf (months post fertilization) juveniles of the F2 generation of the established transgenic strains (a-c), shown by the PC-specific membrane-targeted red fluorescent protein GAPmScarlet, reveals signs of neurodegeneration of PC population in the SCA1 transgenic zebrafish (right column) when compared to the control (left column) and *Atx1[30Q]* (middle column) transgenic strains. On the cellular level (d-f), there are signs of neurodegeneration of PCs in the *Atx1[82Q]* transgenic strain (f, white arrows) which are not observed in control (d, white arrows) and *Atx1[30Q]* (e, white arrows) strains. These data suggest that neurodegeneration of PCs is clearly observed at the late juvenile stages expressing human pathogenic Atx1[82Q]. The images are representative for each experimental group (n = 6, 6 and 7 in the control, *Atx1[30Q]* and *Atx1[82Q]* groups, respectively) and display a dorsal view of late juvenile zebrafish cerebellum, anterior is to the left. Scale bar (a-c): 100 µm, (d-f): 10 µm.

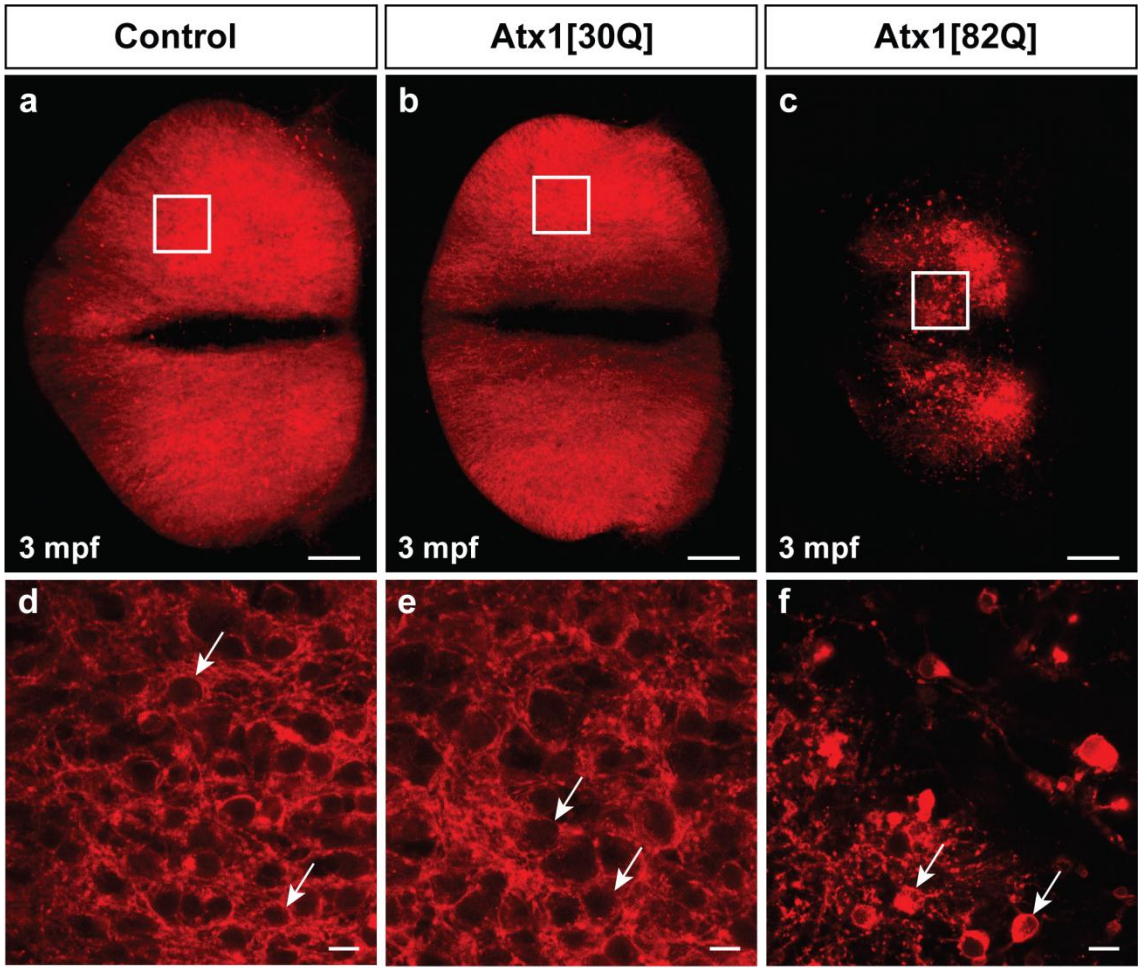

Figure 3.7 Severe neurodegeneration of Purkinje cell population in the adult SCA1 transgenic zebrafish

Morphology of zebrafish cerebellum at 3 mpf (months post fertilization) juveniles of the F2 generation of the established transgenic strains (a-c), shown by the PC-specific membrane-targeted red fluorescent protein GAPmScarlet, reveals signs of neurodegeneration of PC population in the SCA1 transgenic zebrafish (right column) when compared to the control (left column) and *Atx1[30Q]* (middle column) transgenic strains. On the cellular level (d-f), the PC population in the *Atx1[82Q]* transgenic strain is significantly affected with a severely disturbed outline, large discontinuities of cells, a small size and a granular appearance (f, white arrows). Such irregularities were not observed in control (d, white arrows) and *Atx1[30Q]* (e, white arrows) strains. These data suggest that neurodegeneration of PCs is clearly observed at the adult stages expressing human pathogenic Atx1[82Q]. The images are representative for each experimental group (n = 6, 6 and 7 in the control, *Atx1[30Q]* and *Atx1[82Q]* groups, respectively) and display a dorsal view of adult zebrafish cerebellum, anterior is to the left. Scale bar (a-c): 100 µm, (d-f): 10 µm.

The robust disruption of the PCL in the adult *Atx1[82Q]* carriers was further revealed by the cerebellar sagittal sections. Although the membrane-targeted expression of mScarlet showed a continuous layer of PCs in the control and *Atx1[30Q]* strains (Fig. 3.8a, b), in SCA1 fish red fluorescent PCs were largely absent, almost entirely in anterior regions of the corpus cerebelli while the posterior region still contained a number of PCs (Fig. 3.8c). To further corroborate that the SCA1 zebrafish model suffer from PC neurodegeneration, sagittal sections from the cerebellum of control, *Atx1[30Q]* and *Atx1[82Q]* adult fish were stained with anti-ZebrinII immunostainig, a specific antibody staining for PCs (Brochu et al. 1990). Such sections displayed disrupted cellular organization in the PCL of *Atx1[82Q]* fish with apparent holes and debris compared to sections from the control alleles (Fig. 3.8d-f).

Moreover, sagittal sections of the PCL in *Atx1[30Q]* and *Atx1[82Q]* zebrafish analyzed by anti-HA immunohistochemistry confirmed that the transgenes were still expressed in PCs during adulthood, yet displaying only sparse labelling in PCs of *Atx1[82Q]* carriers consistent with apparent holes in the PCL, cellular debris and pronounced PC degeneration (Fig. 3.8g, h). These results further support the age-dependent progredient loss of PCs in the *Atx1[82Q]* SCA1 fish as it is observed in SCA1 patients. These findings also confirm an observation from juvenile stages that apparently anterior regions of the corpus cerebelli seem more vulnerable for PC degeneration than posterior regions in this zebrafish SCA1 model.

In addition, histological staining of adult brain sagittal sections with hematoxylin and eosin was performed. It was shown that the pathogenic cellular organization of *Atx1[82Q]* PCs does not seem to affect the gross morphology of the corpus cerebelli (Fig. 3.9a-c). At higher magnifications (Fig. 3.9d-f), large somata (Fig. 3.9d, e, white arrows) characteristic for PCs, between the granule cell layer (GCL) and the molecular layer (ML), were only visible in the cerebelli of control and *Atx1[30Q]* transgenic strains, but were hardly found in the cerebelli of *Atx1[82Q]* transgenic strain. These results revealed the undisturbed cytology of the cerebellum in the SCA1 zebrafish model with an obviously-distinguishable GCL and ML consisting mostly out of neuropil.

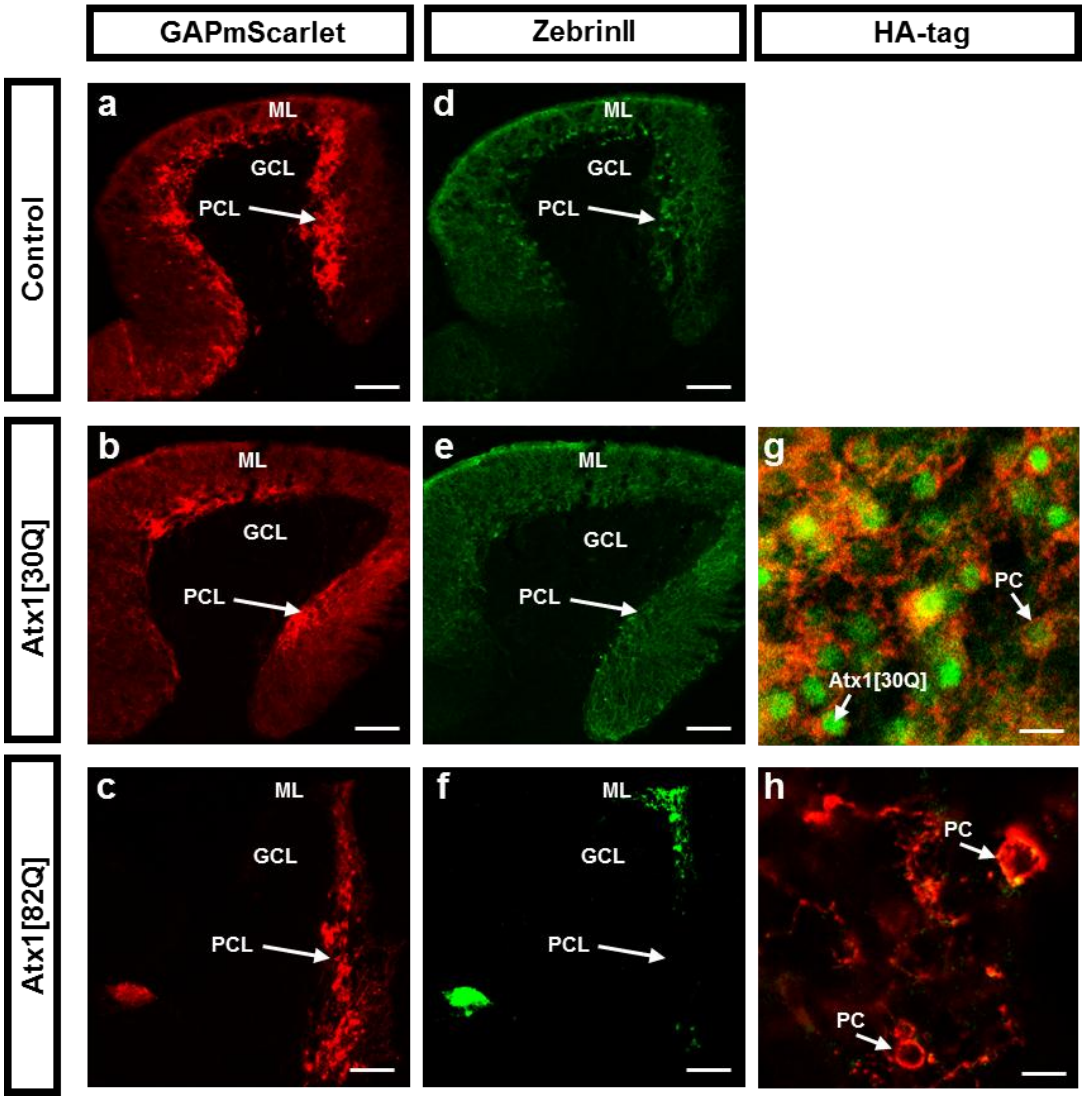

Figure 3.8 Immunohistochemical comparison of adult corpus cerebelli of control and *Atx1*-expressing zebrafish

(a-c) Sagittal sections from the cerebellum of control, *Atx1[30Q]* and *Atx1[82Q]* adult zebrafish, respectively.

(d-f) PC-specific anti-ZebrinII antibody staining of sagittal sections from the cerebellum of control, *Atx1[30Q]* and *Atx1[82Q]* adult zebrafish, respectively.

(g, h) Anti-HA immunostaining of sagittal sections from the cerebellum of *Atx1[30Q]* and *Atx1[82Q]* adult zebrafish, respectively.

Anterior is to the left. Scale bar (a-f): 100 µm, (g, h): 10 µm.

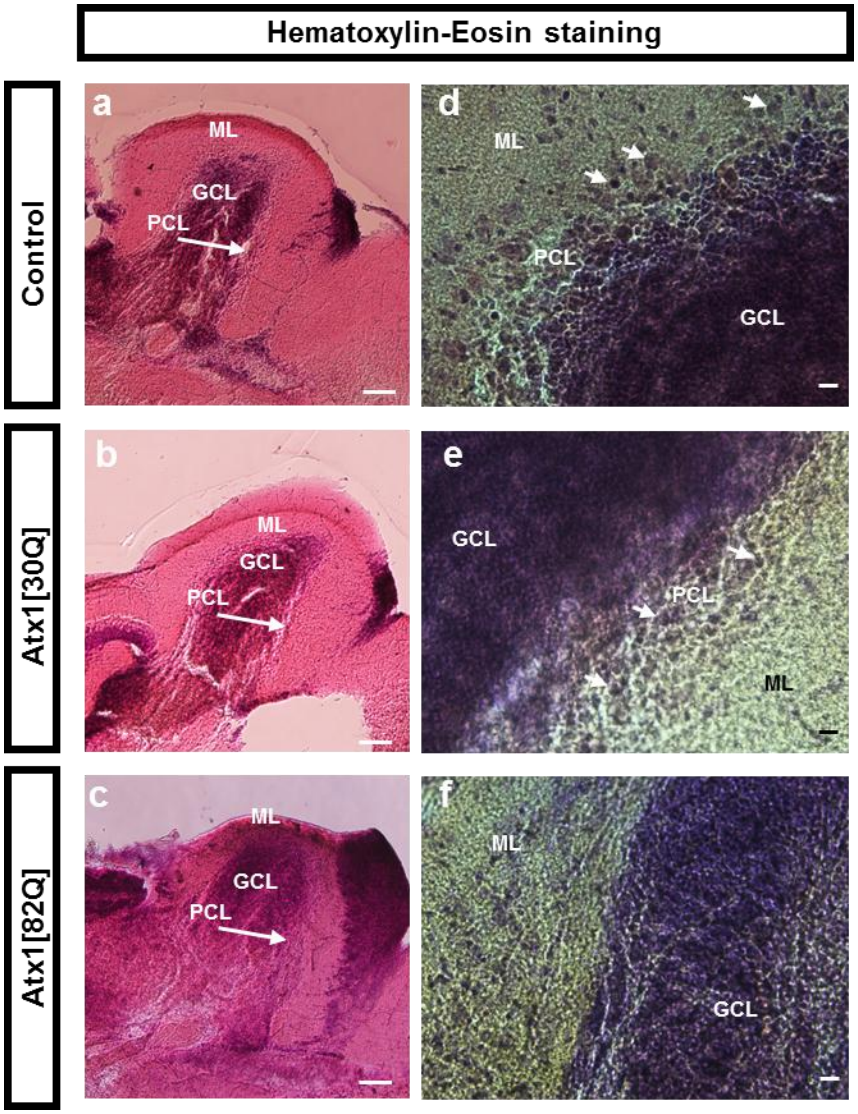

Figure 3.9 Histological comparison of adult corpus cerebelli of control and *Atx1*-expressing zebrafish

(a-c) Hematoxylin-Eosin staining of sagittal sections from the cerebellum of control, *Atx1[30Q]* and *Atx1[82Q]* adult zebrafish, respectively.
(d-f) Higher magnification of a-c, respectively.
Anterior is to the left. Scale bar (a-c): 100 µm, (d-f): 10 µm.

3.3 Age-related progredient loss of Purkinje cell population in zebrafish genetic model of SCA1

Long term analysis was performed for fish groups from the F2 generation of the established transgenic control, *Atx1[30Q]* and *Atx1[82Q]* strains at 40 dpf (early juvenile stage), 2 mpf (late juvenile stage) and 3 mpf (adult stage). At these time points, the body length form the anterior tip of the jaw until the caudal indentation of the tail fin (fork length) of each fish was measured (Fig. 3.10A). This was followed by isolation of the brain for microscopy analysis of PCs and quantification of the brain area covered by PCs across the corpus cerebelli at each age under investigation (Fig. 3.10B). The body length at each time point did not differ significantly among individuals from all three allelic families and the growth in body length continued regularly until adulthood in control and *Atx1[30Q]* zebrafish as well as *Atx1[82Q]* zebrafish (Fig. 3.11).

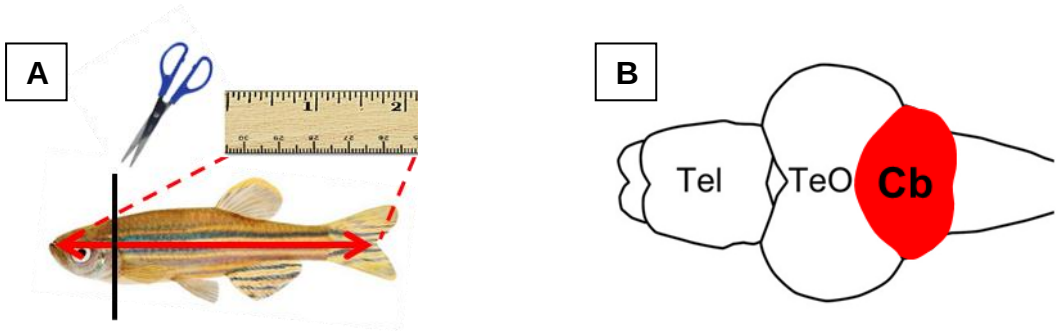

Figure 3.10 Analysis of fish body length and dorsal surface of the cerebellum in dissected brains

(A) Schematic drawing of adult zebrafish to demonstrate measurement of body length form the anterior tip of the jaw until the caudal indentation of the tail fin (fork length) before dissection (lateral view).

(B) The cerebellum in dissected brains from these specimens is easy to identify by the red fluorescent PC population forming a continuous layer of cells across the corpus cerebelli providing a means for measuring the dorsal surface of the cerebellum (dorsal view).

Abbr.: Cb: cerebellum, TeO: optic tectum, Tel: telencephalon.

When the fluorescent cerebellar area covered by PCs (Fig. 3.10B, red area) was quantified and compared among specimens from the three transgenic strains at the three time points

using two-way ANOVA with post hoc Tukey's test, a reduced size of this area was observed only in the *Atx1[82Q]* transgenic strain. This reduction in size of the PC area occurred in an age-dependent progredient manner as the size of PC area stalled in the SCA1 fish from 40 dpf to 2 mpf and there was a significant reduction at 3 mpf. Nevertheless, the area covered by PC population in the control and *Atx1[30Q]* strains increased significantly from 40 dpf to 2 mpf and from 2 mpf to 3 mpf. Moreover, the *Atx1[30Q]* strain never showed a significant difference from the control strain at any time point, which suggests that the transgenic fish expressing non-pathogenic human protein Atx1[30Q] display a regular development of PC population (Fig. 3.12). At 40 dpf, the statistical analysis revealed no significant differences in size of the PC area among fish from all three groups, although signs of neuronal degeneration have been already seen in the SCA1 model. This further confirmed the absence of a major cerebellar atrophy in SCA1 zebrafish at 40 dpf (Fig. 3.12).

The impaired age-dependent expansion of the PC population in the SCA1 fish was obvious because the size of the PC area barely increased in 2 mpf juveniles in comparison to 40 dpf juveniles (Fig. 3.12) despite a regular age-related increase in body size (Fig. 3.11). In young adults, this situation progressed even further. Although the adult SCA1 fish have grown to their normal body size compared to the control and *Atx1[30Q]* counterparts (Fig. 3.11), the area covered by the PC population was quantified to be smaller than in both 40 dpf and 2 mpf SCA1 juveniles and about 5-fold smaller than in the adult control and *Atx1[30Q]* counterparts. However, zebrafish of the control and *Atx1[30Q]* strains displayed a comparable age-related expansion of the PC population in both hemispheres of the corpus cerebelli (Fig. 3.12) in relation to the growth of their body (Fig. 3.11). This age-dependent increase in body length accompanied by an expansion of the PC area continued to young adulthood in 3 months old fish. These findings suggest a progredient neurodegeneration of PCs in the SCA1 zebrafish model expressing the human *Atx1[82Q]* allele in PCs, which like in human patients occurs in an age-related progressive manner.

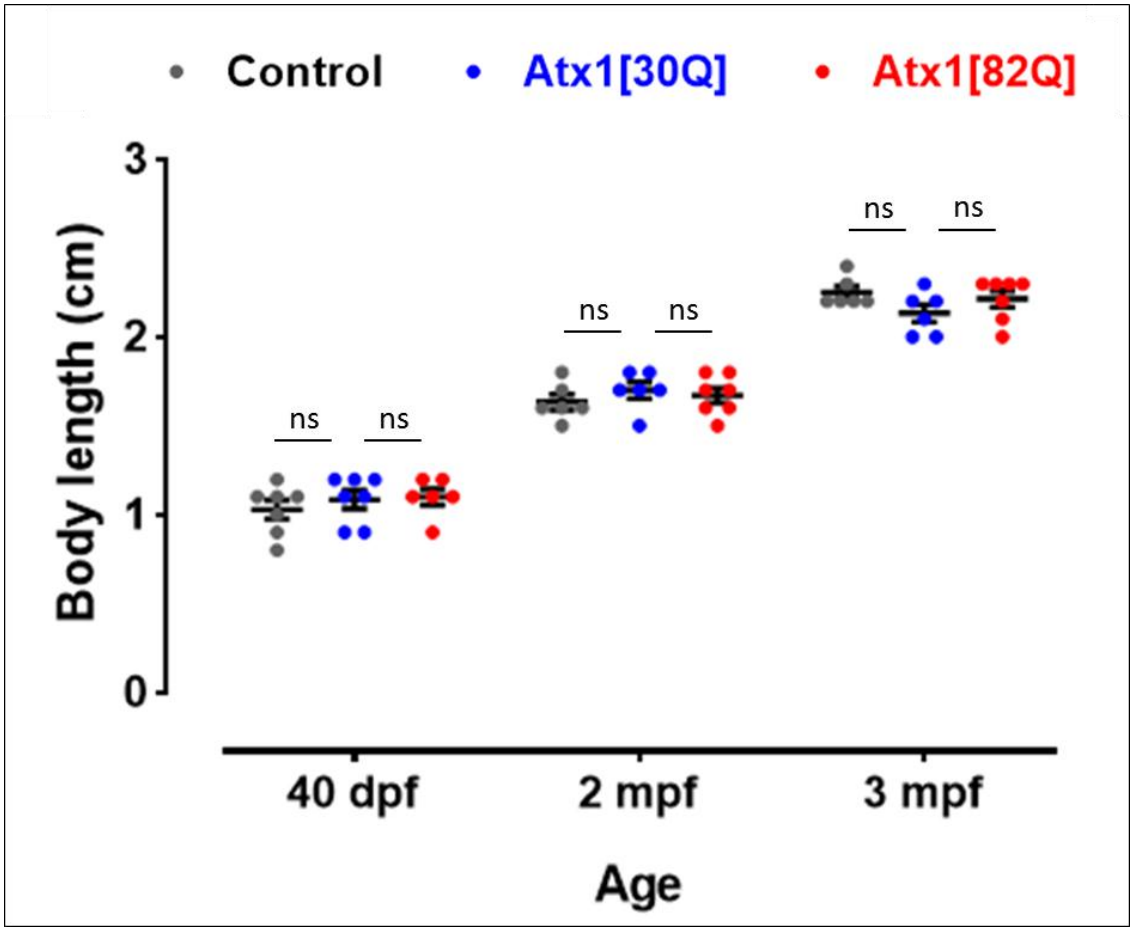

Figure 3.11 Body length analysis in a stable transgenic zebrafish model for SCA1

Age-related analysis of the body length of fish groups from the F2 generation of the established transgenic control, *Atx1[30Q]* and *Atx1[82Q]* strains at early juvenile stage (40 dpf), late juvenile stage (2 mpf) and young adult stage (3 mpf). The body length among individuals from all three allelic families did not differ significantly at each time point. In addition, the growth in body length of the SCA1 zebrafish continued regularly until adulthood as same as the control and *Atx1[30Q]* zebrafish. These findings suggest that abnormal PC development in zebrafish expressing the human pathogenic Atx1[82Q] protein does not interfere with organismic growth. Data are presented as mean ± SEM. N = 7, 6, 6 in 40 dpf, 2 mpf and 3 mpf control groups; N = 7, 6, 6 in 40 dpf, 2 mpf and 3 mpf *Atx1[30Q]* groups; and N = 6, 7, 7 in 40 dpf, 2 mpf and 3 mpf *Atx1[82Q]* groups, respectively.

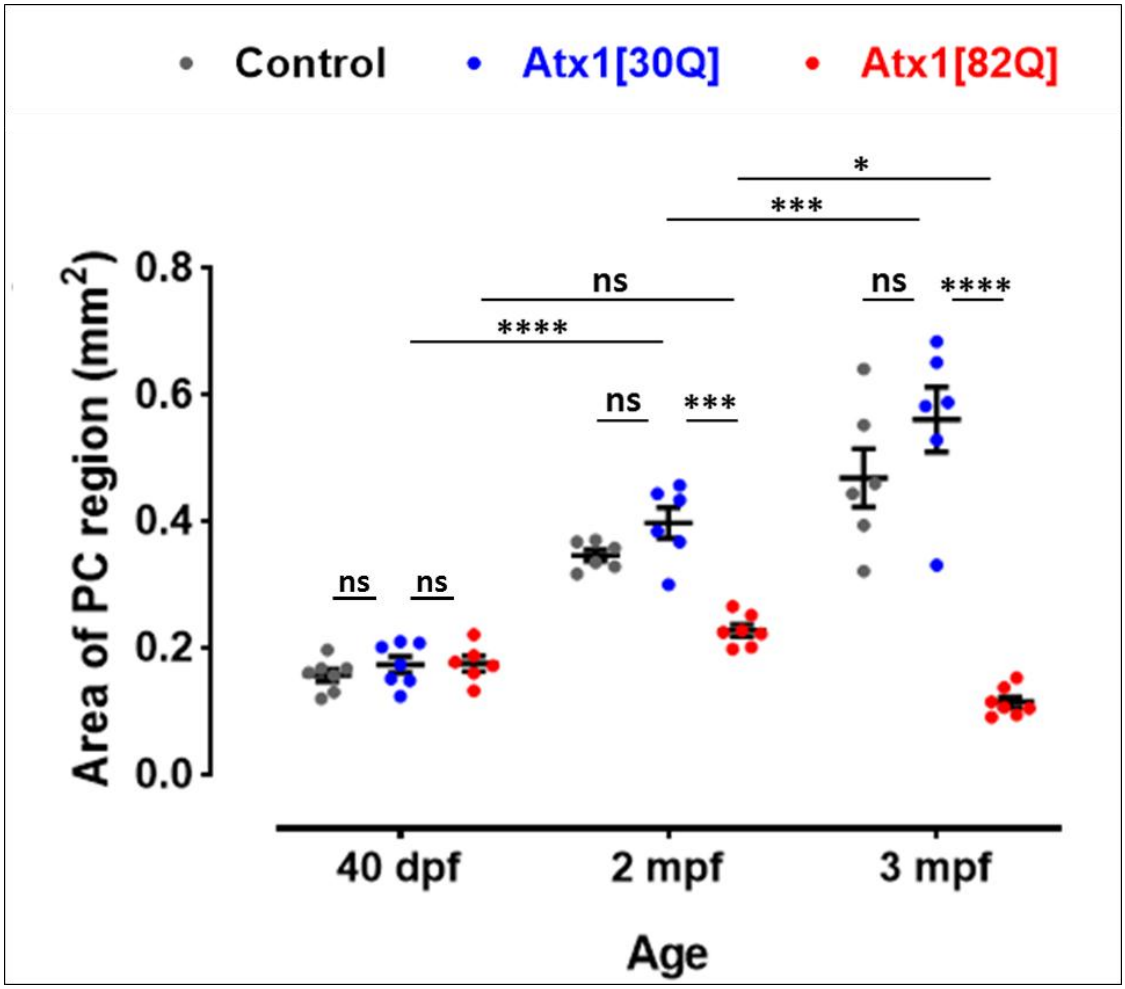

Figure 3.12 Long term analysis of the area covered by Purkinje cell population in a stable transgenic zebrafish model for SCA1

Long term analysis of PC region reveals a robust age-dependent progressive reduction in the cerebellar area covered by Purkinje neurons in the SCA1 zebrafish when compared to the control and *Atx1[30Q]* transgenic strains. Changes in the size of the PC population start in late juvenile stages (2 mpf), although signs of neurodegeneration can be observed already in early juvenile stages (40 dpf). These findings suggest a severe neurodegeneration of PCs in the zebrafish expressing the human *Atx1[82Q]* allele specifically in PCs, which like in human patients occurs in progressive, age-related manner. Data are presented as mean ± SEM; *p < 0.05, ***p < 0.001 and ****p < 0.0001. N = 7, 6, 6 in 40 dpf, 2 mpf and 3 mpf control groups; N = 7, 6, 6 in 40 dpf, 2 mpf and 3 mpf *Atx1[30Q]* groups; and N = 6, 7, 7 in 40 dpf, 2 mpf and 3 mpf *Atx1[82Q]* groups, respectively.

3.4 Physiological properties of zebrafish Purkinje cells expressing human Ataxin-1

The morphological disruption of PCs in the SCA1 zebrafish model has been observed to initiate at 40 dpf (Fig. 3.5d-f). There were no signs of neurodegeneration observed at younger ages. This led to an important question whether the physiology of PCs has already been altered prior to such morphological disruption. To answer this question, *in vivo* calcium imaging was performed to evaluate the activity of PCs in larval stages using the advantage of transparency of the larvae. In order to generate zebrafish expressing a fluorescent indicator for Ca^{2+} transients in PCs, control, *Atx1[30Q]* and *Atx1[82Q]* zebrafish strains were crossed with Tg(*2xcpce-E1b:KALNFB, he1.1:mTagBFP2*)^{bz14} x Tg(*14xUAS:GCaMP6s*)^{mpn101} carriers. The obtained larvae were expressing exclusively in PCs two fluorescent proteins, mScarlet (red) in the cell membrane and GFP (green) in the cytoplasm. The green fluorescence is indicating the Ca^{2+} indicator GCaMP6s. The recording of fluorescent emission of this Ca^{2+} indicator in the PCL was performed for 333 seconds in 6 dpf and 12 dpf larval zebrafish. It was performed for 5 planes (each 10 µm apart) of the PCL, and the GCaMP6s fluorescent emission was analyzed in the third PC plane of all fish (Fig. 3.14E).

It was observed that Ca^{2+} transients in PCs at 6 dpf displayed a disrupted activity in the SCA1 zebrafish. The *Atx1[82Q]*-expressing larvae displayed abnormal pattern of PC neuronal activity when compared to the control and *Atx1[30Q]*-expressing larvae (Fig. 3.13A). At 12 dpf, not only *Atx1[82Q]*-, but also *Atx1[30Q]*-expressing larvae showed altered activity of Ca^{2+} transients in PCs when compared to the control larvae (Fig. 3.13B). Having a closer look at a representative one minute of Ca^{2+}-transient activity in PCs from a single fish per group, the observation of the disrupted activity in the SCA1 fish was confirmed. This representative minute was taken from the middle of the image recording period starting after 160 seconds of recording. The PC activity, indicated by the fluorescent emission of the Ca^{2+} indicator GCaMP6s, in the *Atx1[82Q]* strain at 6 dpf seemed to be weaker than both the control and the *Atx1[30Q]* strains that showed almost similar activity pattern (Fig. 3.14A). However, the *Atx1[30Q]* and the *Atx1[82Q]* transgenic strains displayed affected physiology at 12 dpf (Fig. 3.14B).

Two-way ANOVA with post hoc Tukey's test was performed to compare zebrafish groups from the three transgenic strains at each age. It was confirmed that neuronal activity of PCs in

the *Atx1[82Q]* strain at 6 dpf was reduced with significant differences from the control and the *Atx1[30Q]* strains (Fig. 3.14C). Interestingly, later at 12 dpf, there was no significant difference between the *Atx1[30Q]* and *Atx1[82Q]* transgenic strains. Nevertheless, both of them displayed altered activity with significant differences from the control strain (Fig. 3.14D). The results of calcium imaging suggest that the affected morphology followed by neurodegeneration of zebrafish PCs expressing the human SCA1-causing *Atx1[82Q]* allele was pre-accompanied with an early disruption in the PC physiology. In addition, overexpression of the human non-pathogenic *Atx1[30Q]* allele also seems to affect the physiology of zebrafish PCs, although it does not lead to neurodegeneration. Thus, the human non-pathogenic *Atx1[30Q]* allele affects zebrafish PCs to a lesser extent.

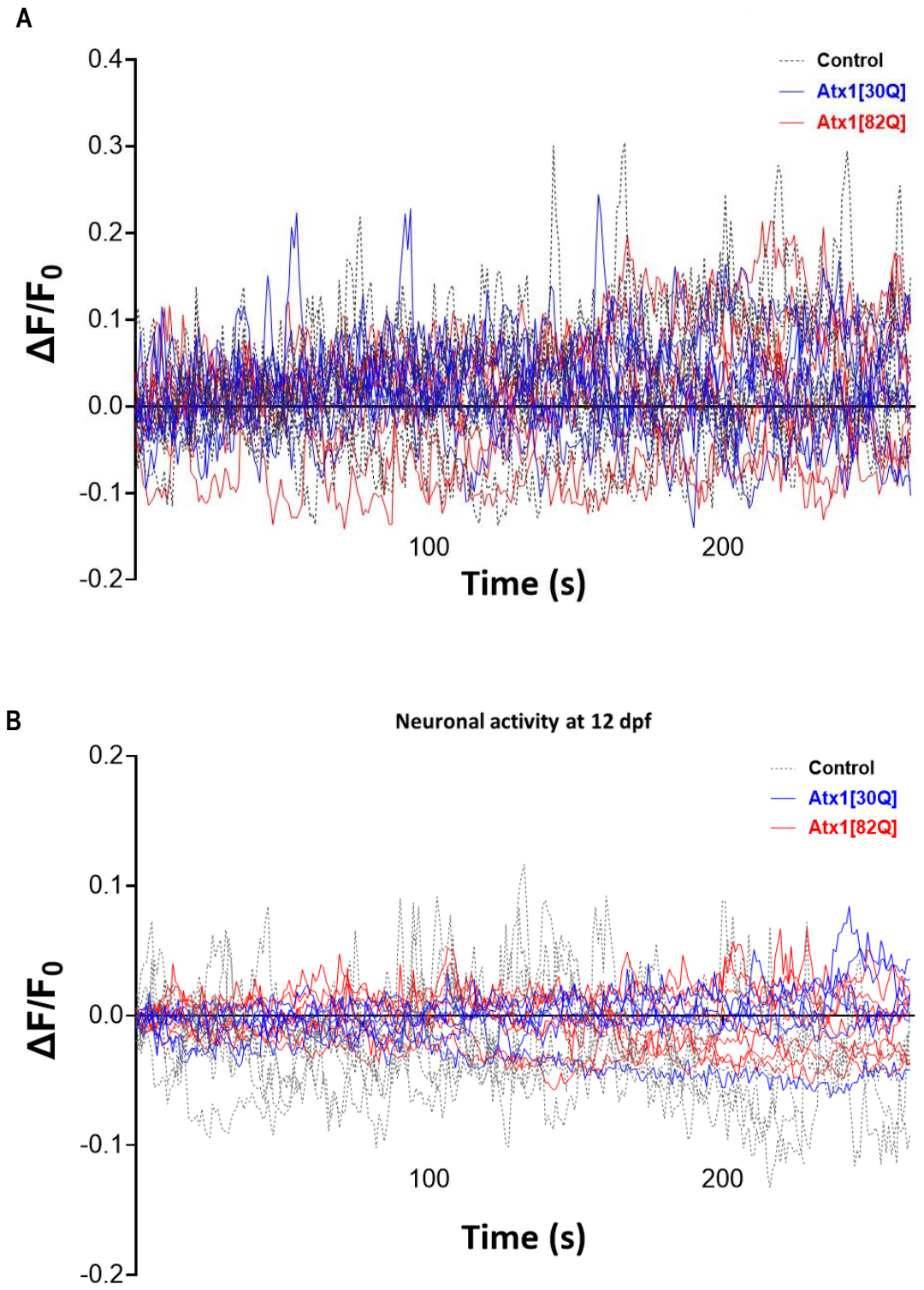

Figure 3.13 Altered neuronal activity of the larval SCA1-affected PCs

(A) At 6 dpf, the fluorescent emission of the calcium indicator GCaMP6s in the PCL of a fish group from each transgenic strain over 265 seconds indicates an abnormally-decreased neuronal activity in the *Atx1[82Q]* strain. N = 7, 8, 7 in control, *Atx1[30Q]* and *Atx1[82Q]* groups, respectively.

(B) At 12 dpf, the fluorescent emission of the calcium indicator GCaMP6s in the PCL of a fish group from each transgenic strain over 265 seconds indicates an abnormally-decreased neuronal activity not only in the *Atx1[82Q]* strain, but also in the *Atx1[30Q]* strain. N = 6, 6, 7 in control, *Atx1[30Q]* and *Atx1[82Q]* groups, respectively.

Each color represents a transgenic strain.

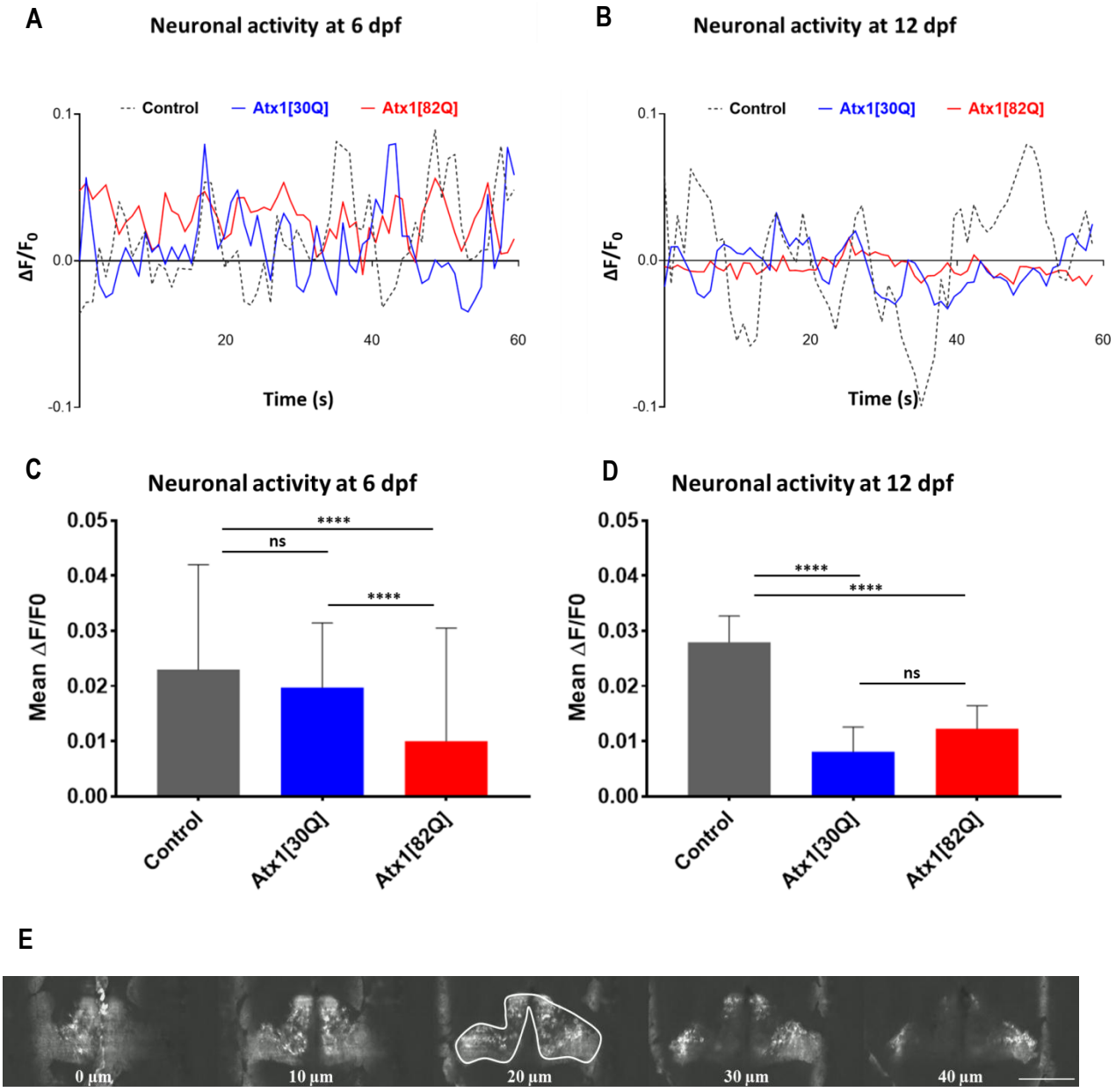

Figure 3.14 Purkinje neurons display disrupted physiology in the *Atx1[82Q]* and *Atx1[30Q]* transgenic strains starting either at 6 dpf or at 12 dpf, respectively

(A) Representative one-minute data of calcium-transient activity in the PCL of individual larva from each transgenic strain at 6 dpf reveal a decreased neuronal activity in the *Atx1[82Q]* strain.

(B) Representative one-minute data of calcium-transient activity in the PCL of individual larva from each transgenic strain at 12 dpf reveal a decreased neuronal activity not only in the *Atx1[82Q]* strain, but also in the *Atx1[30Q]* strain.

(C) Quantitative data analysis of calcium-transient activity in the PCL at 6 dpf confirms the disrupted neuronal physiology in the *Atx1[82Q]* strain. N = 7, 8, 7 in control, *Atx1[30Q]* and *Atx1[82Q]* groups, respectively.

(D) Quantitative data analysis of calcium-transient activity in the PCL at 12 dpf confirms the disrupted neuronal physiology not only in the *Atx1[82Q]* strain, but also in the *Atx1[30Q]* strain. N = 6, 6, 7 in control, *Atx1[30Q]* and *Atx1[82Q]* groups, respectively.

(E) Representative frame shows the stack calcium imaging (5 planes each 10 µm apart) of the PCL by digital light-sheet microscopy. The fluorescent emission of the Ca^{2+} indicator GCaMP6s was analyzed in the third PC plane of all fish.

Each color in A-D represents a transgenic strain. Data in C and D are presented as mean ± SEM; ****p < 0.0001.

3.5 SCA1 zebrafish display behavioral abnormalities

SCA1 zebrafish tended to swim at the bottom of their tanks in the fish facility in case of exposure to any disturbance such as moving the tank to take out some fish for crossing or for an experiment. Therefore, a specific behavioral test to assess such phenotype was needed. The novel tank diving test is a behavioral test used to characterize the exploratory behavior in zebrafish. It exploits the natural tendency of zebrafish to initially dive to the bottom of a novel experimental tank, with a gradual increase in the vertical exploratory activity over time. The novel tank diving test is a comprehensively-studied model for evaluating zebrafish exploratory behavior in a novel environment (Maximino et al. 2010).

Therefore, age-dependent behavioral analysis in the novel tank diving test at 40 dpf, 2 mpf and 3 mpf was performed for fish groups from the control, *Atx1[30Q]* and *Atx1[82Q]* strains. During 6-minute video recording for each individual fish in the novel tank diving test, the aspects that express the exploratory behavior such as the percentage of time spent in the upper half of the tank (Fig. 3.15), the latency until the first visit to the upper half (Fig. 3.16) and the minimum swimming velocity (Fig. 3.17) were measured. Additionally, the whole distance traveled in the novel tank (Fig. 3.18A), the number of transitions to the upper half (Fig. 3.18B), the average swimming velocity (Fig. 3.18C) and the maximum swimming velocity (Fig. 3.18D) were measured to evaluate the locomotor activity. Two-way ANOVA with post hoc Tukey's test was used for data analysis.

On the one hand, the elements indicting the exploratory behavior showed interesting results. Zebrafish expressing the human *Atx1[82Q]* allele specifically in PCs tended to spend less percentage of time in the upper half of the novel tank during the 6-minute test, when compared to the control and *Atx1[30Q]* transgenic strains (Fig. 3.15). Changes in time spent in the upper half started at late juvenile stage (2 mpf) and increased at adult stage (3 mpf). However, at early juvenile stage (40 dpf), there were no significant differences between the three fish strains. In addition, despite the significant increase in the time spent in upper half from 40 dpf to later stages in the control groups, the SCA1 fish showed non-significant increase from 40 dpf to 2 mpf and decrease at 3 mpf (Fig. 3.15). These data suggest that SCA1-affected zebrafish show age-dependent progressive reduction in the exploratory behavior indicated by the progressive escalation of the difference from the control groups in time spent in the upper half of the novel tank.

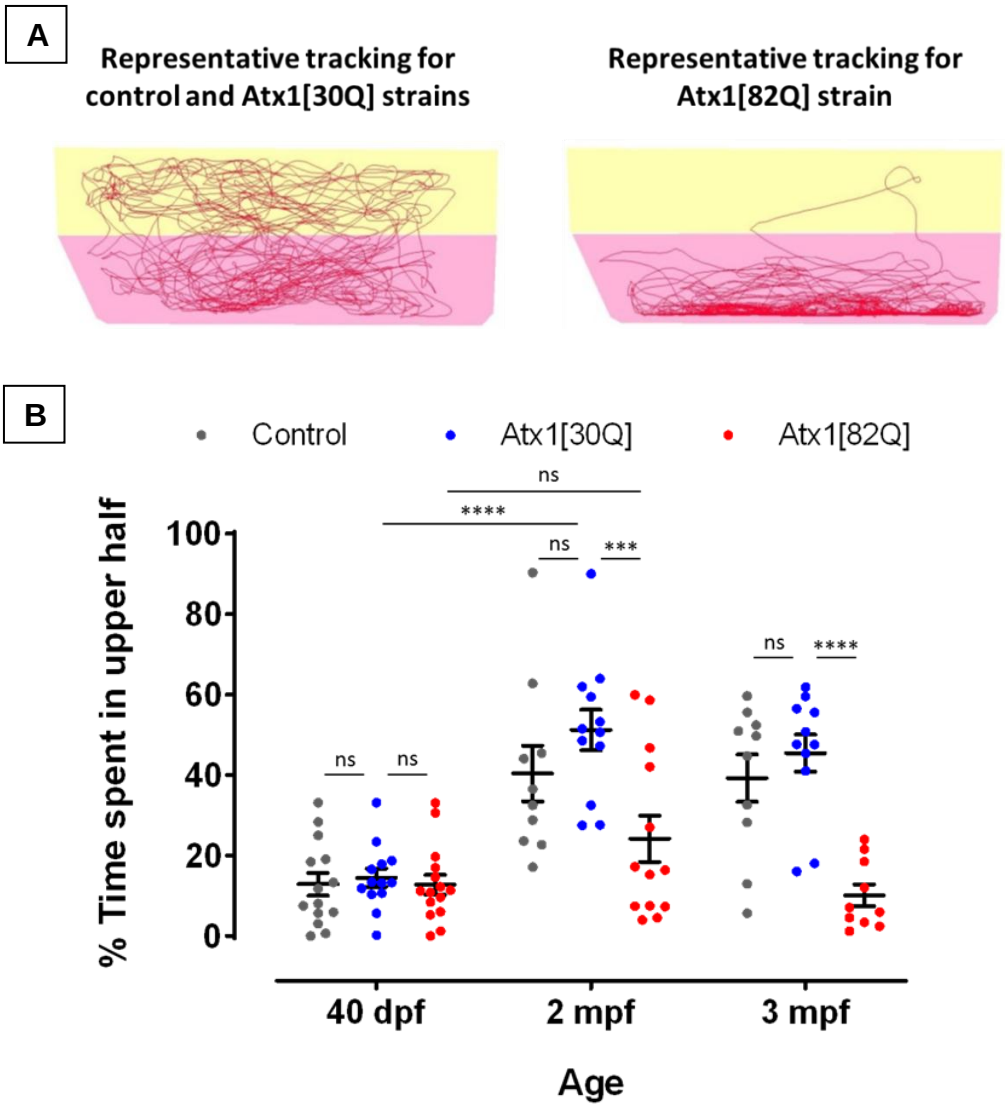

Figure 3.15 Age-dependent analysis of time spent in the upper half during the novel tank diving test for a stable transgenic zebrafish model for SCA1

(A) Representative profile of tracked movements of a 3-mpf individual fish in the novel tank for 6 minutes displays the exploration of the upper half by the fish from control strains and the preference of the *Atx1[82Q]* fish to remain in the bottom for almost the entire recording period.

(B) Long term analysis of zebrafish behavior in the novel tank diving test reveals that fish expressing the human *Atx1[82Q]* allele specifically in PCs showed non-significant increase from 40 dpf to 2 mpf and decrease at 3 mpf in the percentage of time spent in the upper half of the tank during the 6-minute test, although the control groups showed significant increase in the time spent in upper half from 40 dpf to older stages. Data are presented as mean ± SEM; ***$p < 0.001$ and ****$p < 0.0001$. N = 14, 10, 10 in 40 dpf, 2 mpf and 3 mpf control groups; N = 13, 12, 11 in 40 dpf, 2 mpf and 3 mpf *Atx1[30Q]* groups; and N = 15, 13, 10 in 40 dpf, 2 mpf and 3 mpf *Atx1[82Q]* groups, respectively.

SCA1 zebrafish did not display significant decrease from 40 dpf to 2 mpf regarding the time spent in the lower half of the novel tank before the first exploration of the upper half (latency to the first upper visit) (Fig. 3.16). However, the control and *Atx1[30Q]* transgenic strains displayed significant decrease in such latency from 40 dpf to 2 mpf. Nevertheless, not only the *Atx1[82Q]* but also the control and *Atx1[30Q]* transgenic strains showed non-significant decrease in the latency to the first upper visit from 2 mpf to 3 mpf. These data also suggest that SCA1-affected zebrafish show a reduced exploratory behavior as they did not show significantly faster movement to the upper half of the tank from 40 dpf to 2 mpf as shown in the control groups (Fig. 3.16).

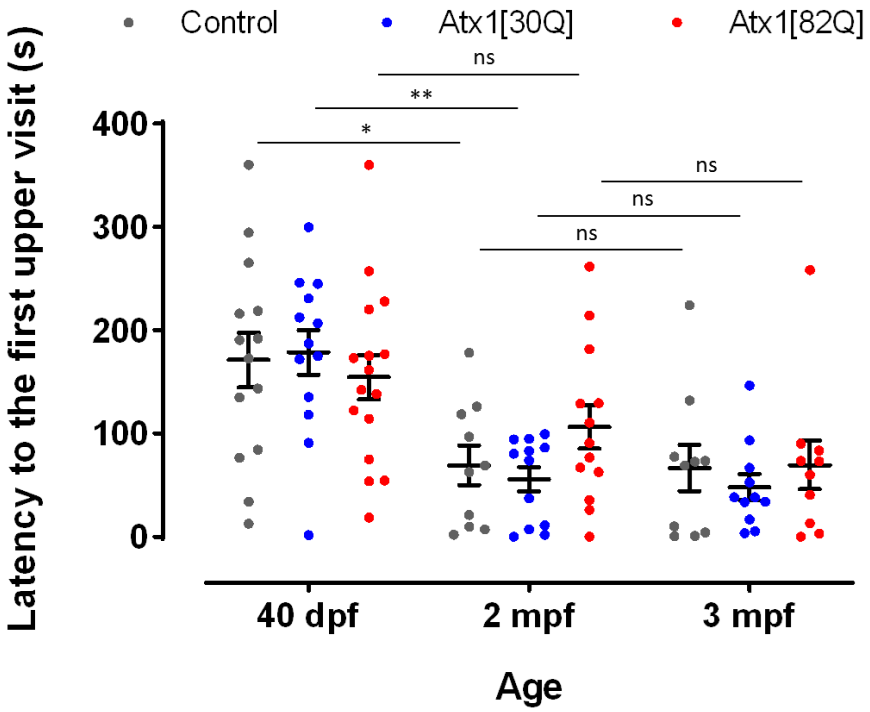

Figure 3.16 Age-dependent analysis of latency until first visit to the upper half at the novel tank diving test for a stable transgenic zebrafish model for SCA1

Long term analysis of zebrafish behavior in the novel tank diving test reveals that fish expressing the human *Atx1[82Q]* allele specifically in PCs showed non-significant decrease in the latency until the first exploration of the upper half from 40 dpf to 2 mpf. The control and *Atx1[30Q]* transgenic strains showed significant decrease. Data are presented as mean ± SEM; *p < 0.05 and **p < 0.01. N = 14, 10, 10 in 40 dpf, 2 mpf and 3 mpf control groups; N = 13, 12, 11 in 40 dpf, 2 mpf and 3 mpf *Atx1[30Q]* groups; and N = 15, 13, 10 in 40 dpf, 2 mpf and 3 mpf *Atx1[82Q]* groups, respectively.

Furthermore, fish expressing the human *Atx1[82Q]* allele specifically in PCs did not display significant increase in the minimum velocity from early juvenile (40 dpf) to adult stage (3 mpf) (Fig. 3.17). However, the control and *Atx1[30Q]* transgenic strains displayed significant increase in the minimum velocity from early juvenile to adult stage. Although the difference between SCA1 fish and control fish at the juvenile stages (40 dpf and 2 mpf) was not significant, there was a significant difference between adult SCA1 fish and adult control fish. These data confirm that SCA1-affected zebrafish show a reduced exploratory behavior indicated by the tendency to freeze in such a novel environment (Fig. 3.17).

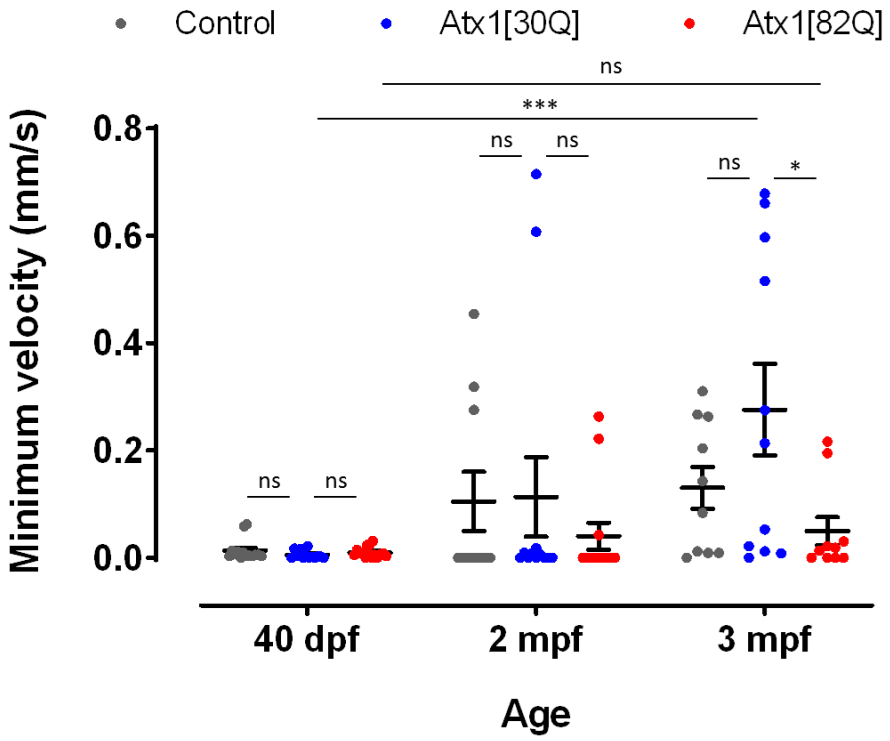

Figure 3.17 Age-dependent analysis of minimum velocity during the novel tank diving test for a stable transgenic zebrafish model for SCA1

Long term analysis of zebrafish behavior in the novel tank diving test reveals that the *Atx1[82Q]* transgenic fish displayed non-significant increase in the minimum velocity from 40 dpf to 3 mpf. The control and *Atx1[30Q]* transgenic strains displayed significant increase in the minimum velocity from 40 dpf to 3 mpf. Data are presented as mean ± SEM; *p < 0.05 and ***p < 0.001. N = 14, 10, 10 in 40 dpf, 2 mpf and 3 mpf control groups; N = 13, 12, 11 in 40 dpf, 2 mpf and 3 mpf *Atx1[30Q]* groups; and N = 15, 13, 10 in 40 dpf, 2 mpf and 3 mpf *Atx1[82Q]* groups, respectively.

On the other hand, when parameters for locomotor activity were analyzed, SCA1 fish did not show significant differences from the control strains at all stages in number of transitions or in average and maximum velocity (Fig. 3.18B-D). However, regarding the distance traveled, although the control strains showed significant increase from early (40 dpf) to late (2 mpf) juvenile stages, the SCA1 fish did not (Fig. 3.18A). These data suggest that SCA1-affected zebrafish are able to move almost as same as the control strains without obvious locomotor abnormalities being detected.

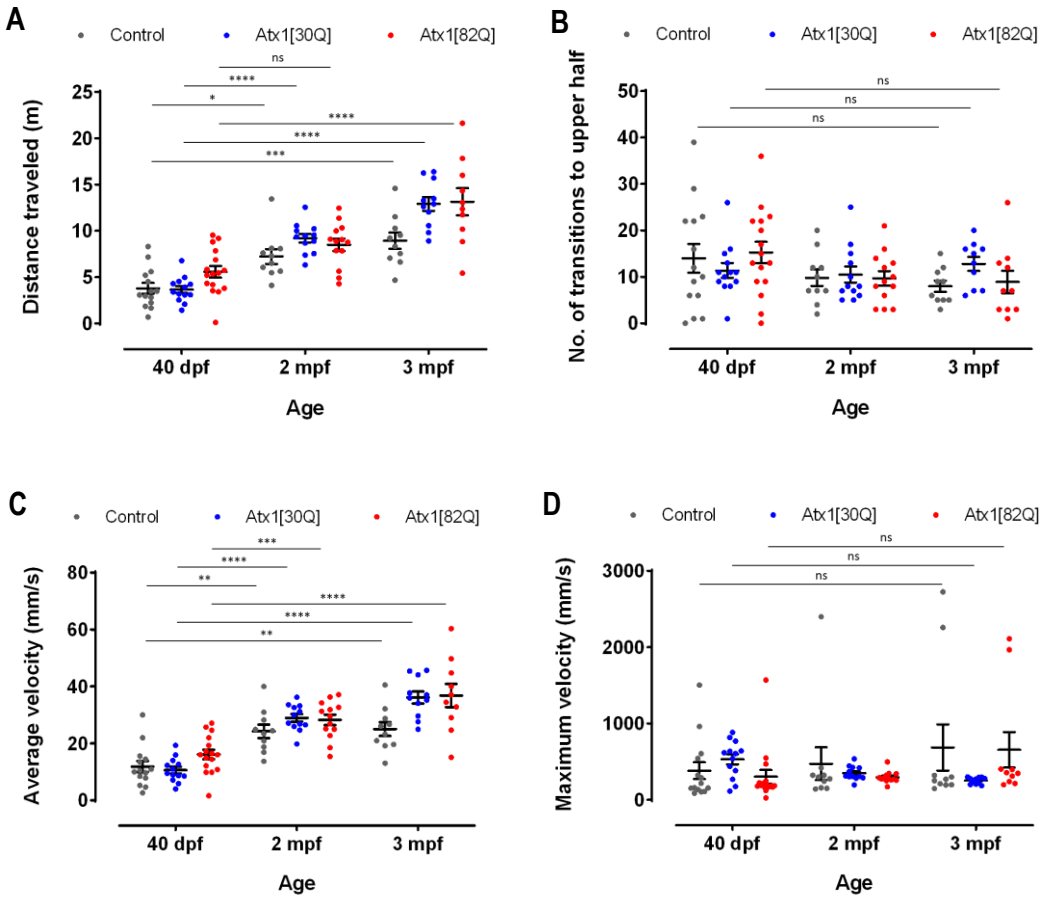

Figure 3.18 Age-dependent analysis of distance traveled, velocity and number of transitions to the upper half in the novel tank diving test for a stable transgenic zebrafish model for SCA1

Long Long term analysis of zebrafish behavior in the novel tank diving test reveals that fish expressing the human *Atx1[82Q]* allele specifically in PCs did not display obvious locomotor deficits. However, they showed some difference from the control strains as they did not show significant increase in the whole distance traveled in the novel tank from 40 dpf to 2 mpf.

(A) Analysis of the whole distance traveled.

(B) Analysis of the number of transitions to the upper half.
(C) Analysis of the average velocity.
(D) Analysis of the maximum velocity.
Data are presented as mean ± SEM; *p < 0.05, **p < 0.01, ***p < 0.001 and ****p < 0.0001. N = 14, 10, 10 in 40 dpf, 2 mpf and 3 mpf control groups; N = 13, 12, 11 in 40 dpf, 2 mpf and 3 mpf *Atx1[30Q]* groups; and N = 15, 13, 10 in 40 dpf, 2 mpf and 3 mpf *Atx1[82Q]* groups, respectively.

4 Discussion

4.1 Genetic modeling of SCA1 in zebrafish

The detailed molecular mechanisms behind polyQ-expanded Atx1 pathogenesis are still unknown (Rousseaux et al. 2018; Lee et al. 2021). In addition, there are at present no disease-modifying cures that exist for SCA1 patients being managed by palliative care only (Bondar et al. 2018; Nitschke et al. 2021). The *Atx1* gene family in zebrafish was characterized and two homologs were identified, *Atx1a* and *Atx1b*, which are conserved in the human *Atx1* gene and expressed in the zebrafish cerebellum; the vulnerable site of SCA1 pathogenesis in humans (Carlson et al. 2009b). Therefore, Carlson and his colleagues suggested that SCA1 can be genetically modeled in zebrafish resulting in a useful model for studying the pathology of SCA1 as well as screening of the toxicity and bioactivity of many candidate drugs before testing on large animal models. In this study, a genetic disease model for SCA1 in zebrafish was generated. Such a novel model with unique features, together with the other established models, will make it easier to better understand the pathological mechanisms, to follow the disease progression *in vivo*, to identify druggable targets, and to faster screen various candidate therapeutic and neuroprotective compounds.

In order to model the SCA1 human disease in zebrafish, a stable transgenic strain expressing the human mutant Atx1[82Q] protein was generated and a systematic analysis was performed in the larval stage (6 dpf and 12 dpf), the juvenile stage (40 dpf and 2 mpf) and the adult stage (3 mpf). Furthermore, as a control, another two stable transgenic strains were established expressing either the red fluorescent protein GAPmScarlet (Bindels et al. 2017) only or the human non-pathogenic Atx1[30Q] protein together with GAPmScarlet. The results revealed pathological phenotypes in the *Atx1[82Q]* strain that started from the early larval stages and got progressively worse. At the larval stages, physiological abnormalities in the activity of PCs were observed. Afterwards, SCA1 zebrafish started to display neurodegeneration of PCs at the early juvenile stage without showing behavioral deficits. Late juvenile as well as adult stages displayed a robust PC neurodegeneration as well as a reduced exploratory behavior.

4.2 Neurodegenerative effects of the polyglutamine toxicity

Some neurodegenerative diseases are characterized by abnormal folding and aggregation of the polyQ-containing proteins due to aberrant expansion of CAG-repeat sequence in the coding region of the corresponding genes, that translates into a long polyQ tract in the proteins (Fan et al. 2014). The length of the expanded CAG repeats may increase while passing from one generation to the next. These so-called polyQ diseases exhibit superior degeneration of specific cell types, in spite of the wide expression of the mutant genes in various cell types. The polyQ neurodegenerative disorders display disease onset in midlife which gets progressively worse (Lieberman et al. 2019). As yet, nine polyQ disorders have been identified: six SCA types 1, 2, 3, 6, 7, 17; Huntington's disease (HD); spinal and bulbar muscular atrophy (SBMA); and dentatorubral pallidoluysian atrophy (DRPLA) (Fan et al. 2014; Lieberman et al. 2019). It has been shown over recent years that the toxicity of polyQ SCAs is induced mainly by genetic and epigenetic deregulations (Niewiadomska-Cimicka et al. 2020).

In order to understand the pathological mechanisms behind polyQ toxicity, various animal models for polyQ disorders were established. Animal models for SCA1 started to be generated after the identification of the SCA1 causative gene (Zoghbi et al. 1991; Ranum et al. 1991) and the gene's mutation involved in the protein's pathogenesis, which is the abnormal expansion of the trinucleotide CAG repeats resulting in an extended polyQ tract (Orr et al. 1993). As a first SCA1 model, a stable transgenic neurodegeneration model in mice could be successfully generated by expressing the human mutant gene *Atx1[82Q]* with an expanded CAG tract specifically in PCs (Burright et al. 1995). As in the current study, Burright and his colleagues generated another transgenic animal expressing the human non-pathogenic gene *Atx1[30Q]* with a normal CAG tract as control. The findings of the current study are consistent with theirs as the *hAtx1[82Q]*-expressing mice and zebrafish displayed PC neurodegeneration and consequently behavioral deficits, while the *hAtx1[30Q]*-expressing mice and zebrafish did not.

The study by Burright and coworkers (1995) stated that the pathological mechanism behind neurodegeneration caused by polyQ expansions is unclear. However, it reported that the neurodegeneration phenotype observed in SCA1 transgenic mice carrying human mutant *Atx1* cDNA obviously reveals that PCs of mice are susceptible to SCA1 pathological mechanisms and that the cellular proteins involved in SCA1 pathology are conserved in mice. Thus, the

neurodegeneration phenotype observed in SCA1 transgenic zebrafish carrying human mutant *Atx1* cDNA indicate that PCs of zebrafish are susceptible to SCA1 pathological mechanisms and that the cellular proteins involved in SCA1 pathology are also conserved in zebrafish.

Moreover, it was shown by immunostaining of human Atx1 protein in transgenic mice using anti-Atx1 antisera that human Atx1 was only detectable in Atx1[30Q]-expressing mice at different ages between 6 and 24 weeks old. However, human Atx1 was not detectable at all in Atx1[82Q]-expressing mice at different ages between 4 and 19 weeks old (Burright et al. 1995). Interestingly, the immunostaining of the HA-tagged human Atx1 protein in the current zebrafish model showed that human Atx1 was detectable in Atx1[30Q]-expressing zebrafish at 4 dpf (Fig. 3.4A) and at the adult stage (Fig. 3.8g). However, in Atx1[82Q]-expressing zebrafish, human Atx1 was only detectable in young PCs at 4 dpf (Fig. 3.4B) and almost entirely disappeared at the adult stage (Fig. 3.8h). It was concluded by Burright and his colleagues that mutant Atx1[82Q] expressed in PCs is either degraded or modified, and this might also be the situation in zebrafsh PCs.

In terms of cellular proteins involved in SCA1 pathology, it was found that the nuclear accumulation of mutant polyQ-expanded Atx1 is insufficient for its pathogenesis. However, its pathogenesis is induced exclusively by the interaction with the transcriptional repressor CIC forming the polyQ-expanded Atx1-CIC large protein complex (Rousseaux et al. 2018). This complex exerted its toxicity in SCA1 patient-derived neurons and PCs of SCA1 transgenic mice by a gain-of-function pathological mechanism. This was concluded through an interesting experiment where the interaction between polyQ-expanded Atx1 and CIC was disrupted in *Atx1[82Q]V591A;S602D* transgenic mice carrying the human pathogenic allele *Atx1[82Q]* with mutations of two critical residues in the AXH domain, valine 591 (V591A) and serine 602 (S602D). Such disruption resulted in the absence of cerebellar pathology, in spite of the presence of aggregates of mutant polyQ-expanded Atx1 in PCs (Rousseaux et al. 2018).

Atx1 forms also another large protein complex by binding to the RNA splicing factor RBM17 (Lim et al. 2008). Mutant polyQ-expanded Atx1 has higher tendency to associate with RBM17 than normal Atx1. Therefore, there was an increase in the polyQ-expanded Atx1-RBM17 protein complexes in SCA1 transgenic mice that could result in irregular splicing of mRNA of important genes leading to neuronal dysfunction and death (Carlson et al. 2009a). Consequently, the conservation of CIC and RBM17 cellular proteins in zebrafish (Woods et al.

2005; Chen et al. 2014; Mehjabin et al. 2019) might play a big role in the vulnerability of zebrafish PCs to SCA1 pathology through their interaction with the human mutant Atx1[82Q] which makes zebrafish a realistic model for SCA1.

Furthermore, a *Drosophila* model for SCA1 was established where combinatorial genetics (GAL4/UAS system) was used to also express either the human wild-type *Atx1[30Q]* or the human pathogenic *Atx1[820Q]* genes in transgenic fruit flies in a controlled manner (Fernandez-Funez et al. 2000). However, the expression was directed to the retina of the eye. It was reported that the relatively high expression of the *Atx1[30Q]* allele can unexpectedly lead to pathological phenotypes as same as those produced by *Atx1[820Q]* allele (Fernandez-Funez et al. 2000). These findings are not fully consistent with the current model where overexpression of the human *Atx1[30Q]* allele in zebrafish did not induce neurodegeneration like overexpression of the human *Atx1[82Q]* allele (Fig. 3.5, 3.6 and 3.7).

In zebrafish, the first model for polyQ toxicity reported that zebrafish embryos can recapitulate the features of the human polyQ diseases, characterized by protein aggregation as well as polyQ length-dependent toxicity, through expressing polyQ tracts of different lengths (19Q, 35Q, 56Q and 80Q) fused to GFP in zebrafish embryos (Miller et al. 2005). The *Atx1[30Q]* and *Atx1[82Q]* transgenic zebrafish strains in the current study replicated this polyQ length-dependent toxicity. On the one hand, the *Atx1[82Q]* strain started to show pathological phenotype in PCs at 6 dpf, earlier than the *Atx1[30Q]* strain which started to show similar pathological phenotype at 12 dpf (Fig. 3.13 and 3.14). On the other hand, the human mutant *Atx1[82Q]* induced neurodegeneration of PCs, while human wild-type *Atx1[30Q]* did not induce such neurodegeneration (Fig. 3.5, 3.6 and 3.7). As Miller and his colleagues expressed polyQ tracts non-specifically in zebrafish embryos, they recommended that developing specific expression systems in the nervous system of zebrafish is required for more precise polyQ disease modeling in such simple vertebrate (Miller et al. 2005). The current SCA1 model with PC-specific expression system could accomplish this goal.

Additionally, transient transgenic zebrafish model for the human polyQ disease, Huntington disease, was generated (Schiffer et al. 2007). It was generated by injection of mRNA expressing an N-terminal fragment of the protein involved in Huntington disease containing different polyQ repeat numbers Htt[4Q], Htt[25Q] and Htt[102Q] into the first or second cell stage of zebrafish embryos. The Htt[4Q] and Htt[25Q] proteins did not show accumulated aggregates. However, the mutant protein Htt[102Q] showed accumulated aggregates after 24

hours in most embryos reminiscent of the aggregates of both human proteins Atx1[30Q] and Atx1[82Q] observed in 4 dpf larvae (Fig. 3.4). Such polyQ disease model in zebrafish was generated in a transient manner by injecting the related mRNA in zebrafish embryos (Schiffer et al. 2007). Therefore, the current SCA1 model is a competitive model, offering a novel zebrafish model of a polyQ disease with a cell-specific expression of the involved pathogenic human protein in a stable transgenic manner, available for future studies.

The neurodegeneration phenotype shown in the current study was getting stronger in an age-related progredient manner (Fig. 3.12). This progressive phenotype highly mimics the progression of the human SCA1 disease which is known to be a progredient disease (Buijsen et al. 2019). Such progressive neurodegeneration phenotype in PCs was also shown in a zebrafish model for SCA13 (Namikawa et al. 2019b). Contrary to the findings in SCA1 zebrafish, overexpression of the SCA13 disease causing gene *kcnc3a*^{R355H} within zebrafish PCs, under control of the same PC-specific enhancer element, resulted in robust neurodegeneration of zebrafish PCs in the SCA13 zebrafish model as early as 4 dpf. In order to establish the SCA13 model, Namikawa and his colleagues isolated a compact regulatory element of 258 bp, *cpce*. The *cpce* enhancer drives expression specifically in PCs. 2x2 Copies of this regulatory element were used to overexpress the SCA13 mutant gene in zebrafish PCs (Namikawa et al. 2019b), while 2x4 copies were used to overexpress the SCA1 mutant gene in PCs of the current SCA1 model. The neurodegeneration in the SCA13 model was clearly earlier than in the current SCA1 model in spite of the fewer copy number of the enhancer (2x2 copies instead of 2x4). However, the progressive neurodegenertaion of PCs indicated by Namikawa and his colleagues in the SCA13 larvae at 4, 7, 11 and 14 dpf was in line with the progressive neurodegenertaion observed in the SCA1 fish in older stages at 40 dpf, 2 mpf and 3 mpf. The difference in the starting age of the neurodegeneration phenotype might be due to the different pathological mechanisms of SCA13 and SCA1 neurodegenerative diseases.

4.3 Purkinje cell physiological deficits in the SCA1 zebrafish model

It was important to investigate whether the physiological properties of larval PCs in the SCA1 zebrafish were affected by the expression of human Atx1[82Q]. Therefore, calcium imaging was performed to assess the activity of PCs and to resolve whether the larval PCs expressing either the human non-pathogenic allele *Atx1[30Q]* or the human disease-causing allele *Atx1[82Q]* were physiologically affected although they did not seem to be morphologically affected. Although *Atx1[30Q]* did not induce neurodegeneration as *Atx1[82Q]* did in juvenile and adult stages, both of the human proteins could induce physiological deficits in larval zebrafish PCs. This might be due to the presence of aggregates of both polyQ human proteins Atx1[30Q] and Atx1[82Q] in larval zebrafish PCs as early as 4 dpf (Fig. 3.4A, B, respectively). However, the difference between both transgenic strains was that the *Atx1[82Q]* strain started to display such deficits at younger ages than the *Atx1[30Q]* strain. At 6 dpf, the *Atx1[82Q]* strain showed weaker activity than both the control and the *Atx1[30Q]* strains (Fig. 3.13A and 3.14A, C). At 12 dpf, both the *Atx1[30Q]* and the *Atx1[82Q]* strains showed weaker activity than the control strain (Fig. 3.13B and 3.14B, D). The activity was assessed by the detection of calcium-transient activity during spontaneous PC activities over time.

Fernandez-Funez and coworkers showed that not only the human pathogenic allele *Atx1[82Q]*, but also the high levels of human non-pathogenic allele *Atx1[30Q]* induced a similar neurodegenerative phenotype in PCs of transgenic mice. The difference was just that the pathology of such high levels of the human wild-type allele *Atx1[30Q]* required longer time to appear. The pathology of *Atx1[82Q]* appeared in the 12-15 week old mice, but the pathology of *Atx1[30Q]* started to be seen in the 59 week old mice (Fernandez-Funez et al. 2000). The current physiology results at 6 and 12 dpf build on this existing evidence as the neuronal-activity data in zebrafish revealed that overexpression of the human wild-type gene *Atx1[30Q]* in PCs caused a pathological phenotype similar to the phenotype induced by the human mutant gene *Atx1[82Q]*. The only difference was also that the pathology of *Atx1[30Q]* was seen at 12 dpf, later than the pathology of *Atx1[82Q]* which appeared already as early as 6 dpf (Fig. 3.13 and 3.14).

Furthermore, interesting results were shown in a polyQ disease model for SCA7 in zebrafish. For modeling the SCA7 disease in zebrafish, the gene Ataxin-7 was knocked down which

consequently impaired the differentiation of PCs (Yanicostas et al. 2012). This loss-of-function disease model is quite different from the current gain-of-function disease model, but both SCA models display a neurodegenerative phenotype of zebrafish PCs. In keeping with the pathophysiological alteration in SCA1 zebrafish at 6 dpf (Fig. 3.13A and 3.14A, C), a pathological phenotype was also observed in PCs of SCA7 zebrafish at an early larval stage (5 dpf). However, such pathological phenotype in SCA7 zebrafish was not just physiological changes in PCs, but a severe reduction in the number of PCs as early as 5 dpf was reported.

In addition, a marked decrease was indicated in the number of PCs expressing retinoid-related orphan nuclear receptor α (RORα), a transcription factor belonging to the family of retinoid-related orphan nuclear-receptors and critical for proper differentiation of PCs (Yanicostas et al. 2012). Interestingly, such down regulation of RORα was also observed in the *hAtx1[82Q]* knock-in neurodegeneration mouse model of SCA1 (Serra et al. 2006). Moreover, a down regulation of the genes controlled by RORα was reported. It was concluded that the decreased expression of RORα enhanced the *hAtx1[82Q]* toxicity and that the down regulation of RORα-mediated genes during development is a key factor in the vulnerability of PCs to SCA1. Therefore, Serra and his colleagues suggested that the failure of neurons to entirely develop, even in the absence of an immediate phenotype, can lead to a weaker ability of adult neurons to survive. This interpretation might also be convenient for the results of the current study as the late juvenile and adult neurons were not able to survive (Fig. 3.6 and 3.7), although the immediate effect of the pathogenic allele *hAtx1[82Q]* on PCs at the early larval stages was not very robust. Therefore, RORα needs to be investigated in the current zebrafish model as it could be down regulated during the development of the *hAtx1[82Q]*-expressing transgenic zebrafish. Such down regulation might have played a role in the altered neuronal activity of PCs at the 6 and 12 dpf larval stages (Fig. 3.13 and 3.14) and consequently the later progredient neurodegeneration and reduction of PCs at juvenile and adult stages (Fig. 3.12).

4.4 Behavioral abnormalities in the SCA1 zebrafish model

PolyQ SCA disorders display progredient degeneration of the cerebellum and its related structures which results in progredient ataxia in addition to other diverse symptoms (Niewiadomska-Cimicka et al. 2020). SCA1 patients suffer from behavioral deficits that do not only comprise locomotor control defects (ataxia), but also cognitive and emotional defects (Mastammanavar et al. 2020). Interestingly, SCA1 zebrafish displayed also behavioral deficits. In the current study, robust behavioral abnormalities were observed in the zebrafish model of SCA1 in terms of exploratory behavior. Late juveniles as well as adults that demonstrated robust neurodegeneration of PCs displayed a reduced-exploration phenotype. Such phenotype was observed starting from 2 mpf along with the loss of PCs and got worse at 3 mpf with the stronger loss of PCs (Fig. 3.15, 3.16 and 3.17). However, the reduced-exploration phenotype was not observed in early juvenile SCA1 fish at 40 dpf most likely due to less-pronounced PC degeneration. This affected exploratory behavior might reflect an anxiety-related phenotype reminiscent of non-ataxic phenotypes observed in SCA1-affected patients (Egan et al. 2009; Mastammanavar et al. 2020).

In terms of locomotion, no gross locomotor deficits in zebrafish expressing the human pathogenic protein Atx1[82Q] were observed neither at juveniles nor at adults (Fig. 3.18), despite the robust loss of PCs. The regular growth of body size observed in SCA1 zebrafish also suggests that they do not seem to have major locomotor deficits interfering with proper feeding (Fig 3.11). Moreover, the ability of SCA1 fish to mate reflects a proper motor coordination. Since the loss of PCs in the SCA1 zebrafish was observed to be more robust in the anterior region of the PCL (Fig. 3.8c), the unaffected locomotor behavior might be due to the less-pronounced PC degeneration in the medial and dorsal regions of the PCL (Fig. 3.8c). This finding fits to recent results from the Köster lab which demonstrated that PCs in the anterior cerebellum do not show neuronal activity during swimming like PCs in the medial region of the cerebellum (Matsui et al. 2014) (Fig. 4.1).

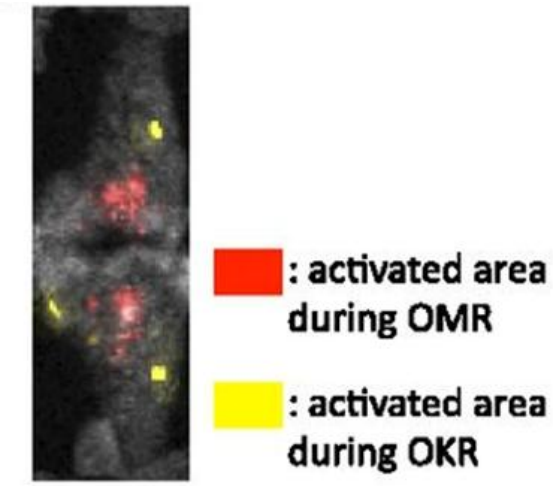

Figure 4.1 Signals of genetically-encoded calcium indicator in the Purkinje cell layer reveal the spatially distinct regions responding to different behavioral paradigms

The figure displays the PC neuronal activity during optomotor response (OMR, red) and optokinetic response (OKR, yellow). It is noticed that there is almost no calcium activity in the anterior PC region during OMR. The image is representative for the experimental group (n = 10/group) and display a dorsal view of larval zebrafish cerebellum (6 dpf), anterior is to the left (Matsui et al. 2014).

In the previously-established polyQ disease model in zebrafish for SCA3 (Machado–Joseph) disease, where either the human non-pathogenic *Atx3[23Q]* or disease causing *Atx3[84Q]* genes were expressed in zebrafish neurons (Watchon et al. 2017) under control of a HuC (*elav*) neuronal specific promoter (Park et al. 2000), the locomotor behavior results were different. Watchon and his colleagues indicated motor impairment in the *Atx3[84Q]* zebrafish that swam shorter distances than the *Atx3[23Q]* zebrafish in an open field behavioral test as early as 6 dpf. However, no significant differences were observed between *Atx1[30Q]* and *Atx1[82Q]* zebrafish in terms of the distance swum in the novel tank diving test until the adult stage (3 mpf) (Fig. 3.18A). Watchon and his colleagues explained that the locomotor deficits they observed are driven by expression of the human mutant *Atx3[84Q]* gene in all zebrafish neurons including the motor neurons. In the current SCA1 model expressing the human mutant polyQ gene *Atx1[82Q]* exclusively in PCs and showing less-pronounced PC loss in the medial and dorsal regions, the exploratory behavior has been affected without major detectable effects on the swimming ability.

4.5 Conclusion and outlook

In this study, zebrafish is introduced to the ataxia research community as a novel SCA1 genetic model with unique characteristics. This neurodegeneration model in zebrafish, mimicking human SCA1 pathology, is a powerful tool to reveal *in vivo* the causative mechanisms of cytotoxicity in SCA1, a neurodegenerative disease for which no cure at present exists. Zebrafish SCA1 model allows for observing affected PCs using fluorescent protein reporters and biosensors and for monitoring the behavioral performance of affected fish in relation to their disease progression. With the accessibility for *in vivo* imaging approaches, these SCA1 zebrafish provide a model to interconnect cellular and molecular pathological mechanisms of PC degeneration with physiological and behavioral studies to offer longitudinal structure-function-behavior relationship insights. The region-specific PC contributions to cerebellar neurodegeneration phenotypes can also be investigated. Furthermore, this model can be used for validating potential compounds against such a devastative neurological disease for their efficacy, blood brain barrier passage and side effects.

In order to perform future studies on this model, it is very important to use the proper control transgenic strains. Therefore, depending on the results of this study that showed physiological abnormalities in PCs of the *Atx1[30Q]* transgenic strain expressing the human non-pathogenic allele *Atx1[30Q]*, it is recommended to use an additional control strain. The additional control transgenic strain used in this study which expresses only a fluorescent reporter protein is a good candidate. A transgenic strain expressing an engineered human *Atx1* allele with a shorter polyQ tract might be also a good candidate control strain.

The interaction of the Atx1 protein with the proteins involved in the SCA1 pathology such as CIC and RBM17 needs to be studied in zebrafish PCs to investigate how the neurodegeneration happened. Furthermore, motor coordination as well as learning of SCA1 zebrafish needs to be investigated in detail for further characterization of the model. A swim channel test is recommended for evaluating locomotor control of the fish against water current with gradually increasing speed (rheotaxis), and classical and operant conditioning tests are recommended for evaluating learning abilities.

It is suggested using 6-dpf larval SCA1 zebrafish for compound-screening studies as it is a good transparent model accessible for *in vivo* bioimaging and it displays an early pathophysiological phenotype to be investigated. Ultimately, this track of research, aiming at modeling neurodegenerative disorders in such cheaply-maintained small vertebrate animal with large amounts of easily-accessible embryos and larvae as well as rapid development, could lead to faster discovery of the pathological mechanisms underlying these disorders and introducing novel paths to treatment.

5 Appendix

5.1 List of figures

Figure no.	Figure legend	Page
1.1	Sagittal MRI from unaffected control (left) and SCA patient (right)	8
1.2	Human Ataxin-1 protein	9
1.3	Schematic model of SCA1 pathology	10
1.4	Illustration of the abnormal protein interactions in SCA1	11
1.5	Purkinje cell morphology in unaffected control mouse (left) and transgenic mouse model of SCA1 (right)	14
1.6	Phenotypes of a SCA1 knock-in mouse model	15
1.7	*Atx1[82Q]-A*^{776} shows a decreased rate of formation of nuclear inclusions in Purkinje cells of a transgenic mouse model of SCA1	16
1.8	The zebrafish cerebellum	19
1.9	Expression pattern of PC-specific GFP under control of the regulatory element *cpce* (*ca8* promoter-derived PC-specific enhancer element) in Tg(*en.cpce-E1B:GFP*)^{bz13} stable transgenic strain	21
1.10	Comparison of the Ataxin-1 protein between human and zebrafish	22
3.1	Genetic modeling of the human SCA1 disease in zebrafish	54
3.2	Generation of stable transgenic zebrafish model for PC-specific SCA1	56
3.3	Expression pattern of GAPmScarlet in the established transgenic strains compared with PC-specific GFP in the transgenic strain Tg(*-7.5ca8:GFP*)^{bz12}	57
3.4	Analysis of human *Atx1*-allele expression in the stable zebrafish transgenic strains	59

3.5	Neurodegenerative effects of overexpression of the human mutant Atx1[82Q] on Purkinje cells of the early juvenile zebrafish	63
3.6	Neurodegenerative effects of overexpression of the human mutant Atx1[82Q] on Purkinje cells of the late juvenile zebrafish	64
3.7	Severe neurodegeneration of Purkinje cell population in the adult SCA1 transgenic zebrafish	65
3.8	Immunohistochemical comparison of adult corpus cerebelli of control and *Atx1*-expressing zebrafish	67
3.9	Histological comparison of adult corpus cerebelli of control and *Atx1*-expressing zebrafish	68
3.10	Analysis of fish body length and dorsal surface of the cerebellum in dissected brains	69
3.11	Body length analysis in a stable transgenic zebrafish model for SCA1	71
3.12	Long term analysis of the area covered by Purkinje cell population in a stable transgenic zebrafish model for SCA1	72
3.13	Altered neuronal activity of the larval SCA1-affected PCs	75
3.14	Purkinje neurons display disrupted physiology in the *Atx1[82Q]* and *Atx1[30Q]* transgenic strains starting either at 6 dpf or at 12 dpf, respectively	77
3.15	Age-dependent analysis of time spent in the upper half during the novel tank diving test for a stable transgenic zebrafish model for SCA1	80
3.16	Age-dependent analysis of latency until first visit to the upper half at the novel tank diving test for a stable transgenic zebrafish model for SCA1	81
3.17	Age-dependent analysis of minimum velocity during the novel tank diving test for a stable transgenic zebrafish model for SCA1	82
3.18	Age-dependent analysis of distance traveled, velocity and number of transitions to the upper half in the novel tank	83

	diving test for a stable transgenic zebrafish model for SCA1	
4.1	Signals of genetically-encoded calcium indicator in the Purkinje cell layer reveal the spatially distinct regions responding to different behavioral paradigms	93

5.2 List of tables

Table no.	Table legend	Page
2.1	Equipment	26
2.2	Chemicals	28
2.3	Enzymes	30
2.4	Antibodies	30
2.5	Fish-related solutions	31
2.6	Cloning solutions	32
2.7	Fixation and staining buffers	33
2.8	Purification kits	33
2.9	Oligonucleotides	34

5.3 List of abbreviations

ANOVA	Analysis of variance
APP	β-Amyloid precursor protein
Atx1	Ataxin-1
AXH	Ataxin-1 and HMG-box protein 1
bp	Base pair
Ca^{2+}	Calcium
Ca8	Carbonic anhydrase VIII
CAG	Cytosine-adenine-guanine
CaM	Calmodulin
Cb	Cerebellum
CC	Crista cerebellaris
CCe	Corpus cerebelli
CFs	Climbing fibers
CIC	Capicua
Cpce	Ca8 promoter-derived PC-specific enhancer element
DAPI	4', 6-Diamidino-2-phenylindole, dihydrochloride
DCN	Deep cerebellar nuclei
dpf	Days post fertilization
ECs	Eurydendroid cells
GABA	γ-Aminobutyric acid
GAP	Growth Associated Protein
GCL	Granule cell layer
GCs	Granule cells

GFP	Green fluorescent protein
GL	Granular layer
hAtx1	Human Ataxin-1
HPLC	High performance liquid chromatography
IO	Inferior olivary nucleus
LB medium	Luria Bertani medium
LCa	Lobus caudalis cerebelli
MFs	Mossy fibers
mir181aT	miRNA181aT
ML	Molecular layer
MON	Medial octavolateralis nucleus
mpf	Months post fertilization
MRI	Magnetic resonance imaging
NLS	Nuclear localization signal
OCT	Optimal cutting temperature compound
pA	Polyadenine
PCL	Purkinje cell layer
Pcp2	Purkinje cell protein 2
PCR	Polymerase chain reaction
PCs	Purkinje cells
PFs	Parallel fibers
PolyQ	Polyglutamine
RBM17	mRNA-binding motif protein 17
RFP	Red fluorescent protein
RORα	Retinoid-related orphan nuclear receptor α

SCA	Spinocerebellar ataxia
SCA1	Spinocerebellar ataxia type 1
Ser	Serine residue
Tel	Telencephalon
TeO	Tectum opticum
TeO	Optic tectum
Tg	Transgene
Va	Valvula cerebelli
zAtxn1a	Zebrafish Ataxin-1a
zAtxn1b	Zebrafish Ataxin-1b

6 References

Aleström, Peter; D'Angelo, Livia; Midtlyng, Paul J.; Schorderet, Daniel F.; Schulte-Merker, Stefan; Sohm, Frederic; Warner, Susan (2019): Zebrafish: Housing and husbandry recommendations. In: *Laboratory animals*, 23677219869037. DOI: 10.1177/0023677219869037.

Bae, Young-Ki; Kani, Shuichi; Shimizu, Takashi; Tanabe, Koji; Nojima, Hideaki; Kimura, Yukiko et al. (2009): Anatomy of zebrafish cerebellum and screen for mutations affecting its development. In: *Developmental Biology* 330 (2), p. 406–426. DOI: 10.1016/j.ydbio.2009.04.013.

Bindels, Daphne S.; Haarbosch, Lindsay; van Weeren, Laura; Postma, Marten; Wiese, Katrin E.; Mastop, Marieke et al. (2017): mScarlet: a bright monomeric red fluorescent protein for cellular imaging. In: *Nature methods* 14 (1), p. 53–56. DOI: 10.1038/nmeth.4074.

Bondar, Vitaliy V.; Adamski, Carolyn J.; Onur, Tarik S.; Tan, Qiumin; Wang, Li; Diaz-Garcia, Javier et al. (2018): PAK1 regulates ATXN1 levels providing an opportunity to modify its toxicity in spinocerebellar ataxia type 1. In: *Human molecular genetics* 27 (16), p. 2863–2873. DOI: 10.1093/hmg/ddy200.

Brochu, G.; Maler, L.; Hawkes, R. (1990): Zebrin II: a polypeptide antigen expressed selectively by Purkinje cells reveals compartments in rat and fish cerebellum. In: *The Journal of comparative neurology* 291 (4), p. 538–552. DOI: 10.1002/cne.902910405.

Buijsen, Ronald A. M.; Toonen, Lodewijk J. A.; Gardiner, Sarah L.; van Roon-Mom, Willeke M. C. (2019): Genetics, Mechanisms, and Therapeutic Progress in Polyglutamine

Spinocerebellar Ataxias. In: *Neurotherapeutics : the journal of the American Society for Experimental NeuroTherapeutics* 16 (2), p. 263–286. DOI: 10.1007/s13311-018-00696-y.

Bullock, W. O.; Fernandez, J. M.; Short J. M. (1987): XL1-Blue, a high-efficiency plasmid transforming recA *Escherichia coli* strain with ß-galactosidase selection. In: *Biotechniques* 5 (3), p. 376–379.

Burright, Eric N.; Brent Clark, H.; Servadio, Antonio; Matilla, Toni; Feddersen, Rodney M.; Yunis, Wael S. et al. (1995): SCA1 transgenic mice: A model for neurodegeneration caused by an expanded CAG trinucleotide repeat. In: *Cell* 82 (6), p. 937–948. DOI: 10.1016/0092-8674(95)90273-2.

Cachat, Jonathan; Stewart, Adam; Grossman, Leah; Gaikwad, Siddharth; Kadri, Ferdous; Chung, Kyung Min et al. (2010): Measuring behavioral and endocrine responses to novelty stress in adult zebrafish. In: *Nature protocols* 5 (11), p. 1786–1799. DOI: 10.1038/nprot.2010.140.

Carlson, Kerri M.; Andresen, J. Michael; Orr, Harry T. (2009a): Emerging pathogenic pathways in the spinocerebellar ataxias. In: *Current opinion in genetics & development* 19 (3), p. 247–253. DOI: 10.1016/j.gde.2009.02.009.

Carlson, Kerri M.; Melcher, Laura; Lai, Shaojuan; Zoghbi, Huda Y.; Clark, H. Brent; Orr, Harry T. (2009b): Characterization of the zebrafish atxn1/axh gene family. In: *Journal of neurogenetics* 23 (3), p. 313–323. DOI: 10.1080/01677060802399976.

Chang, Weipang; Pedroni, Andrea; Hohendorf, Victoria; Giacomello, Stefania; Hibi, Masahiko; Köster, Reinhard W.; Ampatzis, Konstantinos (2020): Functionally distinct Purkinje cell types show temporal precision in encoding locomotion. In:

Proceedings of the National Academy of Sciences of the United States of America 117 (29), p. 17330–17337. DOI: 10.1073/pnas.2005633117.

Chen, TieLin; Zhou, Li; Yuan, Yue; Fang, Yin; Guo, Yue; Huang, HuiZhe et al. (2014): Characterization of Bbx, a member of a novel subfamily of the HMG-box superfamily together with Cic. In: *Development genes and evolution*, p. 261–268. DOI: 10.1007/s00427-014-0476-x.

Chen, Tsai-Wen; Wardill, Trevor J.; Sun, Yi; Pulver, Stefan R.; Renninger, Sabine L.; Baohan, Amy et al. (2013): Ultrasensitive fluorescent proteins for imaging neuronal activity. In: *Nature* 499 (7458), p. 295–300. DOI: 10.1038/nature12354.

Chen, Yu Wai; Allen, Mark D.; Veprintsev, Dmitry B.; Löwe, Jan; Bycroft, Mark (2004): The structure of the AXH domain of spinocerebellar ataxin-1. In: *The Journal of Biological Chemistry* 279 (5), p. 3758–3765. DOI: 10.1074/jbc.M309817200.

Chiara, Cesira de; Menon, Rajesh P.; Strom, Molly; Gibson, Toby J.; Pastore, Annalisa (2009): Phosphorylation of S776 and 14-3-3 binding modulate ataxin-1 interaction with splicing factors. In: *PloS one* 4 (12), e8372. DOI: 10.1371/journal.pone.0008372.

Crespo-Barreto, Juan; Fryer, John D.; Shaw, Chad A.; Orr, Harry T.; Zoghbi, Huda Y. (2010): Partial loss of ataxin-1 function contributes to transcriptional dysregulation in spinocerebellar ataxia type 1 pathogenesis. In: *PLoS genetics* 6 (7), e1001021. DOI: 10.1371/journal.pgen.1001021.

Dallal, Gerard E.; Wilkinson, Leland (1986): An Analytic Approximation to the Distribution of Lilliefors's Test Statistic for Normality. In: *The American Statistician* 40 (4), p. 294. DOI: 10.2307/2684607.

Dohaku, Ryuji; Yamaguchi, Masahiro; Yamamoto, Naoyuki; Shimizu, Takashi; Osakada, Fumitaka; Hibi, Masahiko (2019): Tracing of Afferent Connections in the Zebrafish Cerebellum Using Recombinant Rabies Virus. In: *Frontiers in neural circuits* 13, p. 30. DOI: 10.3389/fncir.2019.00030.

Egan, Rupert J.; Bergner, Carisa L.; Hart, Peter C.; Cachat, Jonathan M.; Canavello, Peter R.; Elegante, Marco F. et al. (2009): Understanding behavioral and physiological phenotypes of stress and anxiety in zebrafish. In: *Behavioural brain research* 205 (1), p. 38–44. DOI: 10.1016/j.bbr.2009.06.022.

Emamian, Effat S.; Kaytor, Michael D.; Duvick, Lisa A.; Zu, Tao; Tousey, Susan K.; Zoghbi, Huda Y. et al. (2003): Serine 776 of Ataxin-1 Is Critical for Polyglutamine-Induced Disease in SCA1 Transgenic Mice. In: *Neuron* 38 (3), p. 375–387. DOI: 10.1016/S0896-6273(03)00258-7.

Fan, Hueng-Chuen; Ho, Li-Ing; Chi, Ching-Shiang; Chen, Shyi-Jou; Peng, Giia-Sheun; Chan, Tzu-Min et al. (2014): Polyglutamine (PolyQ) Diseases: Genetics to Treatments. In: *Cell Transplant* 23 (4-5), p. 441–458. DOI: 10.3727/096368914X678454.

Fernandez-Funez, P.; Nino-Rosales, M. L.; Gouyon, B. de; She, W. C.; Luchak, J. M.; Martinez, P. et al. (2000): Identification of genes that modify ataxin-1-induced neurodegeneration. In: *Nature* 408 (6808), p. 101–106. DOI: 10.1038/35040584.

Goold, Robert; Hubank, Michael; Hunt, Abigail; Holton, Janice; Menon, Rajesh P.; Revesz, Tamas et al. (2007): Down-regulation of the dopamine receptor D2 in mice lacking ataxin 1. In: *Human molecular genetics* 16 (17), p. 2122–2134. DOI: 10.1093/hmg/ddm162.

Gross, Jeffrey M.; Perkins, Brian D. (2008): Zebrafish mutants as models for congenital ocular disorders in humans. In: *Mol. Reprod. Dev.* 75 (3), p. 547–555. DOI: 10.1002/mrd.20831.

Gruol, Donna L.; Koibuchi, Noriyuki; Manto, Mario; Molinari, Marco; Schmahmann, Jeremy D.; Shen, Ying (Hg.) (2016): Essentials of Cerebellum and Cerebellar Disorders. A Primer For Graduate Students. Cham: Springer International Publishing; Imprint Springer.

Hibi, Masahiko; Matsuda, Koji; Takeuchi, Miki; Shimizu, Takashi; Murakami, Yasunori (2017): Evolutionary mechanisms that generate morphology and neural-circuit diversity of the cerebellum. In: *Development, growth & differentiation* 59 (4), p. 228–243. DOI: 10.1111/dgd.12349.

Hibi, Masahiko; Shimizu, Takashi (2012): Development of the cerebellum and cerebellar neural circuits. In: *Developmental neurobiology* 72 (3), p. 282–301. DOI: 10.1002/dneu.20875.

Huang, Mei; Jia, Fang-Jun; Yan, Yuan-Chang; Guo, Li-He; Li, Yi-Ping (2006): Transactivated minimal E1b promoter is capable of driving the expression of short hairpin RNA. In: *Journal of virological methods* 134 (1-2), p. 48–54. DOI: 10.1016/j.jviromet.2005.11.016.

Kalueff, Allan V.; Stewart, Adam Michael; Gerlai, Robert (2014): Zebrafish as an emerging model for studying complex brain disorders. In: *Trends in pharmacological sciences* 35 (2), p. 63–75. DOI: 10.1016/j.tips.2013.12.002.

Kang, Seongman; Hong, Sunghoi (2009): Molecular pathogenesis of spinocerebellar ataxia type 1 disease. In: *Molecules and cells* 27 (6), p. 621–627. DOI: 10.1007/s10059-009-0095-y.

Kani, Shuichi; Bae, Young-Ki; Shimizu, Takashi; Tanabe, Koji; Satou, Chie; Parsons, Michael J. et al. (2010): Proneural gene-linked neurogenesis in zebrafish cerebellum. In: *Developmental Biology* 343 (1-2), p. 1–17. DOI: 10.1016/j.ydbio.2010.03.024.

Kim, Eunji; Lu, Hsiang-Chih; Zoghbi, Huda Y.; Song, Ji-Joon (2013): Structural basis of protein complex formation and reconfiguration by polyglutamine disease protein Ataxin-1 and Capicua. In: *Genes & development* 27 (6), p. 590–595. DOI: 10.1101/gad.212068.112.

Kimmel, C. B.; Ballard, W. W.; Kimmel, S. R.; Ullmann, B.; Schilling, T. F. (1995): Stages of embryonic development of the zebrafish. In: *Developmental dynamics: an official publication of the American Association of Anatomists* 203 (3), p. 253–310. DOI: 10.1002/aja.1002030302.

Klement, Ivan A.; Skinner, Pamela J.; Kaytor, Michael D.; Yi, Hong; Hersch, Steven M.; Clark, H.Brent et al. (1998): Ataxin-1 Nuclear Localization and Aggregation. In: *Cell* 95 (1), p. 41–53. DOI: 10.1016/S0092-8674(00)81781-X.

Koga, Akihiko; Cheah, Felicia S. H.; Hamaguchi, Satoshi; Yeo, Gare Hoon; Chong, Samuel S. (2008): Germline transgenesis of zebrafish using the medaka Tol1 transposon system. In: *Developmental dynamics: an official publication of the American Association of Anatomists* 237 (9), p. 2466–2474. DOI: 10.1002/dvdy.21688.

Lee, Won-Seok; Lavery, Laura; Rousseaux, Maxime W. C.; Rutledge, Eric B.; Jang, Youjin; Wan, Ying-Wooi et al. (2021): Dual targeting of brain region-specific kinases potentiates neurological rescue in Spinocerebellar ataxia type 1. In: *The EMBO journal* 40 (7), e106106. DOI: 10.15252/embj.2020106106.

Lee, Yoontae; Fryer, John D.; Kang, Hyojin; Crespo-Barreto, Juan; Bowman, Aaron B.; Gao, Yan et al. (2011): ATXN1 protein family and CIC regulate extracellular matrix

remodeling and lung alveolarization. In: *Developmental cell* 21 (4), p. 746–757. DOI: 10.1016/j.devcel.2011.08.017.

Lieberman, Andrew P.; Shakkottai, Vikram G.; Albin, Roger L. (2019): Polyglutamine Repeats in Neurodegenerative Diseases. In: *Annual review of pathology* 14, p. 1–27. DOI: 10.1146/annurev-pathmechdis-012418-012857.

Lieschke, Graham J.; Currie, Peter D. (2007): Animal models of human disease: zebrafish swim into view. In: *Nature reviews. Genetics* 8 (5), p. 353–367. DOI: 10.1038/nrg2091.

Lim, Janghoo; Crespo-Barreto, Juan; Jafar-Nejad, Paymaan; Bowman, Aaron B.; Richman, Ronald; Hill, David E. et al. (2008): Opposing effects of polyglutamine expansion on native protein complexes contribute to SCA1. In: *Nature* 452 (7188), p. 713–718. DOI: 10.1038/nature06731.

Lorenzetti, D.; Watase, K.; Xu, B.; Matzuk, M. M.; Orr, H. T.; Zoghbi, H. Y. (2000): Repeat instability and motor incoordination in mice with a targeted expanded CAG repeat in the Sca1 locus. In: *Human molecular genetics* 9 (5), p. 779–785. DOI: 10.1093/hmg/9.5.779.

Mastammanavar, Vinayakumar S.; Kamble, Nitish; Yadav, Ravi; M, Netravathi; Jain, Sanjeev; Kumar, Keshav; Pal, Pramod Kumar (2020): Non-motor symptoms in patients with autosomal dominant spinocerebellar ataxia. In: *Acta neurologica Scandinavica* 142 (4), p. 368–376. DOI: 10.1111/ane.13318.

Matilla, Antoni; Roberson, Erik D.; Banfi, Sandro; Morales, Joanella; Armstrong, Dawna L.; Burright, Eric N. et al. (1998): Mice Lacking Ataxin-1 Display Learning Deficits and Decreased Hippocampal Paired-Pulse Facilitation. In: *J. Neurosci.* 18 (14), p. 5508–5516. DOI: 10.1523/JNEUROSCI.18-14-05508.1998.

Matilla-Dueñas, Antoni; Goold, Robert; Giunti, Paola (2008): Clinical, genetic, molecular, and pathophysiological insights into spinocerebellar ataxia type 1. In: *Cerebellum (London, England)* 7 (2), p. 106–114. DOI: 10.1007/s12311-008-0009-0.

Matsui, Hideaki; Namikawa, Kazuhiko; Babaryka, Andreas; Köster, Reinhard W. (2014): Functional regionalization of the teleost cerebellum analyzed in vivo. In: *Proceedings of the National Academy of Sciences of the United States of America* 111 (32), p. 11846–11851. DOI: 10.1073/pnas.1403105111.

Mattern, Kai; Trotha, Jakob William von; Erfle, Peer; Köster, Reinhard Wolfgang; Dietzel, Andreas (2020): NeuroExaminer: an all-glass microfluidic device for whole-brain in vivo imaging in zebrafish. In: *Communications biology* 3 (1), p. 311. DOI: 10.1038/s42003-020-1029-7.

Matthews, Monte; Trevarrow, Bill; Matthews, Jennifer (2002): A virtual tour of the Guide for zebrafish users. In: *Lab animal* 31 (3), p. 34–40. DOI: 10.1038/5000140.

Maximino, Caio; Brito, Thiago Marques de; da Silva Batista, Annanda Waneza; Herculano, Anderson Manoel; Morato, Silvio; Gouveia, Amauri (2010): Measuring anxiety in zebrafish: a critical review. In: *Behavioural brain research* 214 (2), p. 157–171. DOI: 10.1016/j.bbr.2010.05.031.

Mehjabin, Rumana; Chen, Liangming; Huang, Rong; Zhu, Denghui; Yang, Cheng; Li, Yongming et al. (2019): Expression and localization of grass carp pkc-θ (protein kinase C theta) gene after its activation. In: *Fish & shellfish immunology*, p. 788–795. DOI: 10.1016/j.fsi.2019.01.057.

Meshalkina, Darya A.; Kysil, Elana V.; Warnick, Jason E.; Demin, Konstantin A.; Kalueff, Allan V. (2017): Adult zebrafish in CNS disease modeling: a tank that's half-full, not

half-empty, and still filling. In: *Lab animal* 46 (10), p. 378–387. DOI: 10.1038/laban.1345.

Miller, Victor M.; Nelson, Rick F.; Gouvion, Cynthia M.; Williams, Aislinn; Rodriguez-Lebron, Edgardo; Harper, Scott Q. et al. (2005): CHIP suppresses polyglutamine aggregation and toxicity in vitro and in vivo. In: *J. Neurosci.* 25 (40), p. 9152–9161. DOI: 10.1523/JNEUROSCI.3001-05.2005.

Namikawa, Kazuhiko; Dorigo, Alessandro; Köster, Reinhard W. (2019a): Neurological Disease Modelling for Spinocerebellar Ataxia Using Zebrafish. In: *Journal of Experimental Neuroscience* 13, 1179069519880515. DOI: 10.1177/1179069519880515.

Namikawa, Kazuhiko; Dorigo, Alessandro; Zagrebelsky, Marta; Russo, Giulio; Kirmann, Toni; Fahr, Wieland et al. (2019b): Modeling Neurodegenerative Spinocerebellar Ataxia Type 13 in Zebrafish Using a Purkinje Neuron Specific Tunable Coexpression System. In: *J. Neurosci.* 39 (20), p. 3948–3969. DOI: 10.1523/JNEUROSCI.1862-18.2019.

Nethisinghe, Suran; Pigazzini, Maria Lucia; Pemble, Sally; Sweeney, Mary G.; Labrum, Robyn; Manso, Katarina et al. (2018): PolyQ Tract Toxicity in SCA1 is Length Dependent in the Absence of CAG Repeat Interruption. In: *Frontiers in cellular neuroscience* 12, p. 200. DOI: 10.3389/fncel.2018.00200.

Niewiadomska-Cimicka, Anna; Hache, Antoine; Trottier, Yvon (2020): Gene Deregulation and Underlying Mechanisms in Spinocerebellar Ataxias With Polyglutamine Expansion. In: *Frontiers in neuroscience* 14, p. 571. DOI: 10.3389/fnins.2020.00571.

Nitschke, Larissa; Coffin, Stephanie L.; Xhako, Eder; El-Najjar, Dany B.; Orengo, James P.; Alcala, Elizabeth et al. (2021): Modulation of ATXN1 S776 phosphorylation reveals the importance of allele-specific targeting in SCA1. In: *JCI Insight* 6 (3).

Nóbrega, Clévio; Pereira de Almeida, Luís (Hg.) (2018): Polyglutamine Disorders. Cham: Springer International Publishing (Advances in Experimental Medicine and Biology, 1049).

Orr, H. T.; Chung, M. Y.; Banfi, S.; Kwiatkowski, T. J.; Servadio, A.; Beaudet, A. L. et al. (1993): Expansion of an unstable trinucleotide CAG repeat in spinocerebellar ataxia type 1. In: *Nature genetics* 4 (3), p. 221–226. DOI: 10.1038/ng0793-221.

Pérez Ortiz, Judit M.; Orr, Harry T. (2018): Spinocerebellar Ataxia Type 1: Molecular Mechanisms of Neurodegeneration and Preclinical Studies. In: *Advances in experimental medicine and biology* 1049, p. 135–145. DOI: 10.1007/978-3-319-71779-1_6.

Purves, Dale; Augustine, George J.; Fitzpatrick, David; Katz, Lawrence C.; LaMantia, Anthony-Samuel; McNamara, James O.; Williams, S. Mark (Hg.) (2001): Neuroscience. 2nd ed. Sunderland, Mass: Sinauer Associates.

Ranum, L. P.; Duvick, L. A.; Rich, S. S.; Schut, L. J.; Litt, M.; Orr, H. T. (1991): Localization of the autosomal dominant HLA-linked spinocerebellar ataxia (SCA1) locus, in two kindreds, within an 8-cM subregion of chromosome 6p. In: *American Journal of Human Genetics* 49 (1), p. 31–41.

Rocha, Sara; Vieira, Jorge; Vázquez, Noé; López-Fernández, Hugo; Fdez-Riverola, Florentino; Reboiro-Jato, Miguel et al. (2019): ATXN1 N-terminal region explains the binding differences of wild-type and expanded forms. In: *BMC medical genomics* 12 (1), p. 145. DOI: 10.1186/s12920-019-0594-4.

Rousseaux, Maxime W. C.; Tschumperlin, Tyler; Lu, Hsiang-Chih; Lackey, Elizabeth P.; Bondar, Vitaliy V.; Wan, Ying-Wooi et al. (2018): ATXN1-CIC Complex Is the Primary Driver of Cerebellar Pathology in Spinocerebellar Ataxia Type 1 through a Gain-of-Function Mechanism. In: *Neuron* 97 (6), 1235-1243.e5. DOI: 10.1016/j.neuron.2018.02.013.

Royston, Patrick (1995): Remark AS R94: A Remark on Algorithm AS 181: The W-test for Normality. In: *Applied Statistics* 44 (4), p. 547. DOI: 10.2307/2986146.

Sambrook, Joseph; Russell, David William (2001): Molecular cloning. A laboratory manual. 3rd ed. Cold Spring Harbor, N.Y: Cold Spring Harbor Laboratory Press.

Schiffer, Niclas W.; Broadley, Sarah A.; Hirschberger, Thomas; Tavan, Paul; Kretzschmar, Hans A.; Giese, Armin et al. (2007): Identification of anti-prion compounds as efficient inhibitors of polyglutamine protein aggregation in a zebrafish model. In: *The Journal of Biological Chemistry* 282 (12), p. 9195–9203. DOI: 10.1074/jbc.M607865200.

Schramm, Paul; Hetsch, Florian; Meier, Jochen C.; Köster, Reinhard W. (2021): In vivo Imaging of Fully Active Brain Tissue in Awake Zebrafish Larvae and Juveniles by Skull and Skin Removal. In: *Journal of visualized experiments : JoVE* (168). DOI: 10.3791/62166.

Taroni, Franco; DiDonato, Stefano (2004): Pathways to motor incoordination: the inherited ataxias. In: *Nature reviews. Neuroscience* 5 (8), p. 641–655. DOI: 10.1038/nrn1474.

Tsuda, Hiroshi; Jafar-Nejad, Hamed; Patel, Akash J.; Sun, Yaling; Chen, Hung-Kai; Rose, Matthew F. et al. (2005): The AXH domain of Ataxin-1 mediates neurodegeneration through its interaction with Gfi-1/Senseless proteins. In: *Cell* 122 (4), p. 633–644. DOI: 10.1016/j.cell.2005.06.012.

Vauti, Franz; Stegemann, Luisa A.; Vögele, Viktoria; Köster, Reinhard W. (2020): All-age whole mount in situ hybridization to reveal larval and juvenile expression patterns in zebrafish. In: *PloS one* 15 (8), e0237167. DOI: 10.1371/journal.pone.0237167.

Wang, Yubin; Hersheson, Joshua; Lopez, Dulce; Hammer, Monia; Liu, Yan; Lee, Ka-Hung et al. (2016): Defects in the CAPN1 Gene Result in Alterations in Cerebellar Development and Cerebellar Ataxia in Mice and Humans. In: *Cell reports* 16 (1), p. 79–91. DOI: 10.1016/j.celrep.2016.05.044.

Watase, Kei; Weeber, Edwin J.; Xu, Bisong; Antalffy, Barbara; Yuva-Paylor, Lisa; Hashimoto, Kouichi et al. (2002): A Long CAG Repeat in the Mouse Sca1 Locus Replicates SCA1 Features and Reveals the Impact of Protein Solubility on Selective Neurodegeneration. In: *Neuron* 34 (6), p. 905–919. DOI: 10.1016/S0896-6273(02)00733-X.

Watchon, Maxinne; Yuan, Kristy C.; Mackovski, Nick; Svahn, Adam J.; Cole, Nicholas J.; Goldsbury, Claire et al. (2017): Calpain Inhibition Is Protective in Machado-Joseph Disease Zebrafish Due to Induction of Autophagy. In: *The Journal of neuroscience : the official journal of the Society for Neuroscience* 37 (32), p. 7782–7794. DOI: 10.1523/JNEUROSCI.1142-17.2017.

Woods, Ian G.; Wilson, Catherine; Friedlander, Brian; Chang, Patricia; Reyes, Daengnoy K.; Nix, Rebecca et al. (2005): The zebrafish gene map defines ancestral vertebrate chromosomes. In: *Genome research*, p. 1307–1314. DOI: 10.1101/gr.4134305.

Yanicostas, Constantin; Barbieri, Elisa; Hibi, Masahiko; Brice, Alexis; Stevanin, Giovanni; Soussi-Yanicostas, Nadia (2012): Requirement for zebrafish ataxin-7 in differentiation of photoreceptors and cerebellar neurons. In: *PloS one* 7 (11), e50705. DOI: 10.1371/journal.pone.0050705.

Zhang, Can; Browne, Andrew; Child, Daniel; Divito, Jason R.; Stevenson, Jesse A.; Tanzi, Rudolph E. (2010): Loss of function of ATXN1 increases amyloid beta-protein levels by potentiating beta-secretase processing of beta-amyloid precursor protein. In: *The Journal of Biological Chemistry* 285 (12), p. 8515–8526. DOI: 10.1074/jbc.M109.079079.

Zoghbi, H. Y.; Orr, H. T. (2000): Glutamine repeats and neurodegeneration. In: *Annual review of neuroscience* 23, p. 217–247. DOI: 10.1146/annurev.neuro.23.1.217.

Zoghbi, Huda Y.; Jodice, Carla; Sandkuijl, Lodewijk A.; Kwiatkowski, Thomas J.; McCall, Alanna E.; Huntoon, Sally A. et al. (1991): The gene for autosomal dominant spinocerebellar ataxia (SCA1) maps telomeric to the HLA complex and is closely linked to the D6S89 locus in three large kindreds. In: *American Journal of Human Genetics* 49 (1), p. 23–30.

Zoghbi, Huda Y.; Orr, Harry T. (2009): Pathogenic mechanisms of a polyglutamine-mediated neurodegenerative disease, spinocerebellar ataxia type 1. In: *The Journal of Biological Chemistry* 284 (12), p. 7425–7429. DOI: 10.1074/jbc.R800041200.

Zon, Leonard I.; Peterson, Randall T. (2005): In vivo drug discovery in the zebrafish. In: *Nature reviews. Drug discovery* 4 (1), p. 35–44. DOI: 10.1038/nrd1606.

Zuber, M. X.; Strittmatter, S. M.; Fishman, M. C. (1989): A membrane-targeting signal in the amino terminus of the neuronal protein GAP-43. In: *Nature* 341 (6240), p. 345–348. DOI: 10.1038/341345a0.